GROUP II XENOLITHS FROM LUNAR CRATER VOLCANIC FIELD, NEVADA: IMPLICATIONS FOR SUBDUCTED PLATE METASOMATISM

by

JOHN CLARK MOSELY, JR.

Under the Direction of MICHAEL F. RODEN

ABSTRACT

Lunar Crater Volcanic Field (LCVF), a Quaternary volcanic field in central Nevada, is characterized by alkali basalts that host megacrysts of clinopyroxene, amphibole and olivine as well as mafic and ultramafic xenoliths. The Group II xenoliths present at LCVF offer insight in to the complex magmatic processes at play beneath the volcanic field, as well as providing context for Tertiary and Quaternary volcanism in the western United States. Petrologic and geochemical analysis of these xenoliths and the constituent phases are consistent with genesis from a magma enriched in Ti and Al. High modal abundance of amphibole, as well as the presence of anomalously OH and Cl rich apatite within the xenoliths could be attributed to melting of a source rock enriched in water and chlorine. The geochemistry of xenoliths at LCVF is similar to that of subduction driven magmatism observed at island arcs and convergent margins but occurs well inland. Mantle enrichment by the dehydration of the shallowly subducted Farallon plate and subsequent melting of this enriched mantle allows for and is consistent with the hydrous xenoliths and the anomalous apatite hosted within them.

# GROUP II XENOLITHS FROM LUNAR CRATER VOLCANIC FIELD, NEVADA: IMPLICATIONS FOR SUBDUCTED PLATE METASOMATISM

by

JOHN CLARK MOSELY, JR.

B.S., University of Georgia, 2010

A Thesis Submitted to the Graduate Faculty of The University of Georgia in Partial Fulfillment of the Requirements for the Degree

MASTER OF SCIENCE

ATHENS, GEORGIA

2015

# GROUP II XENOLITHS FROM LUNAR CRATER VOLCANIC FIELD, NEVADA: IMPLICATIONS FOR SUBDUCTED PLATE METASOMATISM

by

JOHN CLARK MOSELY, JR.

| | |
|---|---|
| Major Professor: | Michael F. Roden |
| Committee: | Douglas E. Crowe |
| | Paul A. Schroeder |

Electronic Version Approved:

Julie Coffield
Interim Dean of the Graduate School
The University of Georgia
May 2015

ACKNOWLEDGEMENTS

First and foremost, I would like to thank Mike Roden for the time and effort expended helping me to bring this paper baby to term. His patience and subtle encouragement were instrumental in all phases of my research as well as the writing of this thesis, and I could not have done this without him. I would also like to thank Doug Crowe, for encouraging me to pursue graduate studies in Geology, and for allowing me to pursue them. I'd like to thank Paul Schroeder for his time, his sense of humor, for calling me "dude" and for the XRD experience he provided that will serve me well in my next job. Chris Fleisher is more than a colleague to me, he has been a friend, a mentor, an example, and voice of reason all rolled into one lanky ball. Time spent with Chris running the microprobe in the basement was some of the most enjoyable time I've spent during these past two years and I thank him; when I grow up I want to be like Chris Fleisher. Thanks to Steve Holland for the use of his photomicrograph set-up. Thanks to Sam Swanson for being a good boss and for helping me hone my skills in mineralogy and microscopy. I'd like to thank Gilles Allard and the Allard Fund, for funding my fieldwork, and not a junket in Las Vegas; unfortunately I have been forced to realize that magic is probably not the source of the magmatism at LCVF. I'd like to thank John Norris for his thesis and the data and insight it provided. I'd like to thank Joanna Wilford, for keeping me relatively sane, and for showing me what hard work can accomplish. Finally I'd like to thank my Mom and Dad, Ann and John Mosely, for not giving up on me, I couldn't have done this with out them.

TABLE OF CONTENTS

Page

LIST OF TABLES

Page

LIST OF FIGURES

Page

## 1.0 INTRODUCTION AND GEOLOGIC CONTEXT

The Lunar Crater Volcanic Field (LCVF) is located in central Nevada in northern Nye County (Figure 1.0) and is considered part of the Great Basin region of the Basin and Range Province of Western North America. The Great Basin is the northwestern portion of the Basin and Range Province and is bordered by the Sierra Nevada Mountains to the west, the Snake River Plain to the north, the Colorado Plateau to the east, and the Mojave Desert to the south. The topography of the Great Basin is consistent with that of the greater Basin and Range and exhibits NE-SW trending mountain ranges separated by flat valleys (basins). This topography is the result of crustal extension that results in steeply dipping normal faults that meet basal detachment faults at a depth of 10-20km (Hamilton, 1987). The Great Basin has been characterized by crustal extension and thinning since the Oligocene (Allmendinger et al., 1987). The LCVF is located in the central portion of the Great Basin, is about 80 km long and 20 km wide, and forms a north-northeast trending group of group of cinder cones, maars, and basaltic lava flows between the Reveille and Pancake Ranges (Scott and Trask, 1971). Easy Chair Volcano, the subject of this study, is near the center of the field just south of U.S. Highway 6, has a $^{40}Ar/^{39}Ar$ age of approximately 140 kya (Heizler, 2013), and forms a 2.5 km long ridge that rises to a maximum height of 240 m above the valley floor (Valentine and Cortes, 2013). Easy Chair Volcano exhibits a maar on the southern flank called Easy Chair Crater (Figure 1.1).


Figure 1.0: Location of Lunar Crater Volcanic Field (LCVF). Map Data © Google, INEGI


Figure 1.1: Satellite image of LCVF. Image © Google.

The lavas that comprise the flows around Easy Chair Crater are primarily alkalic in composition and contain mafic and ultramafic xenoliths originating at the interface of the lower crust and upper mantle as well as amphibole, pyroxene, feldspar and olivine megacrysts (Scott and Trask, 1971). The majority of xenoliths observed in the southwestern US fall within the Group I and Group II categories. Group I xenoliths have metamorphic textures, are olivine-dominated and characterized by Cr-rich pyroxenes and olivine with Mg # = 0.86-0.91. Group II xenoliths have Ti- and Al- augite as a key phase, have cumulate textures, and the silicates are more Fe-rich (Mg # = 0.62-0.78) (Menzies et al., 1987; Frey & Prinz, 1978).

Work on the geochemical composition of both Group I and Group II xenoliths, as well as geothermometry and geobarometry, was performed on samples from the Easy Chair basalt flow by John Norris (1996). The xenoliths described by Norris (1996) consist of several Group I xenoliths composed primarily of olivine and clinopyroxene as well as many Group II xenoliths of more variable modes but with major phases including amphibole, clinopyroxene (with some showing orthopyroxene exsolution lamellae), olivine, and spinel group minerals with a few samples containing plagioclase as well. Interestingly at least one sample (S-1) shows exsolution of single spinel grains into two distinct phases, a hercynite-rich phase and a magnetite-rich phase.

Geothermometry done by Norris as well as work by Roden & Shimizu (1993) and Smith (2000) yielded relatively high temperatures (1230-1290°C) of equilibration in some Group I xenoliths compared to temperatures (840-1080°C) estimated for Group I xenoliths from elsewhere in western North America. A possible explanation for these higher equilibrium temperatures in the LCVF Group I xenoliths is an elevated geotherm, which could be due to the

presence of a mantle plume at the time of volcanic activity (Smith, 2000; McKenzie and Bickle, 1988).

Further evidence of mantle plume activity at LCVF is presented in Saltus and Thompson (1995). They posit that an observed topographic rise between southern Nevada and central Nevada observed along longitude 116° (LCVF is located along 116°) indicates the presence of an underlying mantle plume. Seismic evidence presented in Saltus and Thompson (1995) alongside the topographic data shows that simple crustal isostasy could be responsible for at most 50% of the observed change in elevation. However, although the Battle Mountain High region of high heat flow is near the LCVF, the field itself lies in a region of relatively low heat flow for the Basin and Range Province (Figure 1.2). The possible explanation for low observed heat flow at LCVF is twofold. One, the heat flow data in Figure 1.2 was obtained from existing wells in Nevada (Figure 1.3). Note the lack of wells in the area surrounding LCVF. Lack of data from this area makes published heat flow estimates not verified by actual heat flow measurements. Two, Saltus and Thompson (1995) suggest that because Basin and Range Uplift is relatively recent (<20 Mya) that there has been insufficient time for the heat signature of a relatively young and/or deep heat source (i.e. mantle plume) to be recorded as surface heat flow.

The focus of this thesis is on Group II xenoliths from Easy Chair Crater collected by Deborah Hassler and John Norris. New mineral analyses are combined with data from Norris (1996) to constrain petrogenesis as well as pressure and temperature of equilibration of the Group II xenoliths. Additionally, the chemical composition of apatite in the Group II xenoliths was determined. Apatite ($Ca_5(PO_4)_3(OH,F,Cl)$) is a key accessory mineral in the upper mantle

where it is an important repository of phosphorous and halogens (Smith et al., 1981). The halogens Cl and F are essential components of natural apatites, and they, especially Cl, are thought to be important components of the fluids responsible for mantle metasomatism (Patiño Douce et. al. 2011). Differences in the relative abundance of these components within apatites, while not simply related in absolute abundance to halogen content within the parental melt/fluid, can provide insight into the fluid/melt compositions (O'Reilly & Griffin, 2000). For example, apatites with higher Cl amounts could be a signature of a contribution from subducted lithosphere (Patiño Douce et. al. 2011). In summary, in this thesis, the petrology, and geothermometry, as well as apatite compositions in Group II xenoliths are used to constrain the present state of the upper mantle/lower crust beneath the LCVF.

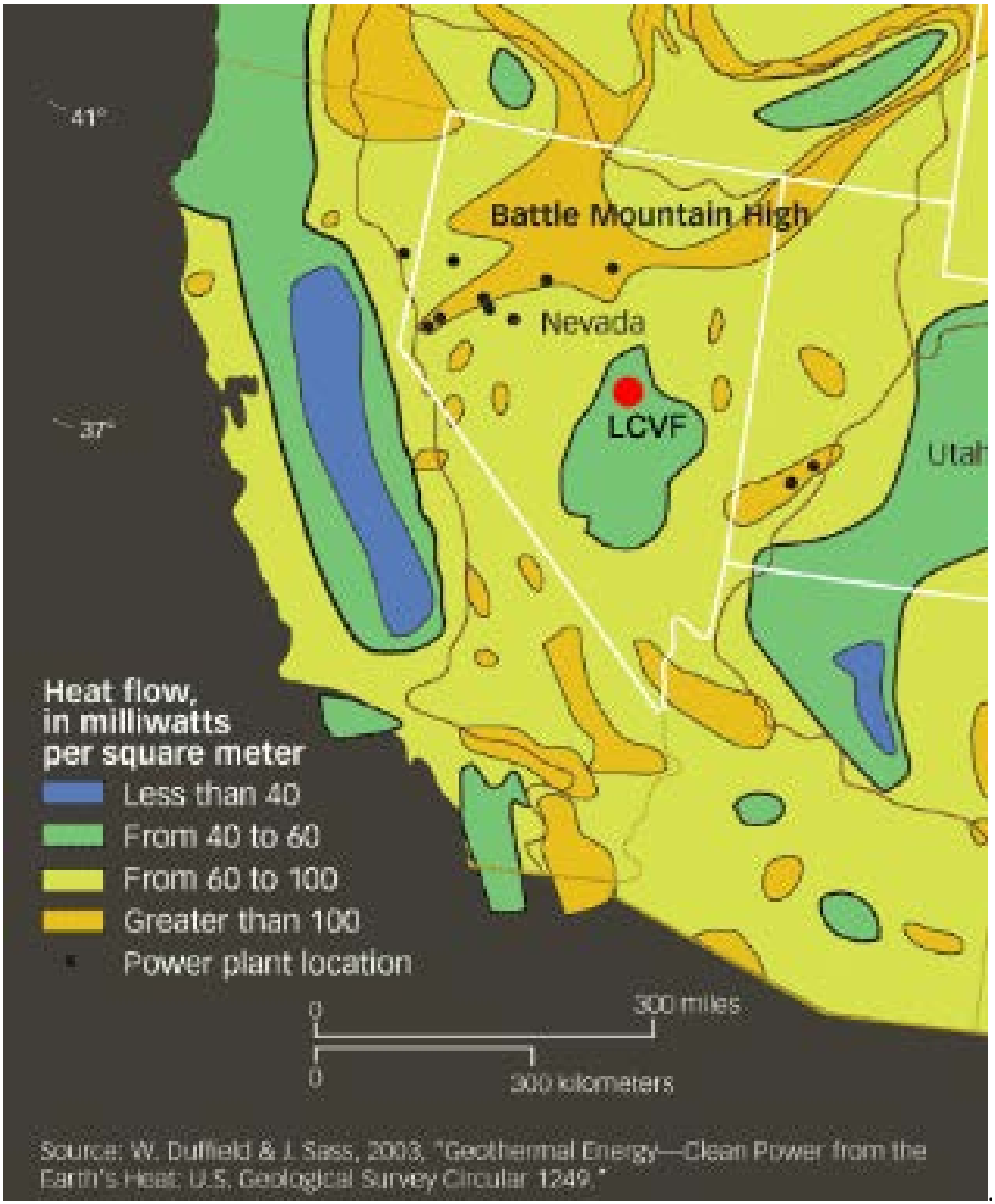


Figure 1.2: Heat flow in the Western U.S. From Dulfield & Sass (2003)

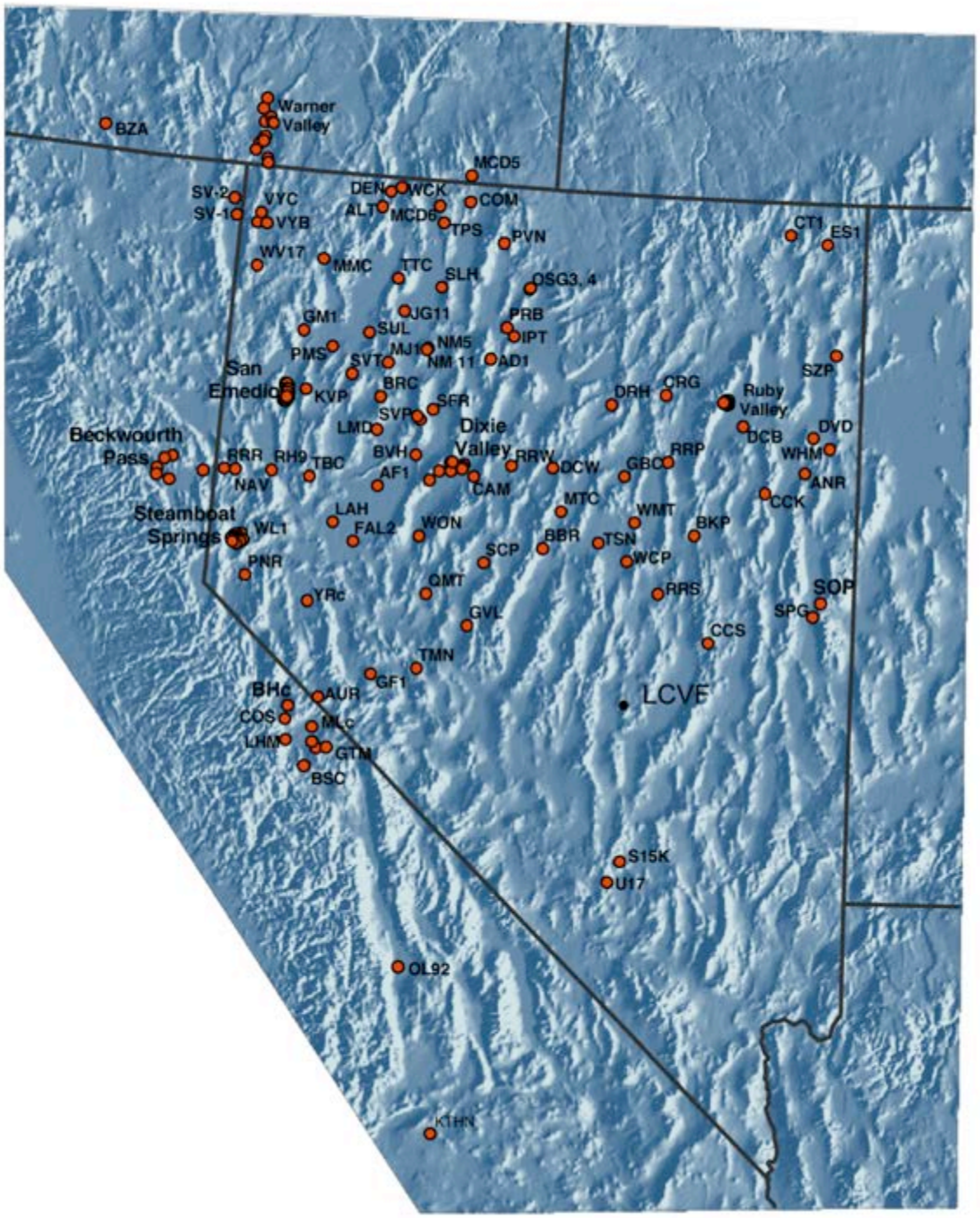


Figure 1.3: Wells used to determine heat flow in Nevada. From Sass et al. (2005)

## 2.0 ANALYTICAL METHODS

### 2.1 Samples

Deborah Hassler and John Norris collected the xenoliths used in this thesis at Easy Chair Crater, Lunar Crater Volcanic Field (LCVF), Nevada during July 1990 and June 1993. Further field data was collected in the fall of 2014 by the author of this thesis. New analytical data obtained during 2013-2014 are combined with bulk-rock major and trace element data as well as mineral composition data from the thesis by John Norris (1996): **Geochemistry of Mafic and Ultramafic Xenoliths From the Easy Chair Crater Basalt Flow, Lunar Crater Volcanic Field, Nevada.**

### 2.2 Methods

Norris analyzed major phase and oxide compositions with a JEOL JXA 8600 electron microprobe at the University of Georgia. These analyses were performed using an accelerating voltage of 15kV and an electron beam current of 15-20nA. The target spot size was 5 micrometers for plagioclase analyses, and 1 micrometer for pyroxenes, olivines, amphiboles and spinels (Norris 1996).

Mineral composition analyses for olivine, pyroxene, amphibole, spinel and sulfide in 2014 at the University of Georgia were performed using a JEOL JXA 8600 electron microprobe, an accelerating voltage of 15kV and an electron beam current of 10nA. The target spot size was 1 micrometer. Mineral grains were qualitatively identified using a Bruker 5010 Silicon Drift

Detector energy dispersive X-ray (EDS) detector controlled by a Bruker Quantax energy dispersive analysis system. Quantitative analyses were performed with wavelength dispersive spectrometers (WDS) automated with Advanced Microbeam, Inc. electronics and Probe for EPMA software, using 10-second count times, and natural and synthetic mineral standards. Analyses were calculated using Armstrong's (1988) Phi-Rho-Z matrix correction model. Backscattered electron images (BEI) were acquired using imaging software from the Quantax analysis system.

For apatite analysis the analytical methods of Patiño-Douce et al. (2011) and Sarafian et al. (2013) for electron microprobe (EMP) analyses were followed. Typical operating conditions were a 15 kV accelerating voltage and a 5 nA beam current. Spot size was a defocused 5-micrometer beam. Eleven elements (P, Ca, Fe, Na, Mg, S, Sr, Y, Ce, F, and Cl) were measured in apatite. $Fe^{+2}$, Sr, Y and the REE (Ce is the most abundant REE) substitute for Ca in apatite and S substitutes for P. Analyzing for these elements helps insure proper stoichiometric totals as well as fully characterizing the composition of apatite. The following synthetic and natural standards were used for EMP analyses:

P, F: Wilberforce apatite, Ca: Durango apatite, Fe: fayalite, Na: plagioclase, Mg: olivine, S: pyrite, Sr: SrTi, Y: $Y_2O_3$, Ce: $CeO_2$, Cl: Chlorapatite

**2.3 Apatite Analytical Screen**

Accurate microprobe analysis of apatites can be complicated by migration of F (Stormer, et al. 1993) as well as complex ionic substitution in the P and Ca sites of apatite. In order to minimize impact of F migration, halogens were analyzed first (Sarafian et al. 2013). The

analytical screen for apatites proposed by Patiño-Douce et al. (2011) was used to reject poor analyses as outlined in the following. Oxide weight percent analyses must total between 98.5 and 100.5%. Analyses were normalized to 25 oxygens (one formula unit). Totals for the Ca site (Ca, Y, Ce, Sr, and Fe) must be between 9.7 and 10.1 cations and the P site (P, S in this case though Si and As also substitute for P) must total between 5.8 and 6.1 cations. The X-site (home of the volatiles) must total less than 2.05 anions.

## 3.0 RESULTS

### 3.1 Xenolith population

Independent surveys of the xenolith population were conducted at a lava flow emanating from the north side of Easy Chair Crater. Xenolith counts were performed *in situ* at two locations where smooth exposures facilitated the xenolith counts (Figure 3.0). A total of 194 xenoliths were examined. Length and width measurements were made on all counted xenoliths. These measurements were tabulated and an outcrop area was calculated for each lithology. Xenolith counts and calculated area are presented in Table 3.0. Observed xenoliths were categorized into three primary lithologies: gabbro, pyroxenite/amphibolite, and peridotite. Samples with significant plagioclase were categorized as gabbro. Samples with significant olivine were categorized as peridotite. Samples composed primarily of pyroxene or amphibole were grouped together as pyroxenite/amphibolite. Pyroxenite/amphibolite was the most abundant xenolith type observed. Gabbro, while observed in less abundance than pyroxenite/amphibolite occupied the most area amongst the three observed xenolith groups. Peridotite was significantly less abundant than either gabbro or pyroxenite/amphibolite.

Table 3.0: Xenolith population count and area

| Lithology | Count | % Population | Area(cm) | % Area |
|---|---|---|---|---|
| Gabbro | 73 | 38 | 590 | 45 |
| Pyroxenite/Amphibolite | 78 | 40 | 436 | 34 |
| Peridotites | 43 | 22 | 272 | 21 |
| Total | 194 | 100 | 1298 | 100 |


Figure 3.0: Xenolith count sites on Easy Chair Crater. Satellite Image © Google.

### 3.2 Petrographic Descriptions

***S-1 Amphibolite (75% amp, 10% cpx, 10% ol, 5% plag/sp)***

Large grains of amphibole (2-10mm) poikilitically enclose anhedral clinopyroxenes (0.1 to 4mm), sub- to anhedral olivines (1-2mm) and anhedral spinels (0.5-1.0mm). Olivines and pyroxenes are unzoned. Clinopyroxenes show exsolution lamellae of orthopyroxene and inclusions of amphibole and spinel. Some spinels show exsolution into pleonaste/magnetite pairs. Small amounts of interstitial plagioclase are present.

***X-1 Clinopyroxenite (30% amp, 35% cpx, 30% ol, 5% plag/sp)***

Phaneritic rock consisting primarily of sub- to anhedral clinopyroxenes (0.5-2.0mm) and olivines (0.5-2.0mm). Clinopyroxenes show exsolution lamellae of orthopyroxene and inclusions of amphibole (Figure 3.1). Olivines and pyroxenes are unzoned. Olivines are rimmed with amphibole. Amphibole also appears interstitially. Spinels occur as inclusions in amphiboles. Small amounts of interstitial plagioclase are present. Apatite is subhedral and appears at amphibole grain boundaries (Figure 3.2).

***S-4 Gabbro (30% amp, 30% cpx, 20% ol, 15% plag/sp)***

Phaneritic rock consisting primarily of sub- to anhedral clinopyroxenes (0.2-1.0mm) and sub- to anhedral olivines (0.2-1.0mm). Olivines and pyroxenes are unzoned. Clinopyroxenes show exsolution lamellae of orthopyroxene and inclusions of amphibole. Amphibole appears interstitially and as large (up to 5mm) subhedral grains poikilitically enclosing olivine and clinopyroxene. Spinel grains are enclosed by or occur along amphibole edges. Plagioclase is interstitial.

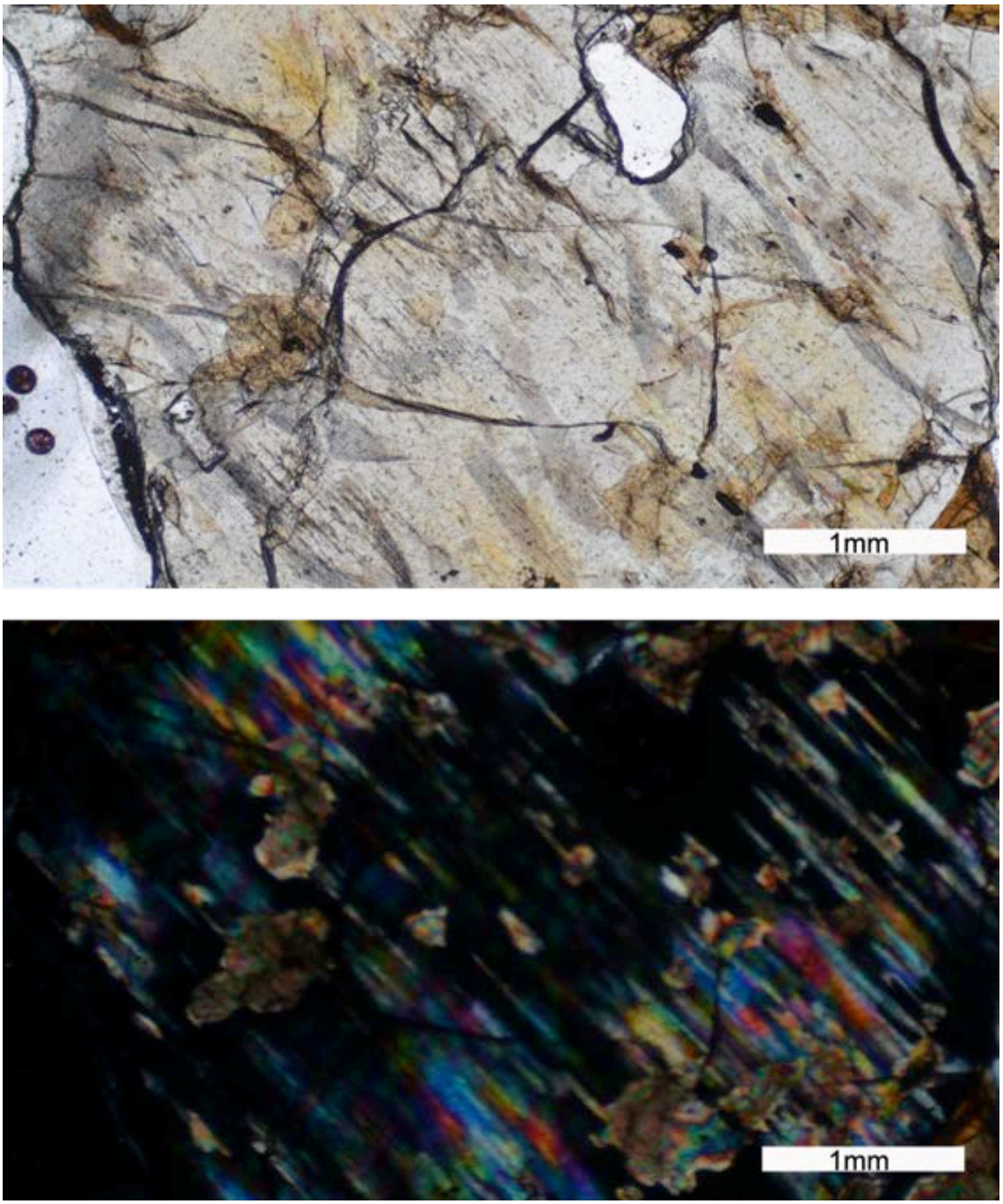


Figure 3.1: Photomicrograph of clinopyroxene with amphibole exsolution in sample X-1. Top image in plain-polarized light, bottom image with crossed nicols.

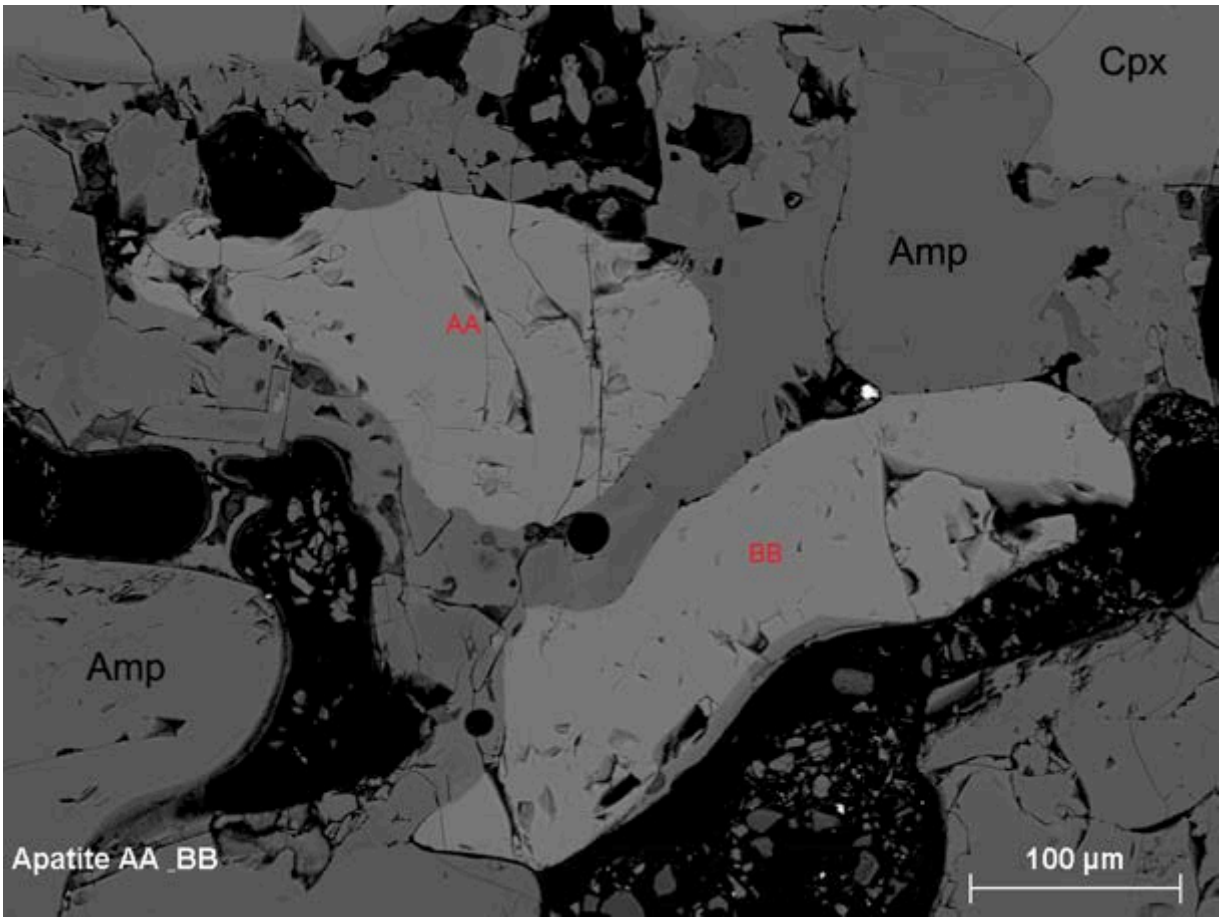


Figure 3.2: BSE (Backscatter Electron) image of apatite grains (AA & BB) in sample X-1.

***90ECC118 Clinopyroxenite (30% amp, 40% cpx, 20% ol, 10% plag/sp)***

Phaneritic rock consisting primarily of grains of sub- to anhedral clinopyroxenes (1-2mm), anhedral (1mm) and interstitial amphibole, and anhedral olivines (0.5-2.0mm). Olivines and pyroxenes are unzoned. Clinopyroxenes show exsolution lamellae of orthopyroxene and inclusions of amphibole. Sub- to anhedral spinels (0.1-0.5mm) are enclosed by amphibole. Small amounts of interstitial plagioclase are present.

***AF-1 Clinopyroxenite (40% amp, 50% cpx, 10% sp)***

Large (2-7mm) anhedral clinopyroxenes along with large (1-6mm) sub- to anhedral amphiboles. Olivines and pyroxenes are unzoned. Amphibole also appears as inclusions and lamellae within clinopyroxenes. Subhedral spinels are enclosed by amphibole. Some spinels show two distinct phases in reflected light. Very small amounts of interstitial plagioclase are present.

***AF-2 Amphibolite (60% amp, 25% cpx, 5% ol, 10% sp)***

Primarily large (2-8mm) sub- to anhedral amphiboles with sub- to anhedral clinopyroxenes (0.5-2mm) and some anhedral olivines (0.2-0.5mm). Olivines and pyroxenes are unzoned. Amphibole also appears as inclusions and lamellae within clinopyroxenes and inclusions within olivine (Figure 3.3). Spinels/oxides are enclosed by amphibole.

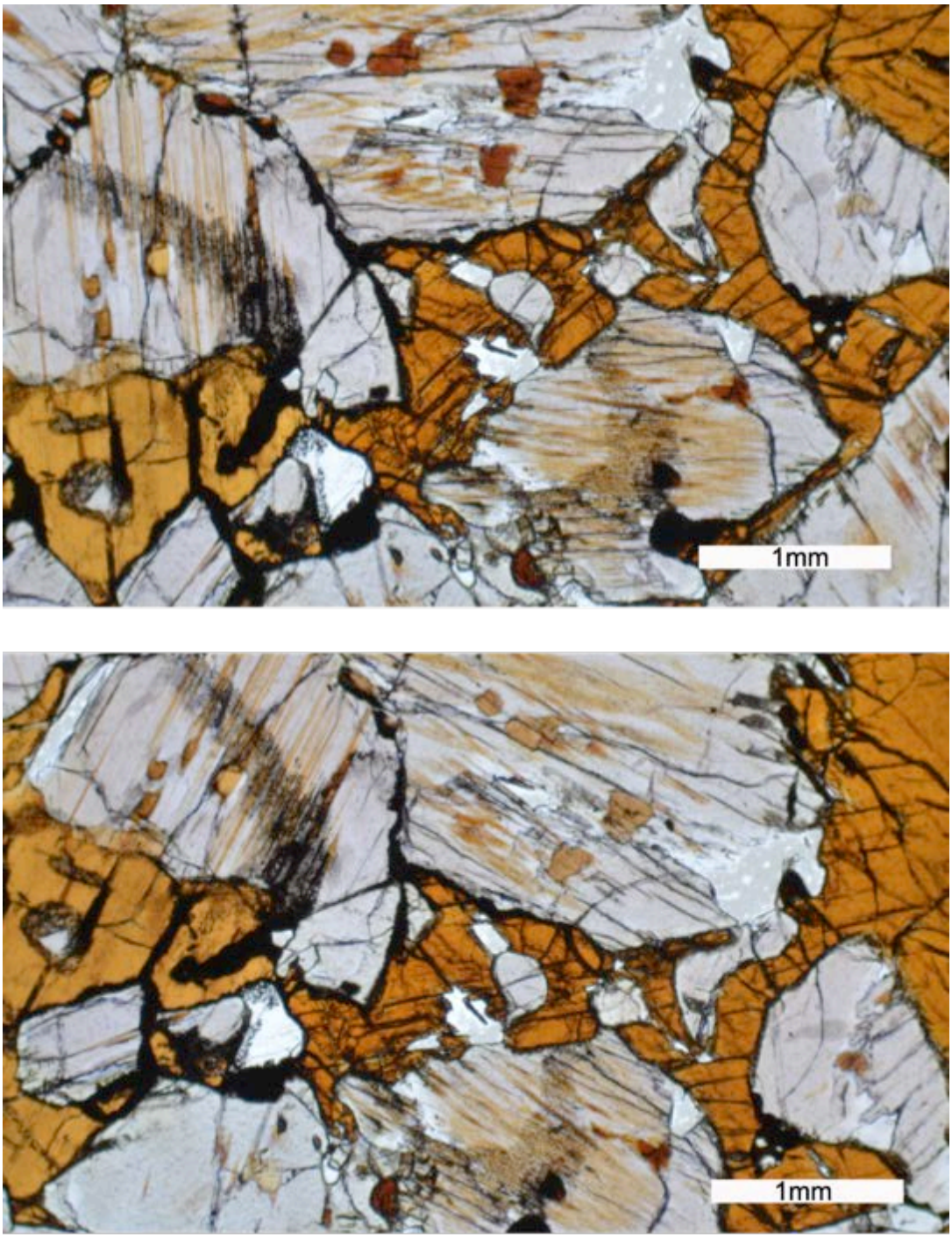


Figure 3.3: Photomicrograph of sample AF-2. Amphibole (colored phase) inclusions and lamellae in clinopyroxene (lighter phase). Thin-section shown at two orientations to highlight pleochroism of inclusions.

***X-6 Clinopyroxenite (35% amp, 35% cpx, 25% ol, 5% sp)***

Phaneritic rock consisting of grains of anhedral olivine (0.5-1.5mm) sub- to anhedral pyroxenes (0.5-1.5mm) and anhedral amphibole (0.5-3.0mm). Olivines and pyroxenes are unzoned. Olivine is highly fractured and altered to iddingsite at grain boundaries and in fractures. Pyroxenes show lamellae of amphibole. Amphibole is interstitial and relatively dark in plain polar light.

***X-8 Clinopyroxenite (10% amp, 45% cpx, 40% ol, 5% sp)***

Phaneritic rock consisting of grains of anhedral olivine (0.5-1.5mm) and sub- to anhedral pyroxenes (0.5-2.0mm) and anhedral amphibole (0.5-3.0mm). Olivines and pyroxenes are unzoned. Olivine is highly fractured and altered to iddingsite at grain boundaries and in fractures. Pyroxenes show lamellae of amphibole. Amphibole appears interstitially and encloses some spinels.

***S-6 Host Basalt/Gabbro xenolith (10% amp, 45% cpx, 30% ol, 15% plag/sp)***

Thin section includes host basalt and a gabbro xenolith. The basalt consists of vesicular glass with some small (<0.5mm) subhedral phenocrysts of plagioclase and pyroxene. Remainder of the slide (gabbro) is a phaneritic rock consisting of grains of subhedral olivine (1-3mm), anhedral plagioclase (1-2mm) and small amounts of altered pyroxene (0.5mm). Olivines and pyroxenes are unzoned. Olivine is extensively altered to iddingsite at grain boundaries and in fractures. Plagioclase appears interstitially. Relic pyroxene grains include amphibole and oxides and show evidence of alteration.

***F-2 Amphibolite (50% amp, 20% cpx, 20% ol, 10% plag/sp)***

Phaneritic rock consisting primarily of sub- to anhedral coarse-grained amphibole (2.0-12.0 mm). Anhedral clinopyroxene (0.5-3.0 mm) and sub- to anhedral olivine (≈1.0mm) are present in approximately equal amounts enclosed poikilitically by amphibole. Olivines and pyroxenes are unzoned. Clinopyroxene exhibits exsolution lamellae and inclusions of amphibole and orthopyroxene. Spinel (0.1-1.0mm) appears as inclusions in amphibole. Small amounts of interstitial plagioclase are present. Apatite is subhedral and appears at grain and vesicle boundaries (Figure 3.4).

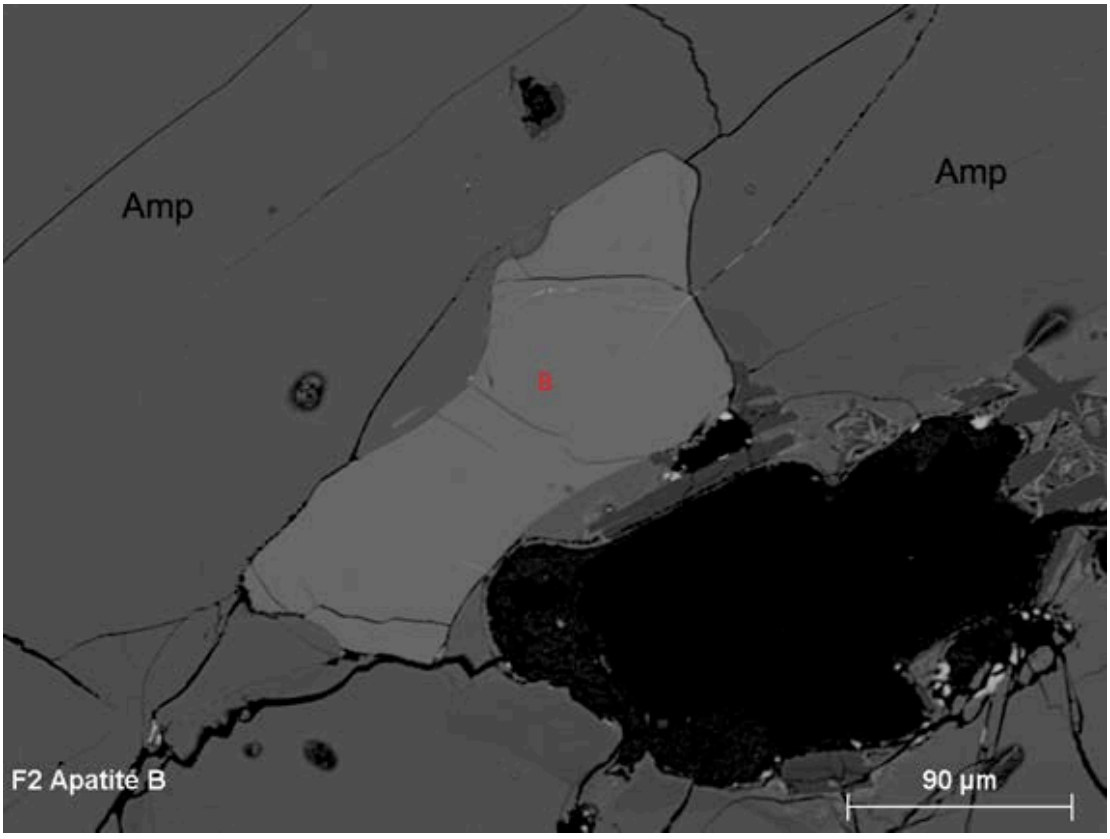


Figure 3.4: BSE image of apatite grain (B) in sample F-2.

***EC-3 Amphibolite (45% amp, 40% cpx, 5% ol, 10% sp/plag)***

Large (>1cm) anhedral amphiboles poikilitically enclose sub- to anhedral clinopyroxenes (0.5-1.0mm) and anhedral olivines (0.5-1.0mm). Olivines and pyroxenes are unzoned. Pyroxenes show some exsolution lamellae of orthopyroxene. Amphibole shows reaction rims of a very fine-grained oxide. Amphibole also encloses relatively large (>0.1mm) spinels that show inclusions of ilmenite in backscatter electron (BSE) images (Figure 3.5).

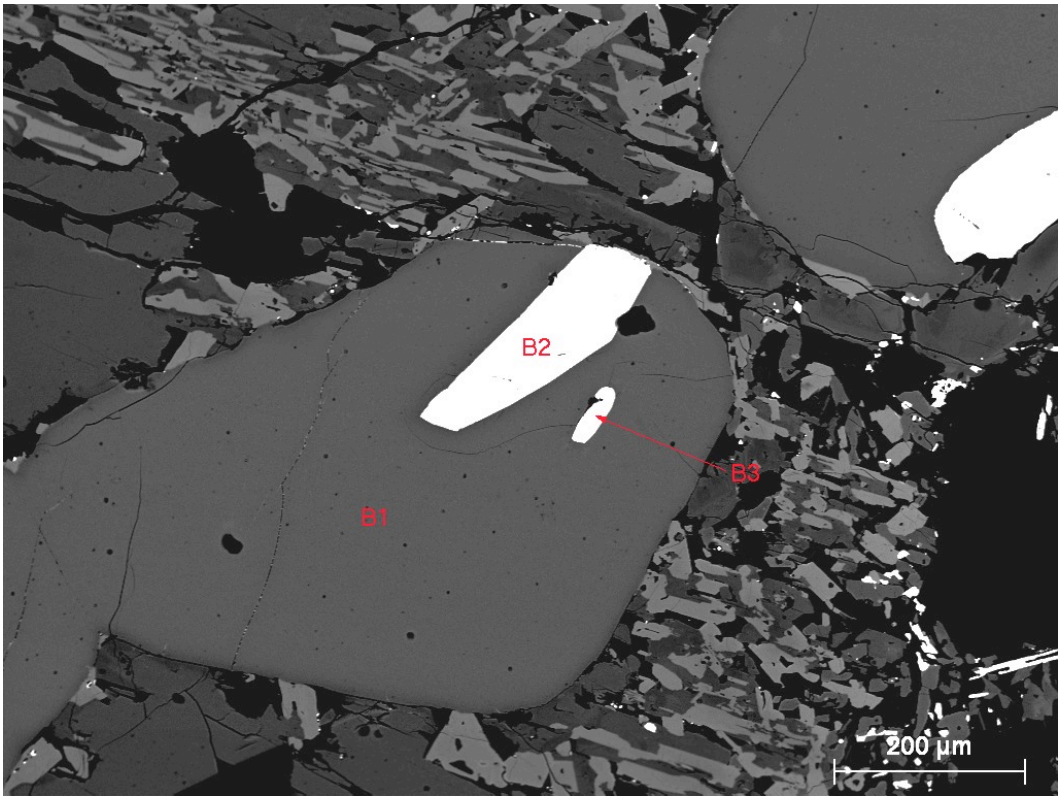


Figure 3.5: BSE image of Hercynite grain (B1) with inclusion of Ilmenite (B2) in sample EC-3

### 3.3 Mineral Chemistry

Norris (1996) initially analyzed the major mineral phases (olivine, pyroxene, amphibole, plagioclase, oxides) in many of the samples. Major mineral phases in several samples not studied by Norris as well as those major mineral phases left unanalyzed in the samples studied by Norris (1996) were further analyzed in this study. Additionally apatite was observed to be abundant in samples X-1 and F-2 and was analyzed for major elements as well as volatiles (F, Cl).

#### 3.3.1 Pyroxenes

All analyses are presented as oxide wt. % and cations were normalized to 6 oxygens (Table 3.1). As noted by Norris (1996), most pyroxenes are diopsides using the classification of Morimoto et al., (1988)(Figure 3.6). Sample EC-3 contains two clinopyroxenes one a diopside, the other is a Fe-rich augite. In backscatter electron images (BSE) it can be seen that the augite appears as small grains at the borders of larger diopside grains as well as in smaller grains in which lathes of augite and diopside alternate (Figure 3.7). Analyzed pyroxenes are Al-rich, Ti-rich , modestly rich in Na, with Mg#s (Mg/Mg+Fe in cation units) ranging from 47.9-62.6.

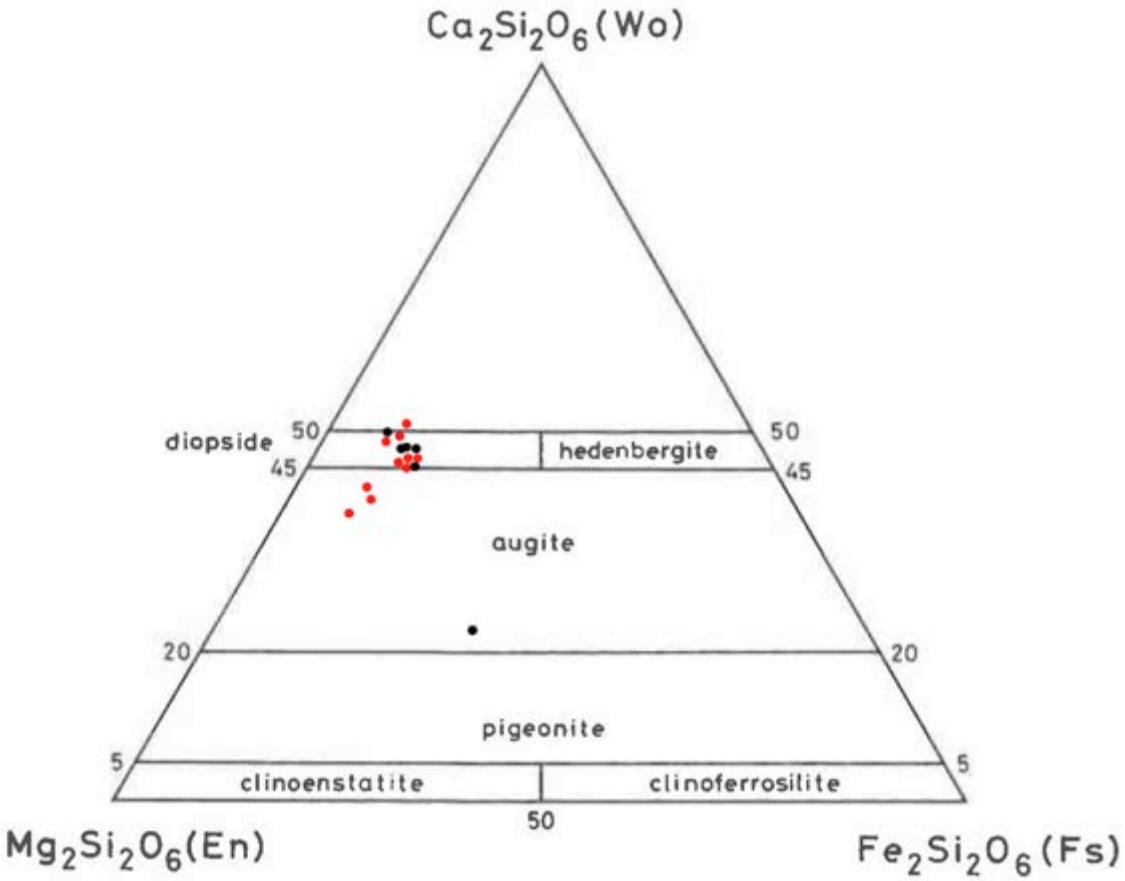


Figure 3.6: Representative pyroxene analyses plotted on the Wo-En-Fs triangle. Analyses from Norris (1996) in red. Figure after Morimoto (1988).

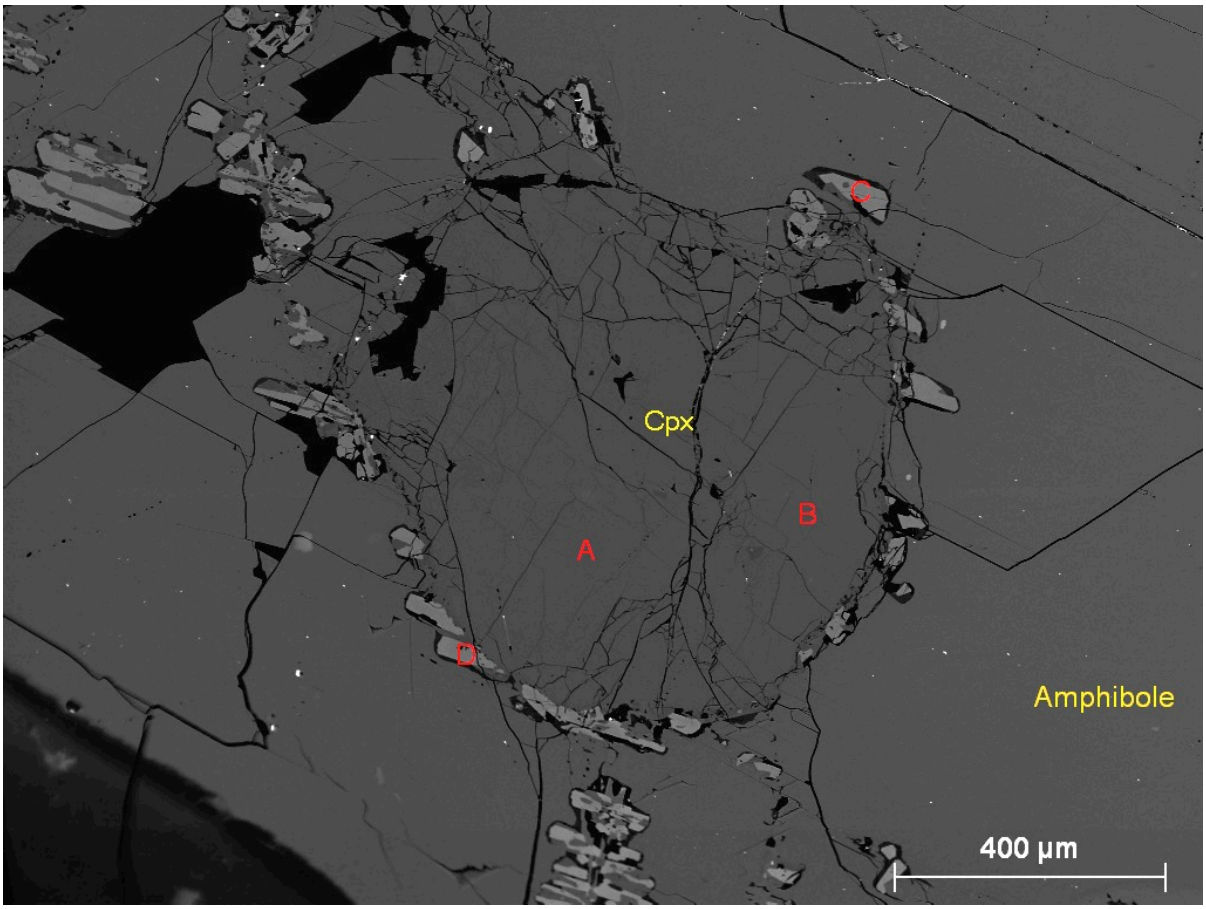


Figure 3.7: EC-3 Grain 1, BSE image. Points A&B are diopside, C&D are augite.

Table 3.1: Representative Analyses of Pyroxene

| Sample | AF-1 | AF-1 | AF-1 | AF-2 | AF-2 | AF-2 | AF-2 | AF-2 |
|---|---|---|---|---|---|---|---|---|
| Mineral | diopside | diopside | diopside | diopside | diopside | diopside | diopside | diopside |
| Grain | B | C | D | A | B | C | D | E |
| SiO2 | 45.72 | 45.03 | 46.09 | 44.71 | 45.64 | 47.05 | 46.28 | 44.80 |
| TiO2 | 2.43 | 1.91 | 2.27 | 2.36 | 2.19 | 1.92 | 2.57 | 2.66 |
| Al2O3 | 8.95 | 9.58 | 9.10 | 9.67 | 9.55 | 8.04 | 9.08 | 9.74 |
| FeO | 8.58 | 8.44 | 8.03 | 7.59 | 7.91 | 7.18 | 7.14 | 7.60 |
| MnO | 0.35 | 0.23 | 0.13 | 0.13 | 0.24 | 0.14 | 0.09 | 0.23 |
| MgO | 11.74 | 11.39 | 11.90 | 11.12 | 11.44 | 12.00 | 11.55 | 11.00 |
| CaO | 20.80 | 21.13 | 20.89 | 22.62 | 20.98 | 22.13 | 22.25 | 22.05 |
| Na2O | 0.75 | 0.79 | 0.90 | 0.69 | 1.16 | 0.72 | 0.72 | 0.82 |
| Cr2O3 | nd | nd | nd | nd | nd | nd | nd | nd |
| Total | 99.34 | 98.57 | 99.43 | 98.92 | 99.23 | 99.22 | 99.72 | 99.05 |
| cations normalized to 6 oxygens | | | | | | | | |
| Si | 1.726 | 1.714 | 1.732 | 1.697 | 1.722 | 1.768 | 1.732 | 1.697 |
| Ti | 0.069 | 0.055 | 0.064 | 0.067 | 0.062 | 0.054 | 0.072 | 0.076 |
| Al | 0.398 | 0.430 | 0.403 | 0.433 | 0.424 | 0.356 | 0.400 | 0.435 |
| Fe 2+ | 0.271 | 0.269 | 0.252 | 0.241 | 0.250 | 0.226 | 0.224 | 0.241 |
| Mn | 0.011 | 0.007 | 0.004 | 0.004 | 0.008 | 0.004 | 0.003 | 0.007 |
| Mg | 0.661 | 0.646 | 0.667 | 0.629 | 0.643 | 0.672 | 0.645 | 0.621 |
| Ca | 0.841 | 0.862 | 0.841 | 0.920 | 0.848 | 0.891 | 0.892 | 0.895 |
| Na | 0.055 | 0.058 | 0.066 | 0.051 | 0.085 | 0.053 | 0.053 | 0.060 |
| Cr | 0.001 | 0.002 | 0.004 | 0.001 | 0.004 | 0.001 | 0.001 | 0.004 |
| Cation Total | 4.033 | 4.044 | 4.033 | 4.044 | 4.045 | 4.026 | 4.021 | 4.037 |
| Mg# | 57.78 | 57.43 | 59.72 | 59.45 | 59.12 | 62.57 | 61.80 | 59.12 |
| Wo | 47.45 | 48.49 | 47.80 | 51.39 | 48.71 | 49.81 | 50.69 | 50.95 |
| En | 37.27 | 36.38 | 37.87 | 35.15 | 36.96 | 37.58 | 36.62 | 35.34 |
| Fs | 15.28 | 15.13 | 14.33 | 13.45 | 14.34 | 12.61 | 12.70 | 13.71 |

| Sample | X-6 | X-6 | EC-4 | EC-4 | EC-4 | EC-3 | EC-3 | EC-3 |
|---|---|---|---|---|---|---|---|---|
| Mineral | diopside | diopside | diopside | diopside | diopside | diopside | augite | diopside |
| Grain | B | C | A | B | C | 1A | 1C | 2B |
| SiO2 | 47.96 | 47.43 | 46.28 | 46.84 | 45.35 | 44.75 | 27.30 | 45.95 |
| TiO2 | 1.18 | 1.37 | 1.35 | 1.41 | 1.93 | 2.44 | 9.78 | 1.98 |
| Al2O3 | 7.75 | 8.15 | 8.74 | 8.73 | 9.14 | 9.54 | 16.09 | 9.41 |
| FeO | 8.55 | 8.85 | 8.85 | 8.32 | 8.79 | 7.12 | 17.55 | 8.53 |
| MnO | 0.24 | 0.13 | 0.21 | 0.16 | 0.14 | 0.09 | 0.14 | 0.14 |
| MgO | 12.79 | 12.38 | 11.41 | 11.50 | 11.54 | 11.99 | 16.25 | 12.18 |
| CaO | 19.99 | 20.31 | 20.88 | 20.95 | 20.82 | 21.96 | 11.23 | 20.86 |
| Na2O | 0.68 | 0.78 | 0.91 | 0.91 | 0.98 | 0.81 | 1.59 | 0.88 |
| Cr2O3 | nd | nd | nd | nd | nd | nd | nd | nd |
| Total | 99.15 | 99.39 | 98.66 | 98.82 | 98.69 | 98.63 | 99.96 | 100.03 |
| cations normalized to 6 oxygens | | | | | | | | |
| Si | 1.805 | 1.782 | 1.739 | 1.755 | 1.715 | 1.689 | 1.026 | 1.733 |
| Ti | 0.033 | 0.039 | 0.038 | 0.040 | 0.055 | 0.069 | 0.276 | 0.056 |
| Al | 0.344 | 0.361 | 0.387 | 0.386 | 0.408 | 0.424 | 0.713 | 0.418 |
| Fe 2+ | 0.269 | 0.278 | 0.278 | 0.261 | 0.278 | 0.225 | 0.552 | 0.269 |
| Mn | 0.008 | 0.004 | 0.007 | 0.005 | 0.005 | 0.003 | 0.005 | 0.005 |
| Mg | 0.718 | 0.694 | 0.639 | 0.642 | 0.651 | 0.675 | 0.911 | 0.685 |
| Ca | 0.807 | 0.818 | 0.841 | 0.841 | 0.844 | 0.888 | 0.452 | 0.843 |
| Na | 0.050 | 0.057 | 0.066 | 0.066 | 0.072 | 0.059 | 0.116 | 0.065 |
| Cr | 0.000 | 0.000 | 0.001 | 0.000 | 0.000 | 0.000 | 0.000 | 0.000 |
| Cation Total | 4.034 | 4.033 | 3.996 | 3.996 | 4.027 | 4.031 | 4.051 | 4.077 |
| Mg# | 59.930 | 58.332 | 56.321 | 58.000 | 56.760 | 62.752 | 48.084 | 58.810 |
| Wo | 44.963 | 45.702 | 47.812 | 48.221 | 47.609 | 49.689 | 23.627 | 46.906 |
| En | 40.024 | 38.763 | 36.365 | 36.820 | 36.704 | 37.742 | 47.562 | 38.116 |
| Fs | 15.014 | 15.534 | 15.823 | 14.959 | 15.687 | 12.569 | 28.811 | 14.977 |

### 3.3.2 Amphiboles

All amphibole analyses are presented on an oxide wt. % basis and cations were normalized to 23 O+OH basis. Cation sites were filled and classified using the methodology of Leake (1997). All observed amphiboles are classified as kaersutite (Ca ≥ 1.50, Na+K ≥ 0.50, Ti ≥ 0.5 based on 23 O+OH; Leake, 1997). These amphiboles are Al- and Ti-rich and have no detectable Cl or F with Mg#s between 50.9-53.3.

Table 3.2: Representative analyses of amphiboles

| Sample | AF-1 | AF-1 | AF-1 | AF-2 | AF-2 | AF-2 |
|---|---|---|---|---|---|---|
| Mineral | Kaersutite | Kaersutite | Kaersutite | Kaersutite | Kaersutite | Kaersutite |
| Grain | A | B | C | A | B | C |
| SiO2 | 39.92 | 38.18 | 39.49 | 39.98 | 38.95 | 39.99 |
| TiO2 | 4.53 | 4.50 | 5.49 | 4.82 | 5.73 | 5.16 |
| Al2O3 | 14.23 | 14.48 | 14.27 | 14.50 | 14.60 | 14.23 |
| FeO | 11.71 | 11.48 | 11.33 | 11.63 | 11.06 | 10.70 |
| MnO | nd | 0.17 | nd | nd | nd | nd |
| MgO | 12.13 | 12.37 | 11.95 | 12.46 | 12.37 | 12.19 |
| CaO | 11.52 | 11.71 | 11.78 | 11.76 | 11.57 | 11.94 |
| Na2O | 2.32 | 2.37 | 2.45 | 2.70 | 2.50 | 2.41 |
| K2O | 1.14 | 0.89 | 0.98 | 1.14 | 0.90 | 0.97 |
| Cl | nd | nd | nd | nd | nd | nd |
| F | nd | nd | nd | nd | nd | nd |
| Total | 97.51 | 96.14 | 97.72 | 98.99 | 97.68 | 97.58 |
| cations normalized to 23 O+OH equivalents | | | | | | |
| Si | 5.920 | 5.765 | 5.846 | 5.853 | 5.760 | 5.902 |
| Ti | 0.505 | 0.511 | 0.611 | 0.531 | 0.637 | 0.573 |
| Al | 2.488 | 2.578 | 2.490 | 2.502 | 2.545 | 2.475 |
| Fe | 1.452 | 1.449 | 1.402 | 1.424 | 1.369 | 1.320 |
| Mn | 0.012 | 0.021 | 0.000 | 0.002 | 0.013 | 0.010 |
| Mg | 2.681 | 2.784 | 2.636 | 2.719 | 2.728 | 2.683 |
| Ca | 1.830 | 1.894 | 1.868 | 1.845 | 1.834 | 1.888 |
| Na | 0.668 | 0.693 | 0.703 | 0.767 | 0.717 | 0.690 |
| K | 0.216 | 0.171 | 0.185 | 0.213 | 0.170 | 0.184 |
| Total | 15.773 | 15.867 | 15.742 | 15.855 | 15.773 | 15.725 |
| Mg# | 50.88 | 51.87 | 51.33 | 51.72 | 52.79 | 53.27 |

### 3.3.3 Olivine

All olivine analyses are presented on an oxide wt. % basis and cations are normalized to 4 oxygens. Olivines are Ni-poor and are relatively rich in Fe with Mg#s between 54.9-60.2. An exemplar olivine grain from sample X-1 is shown in Figure 3.8.

Table 3.3: Representative analyses of olivine

| Sample | EC-3 | EC-3 | X-1 | X-1 | S-1 | S-1 |
|---|---|---|---|---|---|---|
| Grain | A | B | A | B | A | B |
| SiO2 | 36.18 | 35.48 | 35.48 | 36.76 | 34.87 | 35.64 |
| FeO | 27.97 | 27.16 | 25.69 | 25.35 | 25.58 | 28.53 |
| MnO | 0.45 | 0.26 | 0.20 | 0.32 | 0.31 | 0.32 |
| MgO | 34.71 | 35.75 | 37.26 | 37.03 | 38.02 | 35.70 |
| CaO | nd | 0.07 | 0.12 | 0.10 | 0.10 | nd |
| NiO | nd | 0.11 | nd | 0.14 | nd | nd |
| Total | 99.32 | 98.82 | 98.75 | 99.56 | 98.87 | 100.18 |
| Cations normalized to 4 oxygens | | | | | | |
| Si | 0.979 | 0.964 | 0.957 | 0.978 | 0.941 | 0.959 |
| Fe 2+ | 0.633 | 0.617 | 0.580 | 0.564 | 0.577 | 0.642 |
| Mn | 0.010 | 0.006 | 0.005 | 0.007 | 0.007 | 0.007 |
| Mg | 1.400 | 1.448 | 1.498 | 1.468 | 1.530 | 1.432 |
| Ca | 0.000 | 0.002 | 0.003 | 0.003 | 0.003 | 0.000 |
| Ni | 0.000 | 0.002 | 0.000 | 0.003 | 0.000 | 0.000 |
| Total | 3.021 | 3.038 | 3.043 | 3.022 | 3.058 | 3.040 |
| Mg# | 55.37 | 56.83 | 59.19 | 59.36 | 59.78 | 55.58 |

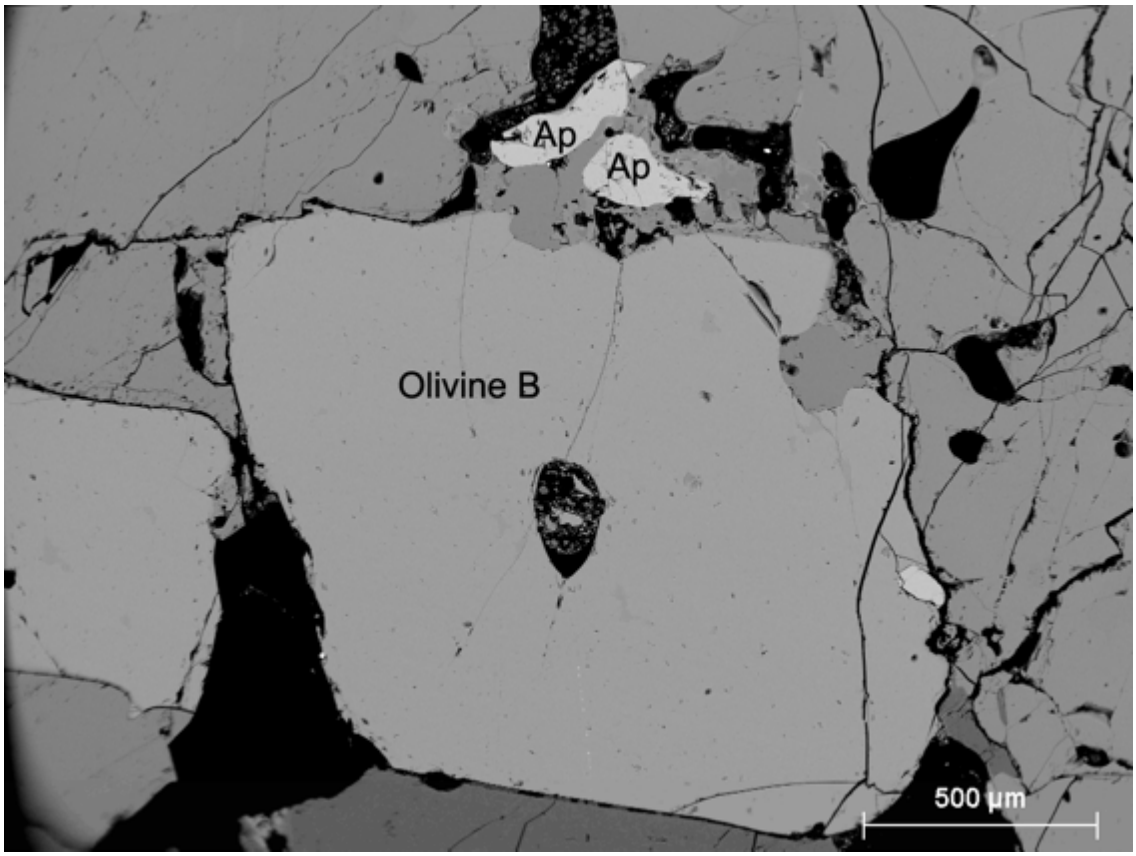


Figure 3.8: Olivine grain B from sample X-1. Also note the apatites (Ap) grains AA & BB. Detailed view in Figure 3.2.

### 3.3.4 Oxides

All oxide analyses are presented as oxide wt. %. Cations were normalized to 4 oxygens for spinels and to 3 oxygens for ilmenite. Fe 3+ was calculated from charge balance. In sample S-1 blebs of magnetite occur in a host hercynite-spinel ("pleonaste") grain consistent with exsolution of magnetite from hercynite (Turnock and Eugster, 1962; Smith and Roden, 1981).

Table 3.4: Representative analyses of oxides

| Sample | EC-3 | EC-3 | EC-3 | EC-3 | S-1 | S-1 |
|---|---|---|---|---|---|---|
| Mineral | Pleonaste | Illmenite | Pleonaste | Illmenite | Pleonaste | Magnetite |
| Grain | A1 | A2 | B1 | B2 | A1 | A2 |
| TiO2 | 0.40 | 53.33 | 0.50 | 53.37 | 0.44 | 0.06 |
| Al2O3 | 60.94 | 0.41 | 56.26 | 0.10 | 60.95 | 1.08 |
| MnO | 0.20 | 0.41 | 0.21 | 0.40 | 0.08 | 0.06 |
| MgO | 16.58 | 8.42 | 14.25 | 8.43 | 13.53 | 0.14 |
| Cr2O3 | 0.21 | nd | 0.14 | nd | 0.34 | nd |
| FeO | 16.99 | 32.60 | 19.25 | 32.60 | 20.74 | 29.28 |
| Fe2O3 | 6.30 | 4.80 | 8.86 | 4.90 | 1.97 | 57.65 |
| Total | 101.62 | 99.96 | 99.46 | 99.80 | 98.05 | 88.27 |
| cations norm to 4 oxygen equivalents for spinel, 3 for illmenite | | | | | | |
| Ti | 0.008 | 0.965 | 0.010 | 0.969 | 0.009 | 0.002 |
| Al | 1.885 | 0.012 | 1.835 | 0.003 | 1.941 | 0.055 |
| Fe 2+ | 0.373 | 0.647 | 0.445 | 0.649 | 0.469 | 1.064 |
| Fe 3+ | 0.124 | 0.078 | 0.184 | 0.087 | 0.040 | 1.885 |
| Mn | 0.004 | 0.008 | 0.005 | 0.008 | 0.002 | 0.002 |
| Mg | 0.648 | 0.302 | 0.588 | 0.303 | 0.545 | 0.009 |
| Ca | 0.000 | 0.000 | 0.000 | 0.000 | 0.001 | 0.000 |
| Cr | 0.004 | 0.000 | 0.003 | 0.000 | 0.007 | 0.000 |
| Sum Cations | 3.047 | 2.012 | 3.071 | 2.019 | 3.014 | 3.018 |

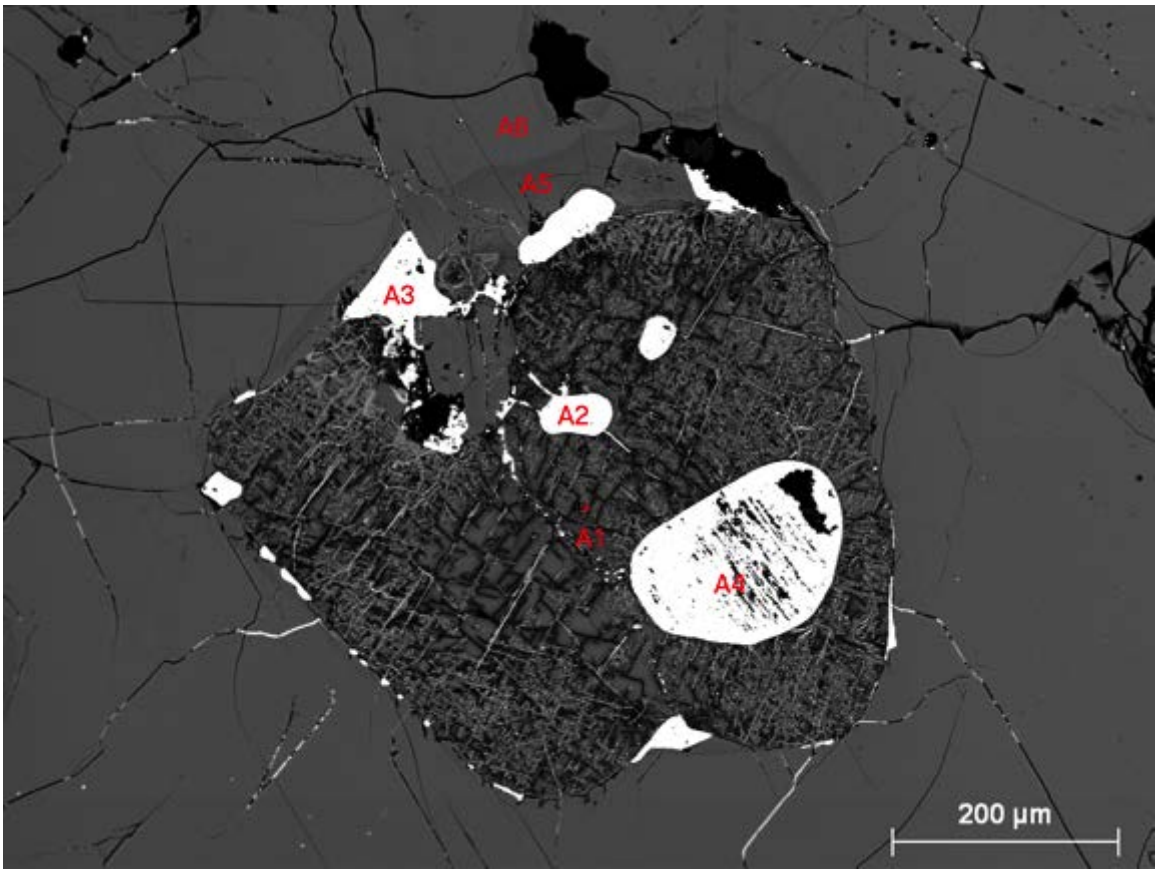


Figure 3.9: Oxide from Sample S-1 showing spinel exsolution. The larger grain (A1) is hercynite, the brighter areas (A2, A3, A4) are magnetite.

### 3.3.5 Apatite

Representative apatite analyses from two xenoliths X-1 and F-2 (Figures 3.2 & 3.4), are presented in Table 3.4, and atomic proportions of F-Cl-OH are plotted in figure 3.10 along with those of apatite analyses from O'Reilly & Griffin (2000) who reported analyses from Group I (Type A apatites) and Group II (Type B apatites) xenoliths. Multiple analyses were performed on each grain and unsatisfactory analyses subsequently culled using the criteria outlined in Patiño-Douce et al. (2011). Stoichiometric OH was calculated by difference. My analyses for F-2 overlap well with those from the same sample published by Patiño-Douce et al. (2011) as well as those categorized as Apatite B by O'Reilly & Griffin (2000). The apatites from X-1 plot as more OH- and Cl-rich than those of F-2. Sr values in apatites from both X-1 and F-2 are comparable to each other and fall within the range for Apatite B of O'Reilly and Griffin (2000). Ce and Y values in both X-1 and F-2 apatites were mostly below detection limits.

Table 3.5: Representative analyses of apatite

| Sample | X-1 | X-1 | X-1 | X-1 | X-1 | F-2 | F-2 | F-2 | F-2 | F-2 | F-2 |
|---|---|---|---|---|---|---|---|---|---|---|---|
| Grain | AA1 | BB1 | BB2 | BB3 | A1 | A2 | A3 | B1 | B2 | C1 | C1 |
| FeO | 0.93 | 0.51 | 0.73 | 0.40 | 0.60 | 1.28 | 3.60 | 0.31 | 0.50 | 0.57 | 1.02 |
| MgO | 0.58 | 0.54 | 0.55 | 0.50 | 0.37 | 0.61 | 0.78 | 0.31 | 0.33 | 0.40 | 0.56 |
| CaO | 55.01 | 54.12 | 54.32 | 54.25 | 54.45 | 53.60 | 51.58 | 53.90 | 53.92 | 55.15 | 55.23 |
| Na2O | 0.19 | 0.21 | 0.23 | 0.23 | 0.12 | 0.12 | nd | nd | 0.12 | 0.31 | 0.22 |
| P2O5 | 41.90 | 41.35 | 41.14 | 41.81 | 42.21 | 40.53 | 41.08 | 42.00 | 42.66 | 42.41 | 42.28 |
| SO3 | nd | nd | nd | 0.05 | 0.10 | 0.09 | 0.14 | nd | nd | nd | nd |
| SrO | 0.19 | 0.18 | 0.14 | 0.21 | 0.23 | 0.24 | 0.27 | nd | 0.11 | 0.15 | 0.15 |
| Ce2O3 | nd | nd | nd | nd | nd | nd | nd | nd | nd | nd | nd |
| Y2O3 | nd | nd | nd | nd | nd | 0.25 | nd | 0.21 | nd | nd | nd |
| F | 0.61 | 0.35 | 0.35 | 0.61 | nd | 2.68 | 2.14 | 1.24 | 1.28 | 1.26 | 1.43 |
| Cl | 0.91 | 0.95 | 0.95 | 0.97 | 1.00 | 0.55 | 0.32 | 0.49 | 0.47 | 0.45 | 0.55 |
| Total | 100.38 | 98.70 | 98.68 | 99.18 | 99.65 | 99.95 | 100.14 | 99.10 | 99.38 | 100.91 | 101.52 |
| O=F, CL | -0.46 | -0.36 | -0.36 | -0.48 | -0.24 | -1.25 | -0.97 | -0.64 | -0.64 | -0.63 | -0.73 |
| total | 99.91 | 98.34 | 98.31 | 98.70 | 99.41 | 98.70 | 99.17 | 98.46 | 98.74 | 100.28 | 100.79 |
| cations norm to 25 oxygen equivalents | | | | | | | | | | | |
| Fe | 0.130 | 0.073 | 0.104 | 0.057 | 0.084 | 0.184 | 0.512 | 0.044 | 0.070 | 0.079 | 0.142 |
| Mg | 0.143 | 0.136 | 0.139 | 0.126 | 0.093 | 0.155 | 0.197 | 0.079 | 0.081 | 0.099 | 0.139 |
| Ca | 9.850 | 9.842 | 9.884 | 9.801 | 9.754 | 9.844 | 9.395 | 9.760 | 9.683 | 9.821 | 9.817 |
| Na | 0.062 | 0.069 | 0.075 | 0.074 | 0.040 | 0.041 | 0.023 | 0.018 | 0.038 | 0.100 | 0.071 |
| P | 5.928 | 5.941 | 5.914 | 5.969 | 5.976 | 5.882 | 5.913 | 6.009 | 6.053 | 5.966 | 5.937 |
| S | 0.000 | 0.000 | 0.003 | 0.006 | 0.013 | 0.011 | 0.018 | 0.002 | 0.002 | 0.000 | 0.000 |
| Sr | 0.018 | 0.018 | 0.014 | 0.021 | 0.022 | 0.024 | 0.026 | 0.002 | 0.011 | 0.014 | 0.015 |
| Ce | 0.000 | 0.029 | 0.007 | 0.000 | 0.032 | 0.000 | 0.000 | 0.032 | 0.000 | 0.011 | 0.000 |
| Y | 0.006 | 0.000 | 0.011 | 0.014 | 0.000 | 0.022 | 0.016 | 0.019 | 0.000 | 0.003 | 0.006 |
| F | 0.325 | 0.190 | 0.190 | 0.326 | 0.020 | 1.451 | 1.149 | 0.665 | 0.678 | 0.660 | 0.748 |
| Cl | 0.257 | 0.274 | 0.274 | 0.277 | 0.283 | 0.160 | 0.092 | 0.142 | 0.133 | 0.127 | 0.155 |
| OH | 1.419 | 1.536 | 1.536 | 1.397 | 1.698 | 0.389 | 0.759 | 1.193 | 1.189 | 1.213 | 1.096 |
| Sum cations | 16.14 | 16.11 | 16.15 | 16.07 | 16.02 | 16.16 | 16.10 | 15.97 | 15.94 | 16.09 | 16.13 |

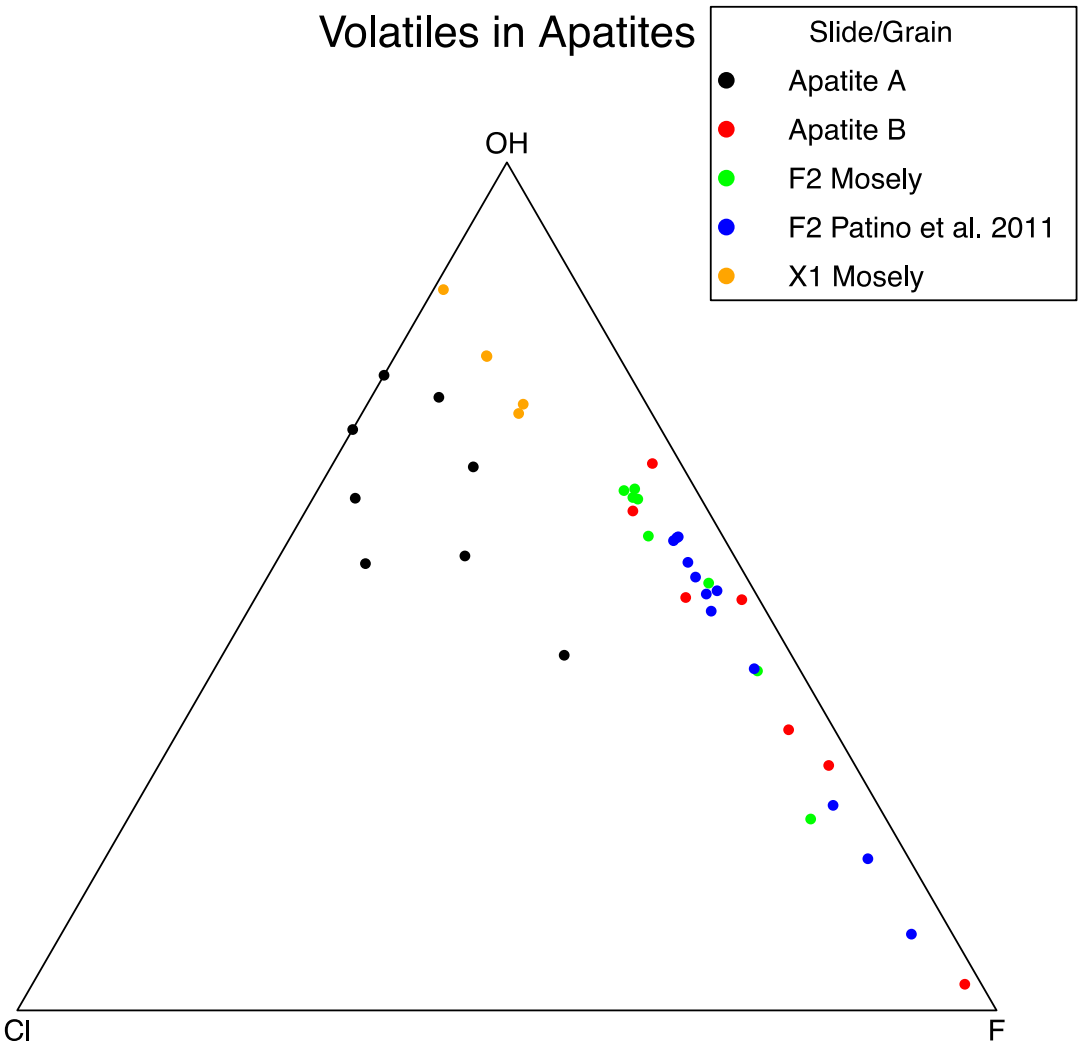


Figure 3.10: Chlorine, F and OH (calculated) in analyzed apatites compared to type A & B apatites from O'Reilly & Griffin (2000)

# 4.0 DISCUSSION

## 4.1 Nature of LCVF Group II Xenoliths

This thesis focuses on those xenoliths from Easy Chair Crater that are pyroxene- or amphibole-dominated and as such can be classified as Group II xenoliths, using the nomenclature of Frey and Prinz (1978) or Al-augite xenoliths using that of Wilshire and Shervais (1975). For the purposes of this thesis, I will use the nomenclature of Frey and Prinz (1978) who describe Group II xenoliths as a clinopyroxene-dominated assemblage of Al-rich, Ti-rich clinopyroxene, olivine, kaersutite (Ti-rich amphibole), and spinel +/- orthopyroxene, magnetite, plagioclase, illmenite, and apatite. These xenoliths commonly, but not always, exhibit poikilitic, cumulate textures. Similarly, Wilshire and Shervais (1975) define Al-Augite xenoliths as characterized by Al-, Ti-rich augite, comparatively Fe-rich olivine and orthopyroxene, and Al-rich spinel. Clinopyroxenes analyzed in this thesis are compared to clinopyroxenes of the Group I and Group II xenoliths from San Carlos, AZ in figure 4.0 (Frey and Prinz, 1978). The Lunar Crater clinopyroxenes, while predominantly classified as diopside due to high Ca and Mg content, have the high Al contents that are typical of Group II, Al-augite xenoliths; moreover their $TiO_2$ contents (1.18-2.66 wt. %) are similar to the range in $TiO_2$ content (0.89-1.68 wt. %) of clinopyroxene in the San Carlos Group II xenoliths. Lunar Crater xenolith amphiboles are kaersutite as is typical of Group II xenoliths. Additionally, spinels are Fe-rich and Cr-poor. Mineralogy and texture in Easy Chair pyroxenite/amphibolite xenoliths are nearly identical to those described for Group II xenoliths in Frey and Prinz (1978). Easy Chair Group II xenoliths

differ from those described by Frey and Prinz in modal abundances: Easy Chair Group II xenoliths have more amphibole, indicating an origin from a relatively hydrous melt (Figure 4.1). Group II xenoliths in general are thought to be derived from near the crust-mantle interface as high-pressure crystal accumulations from an alkali basaltic melt (Menzies et al. 1987). For Lunar Crater group II xenoliths in particular, isotopic constraints indicate a source similar to the host alkaline magmatism (Menzies et al. 1987).

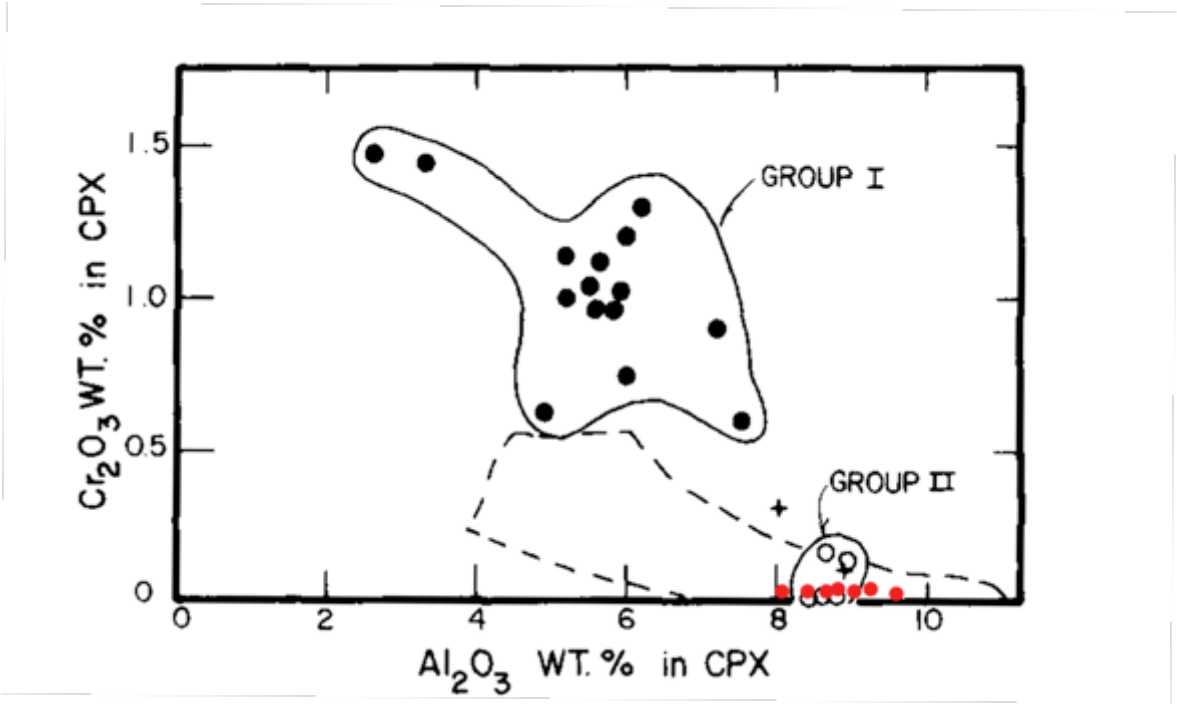


Figure 4.0: $Cr_2O_3$ vs. $Al_2O_3$ in clinopyroxene. Representative pyroxenes (red circles) from Easy Chair Crater xenoliths plotted on a figure from Frey and Prinz (1978). Dashed field encloses Group II xenoliths from Eifel, Germany (Aoki and Kushiro, 1968).

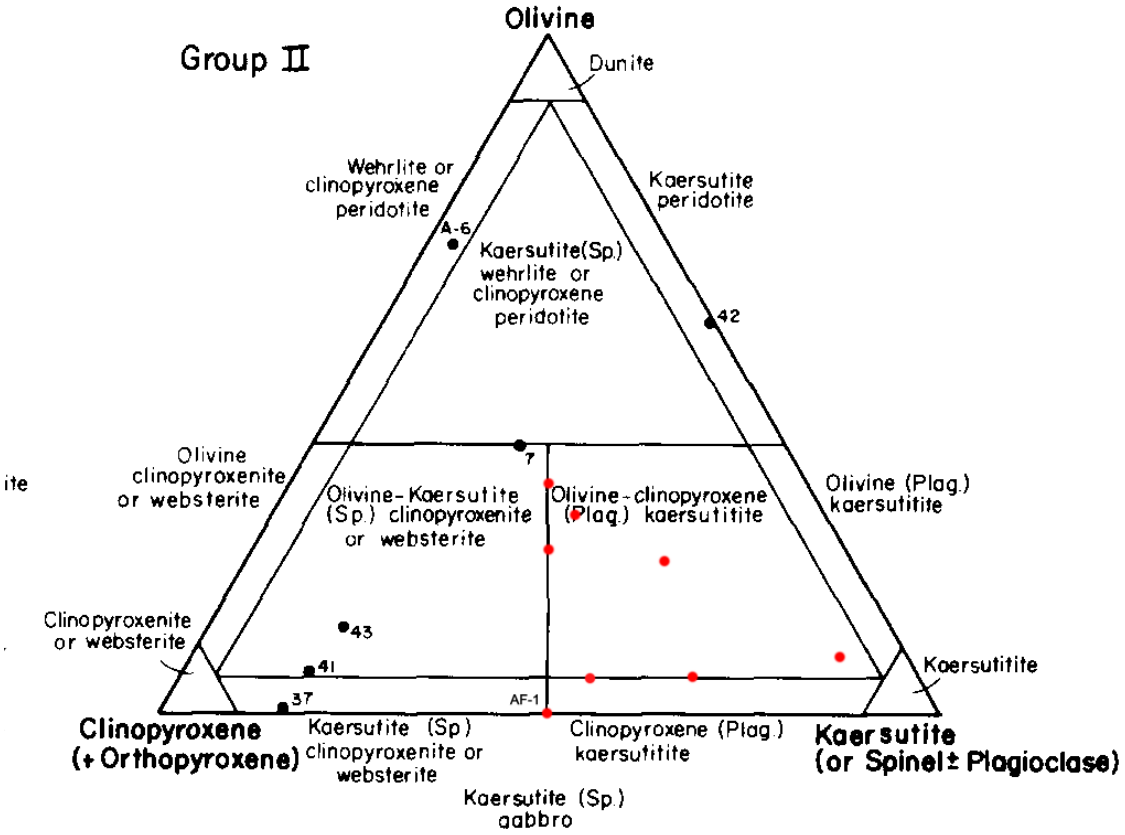


Figure 4.1: Modal composition of Easy Chair Crater Group II xenoliths from this thesis (in red) compared to samples from Frey and Prinz (1978). Diagram from Frey and Prinz (1978)

Wilshire and Shervais (1975) suggest that not all Group II xenoliths should be considered cumulate in origin, especially olivine-rich examples, because they can lack obvious cumulate textures. However, for the xenoliths analyzed in this study, the poikilitic nature of the interstitial kaersutite (Wager et al., 1960), and the widely varying modal proportions implies that these Group II xenoliths are cumulates and the kaersutite represents the intercumulate melt present during the last stages of crystallization (Frey and Prinz, 1978). If so, the relatively high modal abundance of this interstitial high-Ti amphibole suggests that the melt responsible was high in water, alkalis, and Ti. Bergman et al. (1981) examined a Group II Lunar Crater wherlite cut by a

vein of kaersutite. Bergman (1981) thought that the kaersutite vein was from a relatively primitive melt emplaced in a wherlite that formed from crystallization of a more differentiated magma. This magma that is similar to the melt proposed by Bergman (1981) is slightly more evolved as shown by the lower Mg# of the kaersutite from the xenoliths analyzed for this thesis (Figure 4.2).

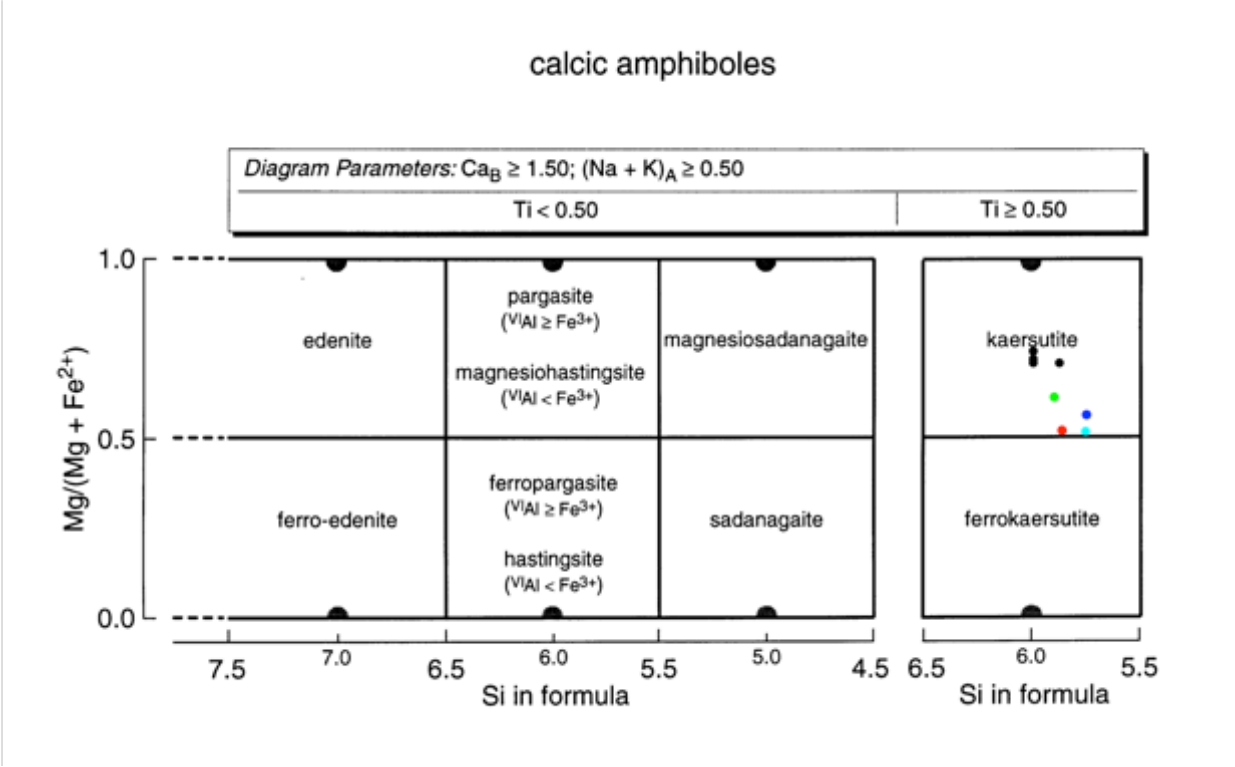


Figure 4.2: Comparison of Easy Chair amphiboles in Group II xenoliths from this thesis to those of Bergman (1981). Bergman analyses in black. Shown are amphiboles from AF-1 (red symbol), S-1 (blue symbol), X-1 (green symbol) and F-2 (cyan). Figure from Leake et al. (1997)

**4.2 Geothermometry**

The Group II xenoliths in this thesis are comprised primarily of olivine, clinopyroxene, amphibole, and spinel. Orthopyroxene was observed as exsolution lamellae within some analyzed clinopyroxenes, but at a scale that precluded accurate microprobe analysis. Because of this lack of coarse orthopyroxene, geothermometers that rely on orthopyroxene/clinopyroxene phase relations were not applicable. The QUILF equilibria program of Andersen et al. (1993) was utilized because it includes thermodynamic models for olivine, clinopyroxene, and spinel, as well as orthopyroxene. The amphibole present in the samples was not considered in these models. For the assemblages present in the analyzed samples the QUILF program utilized the following equilibria:

<u>Olivine - Pyroxene</u>

$Mg_2SiO_4 + (cpx)Fe_2Si_2O_6 = Fe_2SIO_4 + (cpx)Mg_2Si_2O_6$

$Fe_2SiO_4 + (cpx)CaFeSi_2O_6 = CaFeSiO_4 + (cpx)Fe_2Si_2O_6$

$Mg_2SIO_4 + CaMgSi_2O_6 = CaMgSIO_4 + (cpx)Mg_2Si_2O_6$

$Mg_2Si0_4 + (cpx)Fe_2Si_2O_6 = Fe_2SiO_4 + (cpx)Mg_2Si_2O_6$

<u>Silicate – Oxide</u>

$Fe_2SiO_4 + 2MgFe_2O_4 = Mg_2SiO_4 + 2Fe_3O_4$

$Fe_2Si_2O_6 + 2MgFe_2O_4 = Mg_2Si_2O_6 + 2Fe_3O_4$

$Fe_2Si_2O_6 + 2MgFe_2O_4 = Mg_2Si_2O_6 + 2Fe_3O_4$

$Fe_2SiO_4 + 2MgTiO_3 = Mg_2Si0_4 + 2FeTiO_3$

$Fe_2Si_2O_6 + 2MgTi0_3 = Mg_2Si_2O_6 + 2FeTiO_3$

Two Oxide

$Fe_3O_4 + FeTiO_3 = Fe_2TiO_4 + Fe_2O_3$

Observed olivine, clinopyroxene, spinel and in one case illmenite compositions from group II xenoliths taken from Norris (1996) and from analyses in this thesis were entered into the QUILF program. Resulting temperatures were calculated for a range of assumed pressures: 1kbar, 5kbar, 10kbar, and 15kbar because the mineral assemblages do not uniquely constrain pressure (Table 3.5). These pressures can be converted to depths by assuming average density of continental crust as 2850 kg/$m^3$ (Christensen and Mooney, 1995) and utilizing the equation $P= g*\rho*h$, where g is gravitational acceleration, $\rho$ is crustal density, and h is depth. Uncertainty reported by the QUILF program for each temperature increased as pressure increased. Most xenoliths exhibit a positive correlation between depth and calculated temperature except samples S-1 and EC-3 (Figure 4.3). Temperatures estimated by QUILF equilibria of the LCVF Group II xenoliths tend to be in excess of 800° C. The significance of the high temperatures estimated from the QUILF equilibria is uncertain. Group I xenoliths from LCVF yield even higher calculated temperatures (Roden & Shimizu, 1993; Smith 2000). However, composite spinel grains in Group II xenolith S-1, a sample with a pleonaste/magnetite exsolution pair, have compositions consistent with exsolution at low temperatures. Exsolution of an aluminous spinel and magnetite is known to occur at low temperatures from the work of Turnock and Eugster (1962) and was observed in a relatively Fe-rich xenolith from the Navajo Volcanic Field (Smith and Roden, 1981). The exsolution provides an independent constraint on temperatures of equilibration, and points to a low temperature of equilibration (≈500$^oC$, Fig. 4.4). This

temperature possibly represents the final equilibration temperature of the xenolith prior to incorporation in the host basalt.

Table 4.0: QUILF temperatures at various depths

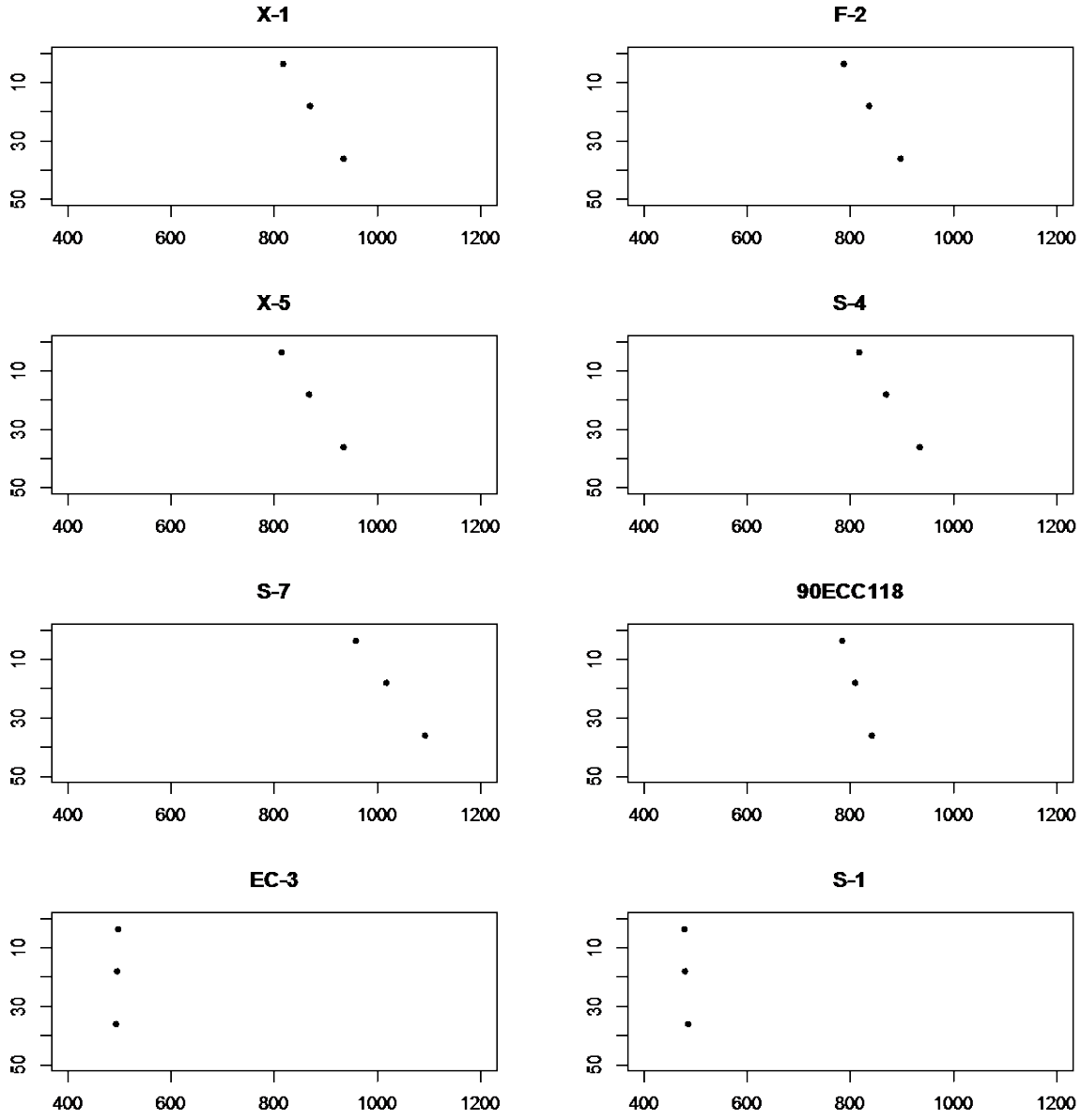


Figure 4.3: Calculated QUILF temperatures, depth (km) vs. temperature(°C), at 3.6, 18, and 36 km.

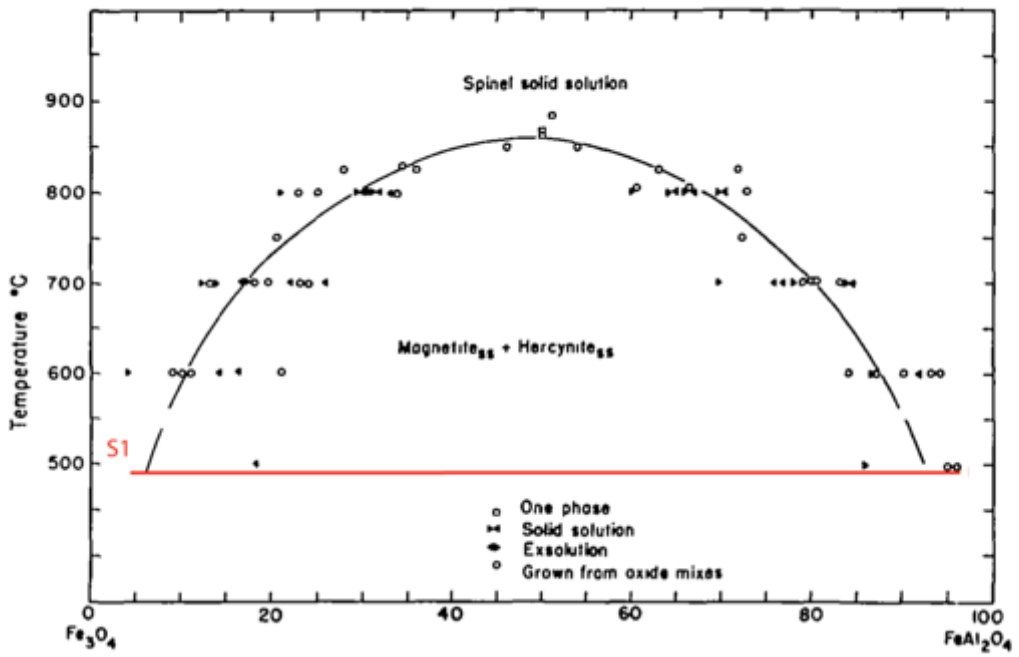


Figure 4.4: Exsolution of spinel pair in sample S-1. Figure modified from Turnock and Eugster (1962)

EC-3 is a sample that contained illmenite and pleonaste and the QUILF algorithm also yields a relatively low temperature (≈500°C) for all depths. The equilibria magnetite + ilmenite = ulvospinel + hematite utilized by QUILF is based on the work of Buddington and Lindsley (1964). The compositions of these phases when in equilibrium are dependent on oxygen fugacity and temperature; for this equilibrium, experimental data shows that for a given temperature an increase in the oxygen fugacity results in a decrease in the amount of $TiO_2$ in the magnetite and an increase in amount of $Fe_2O_3$ of the ilmenite (Buddington and Lindsley 1964). The Ilmenite in sample EC-3 is very near end-member Ilmenite (96 mole%) and the co-existing pleonaste is very low in $TiO_2$ (2 mole% ulvospinel). At these near endmember compositions, the geothermometer is nearly independent of oxygen fugacity.

Because the calculated temperatures of sample EC-3 and S-1 are independent of assumed pressure an absolute depth can be inferred from published geotherms for the area provided that such a steady state geotherm is applicable to the Lunar Crater area. Plotting sample EC-3 and S-1 on the average Basin and Range extensional geotherm of Lachenbruch and Sass (1978) gives a depth of 15km. The remainder of the samples plotted far to the right of the geotherm (at much higher temperatures) indicating that if 15km is a valid depth of equilibration for the bulk of observed samples then the geotherm for Lunar Crater is much higher or was perturbed perhaps due to magmatism (Figure 4.5). Alternatively, the relatively high temperatures may be closing temperatures reflecting ending of chemical communication between minerals as temperature fell. In this case only those assemblages with ilmenite or titanium poor spinel (i.e. EC-3, S-1) are capable of recording the lowest and presumably final temperatures of equilibrium. For comparison, assuming that the calculated equilibria temperatures record ambient temperatures in the lower crust/upper mantle just before the xenolith was incorporated in the host basaltic magma, the samples are plotted along the geotherm in Figure 4.6. If this assumption is valid, then the xenoliths were derived over a range of depths from ≈15 km to ≈45 km

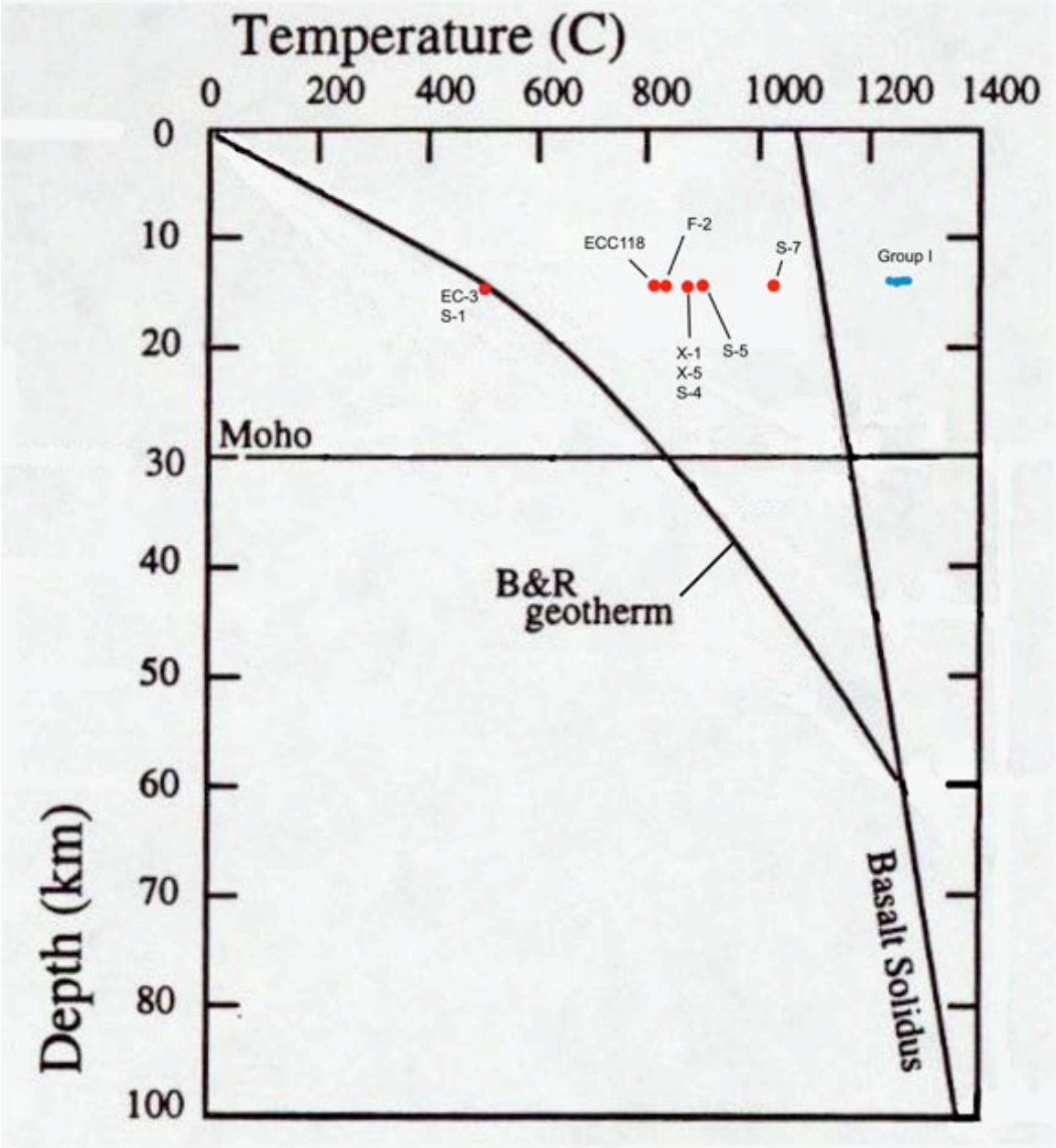


Figure 4.5: Calculated QUILF temperatures of LCVF Group II xenoliths plotted along with representative Group I xenolith LCVF temperatures (Roden & Shimizu, 1983) Geotherm of Lachenbruch and Sass (1978). Figure adapted from Saltus and Thompson (1995).

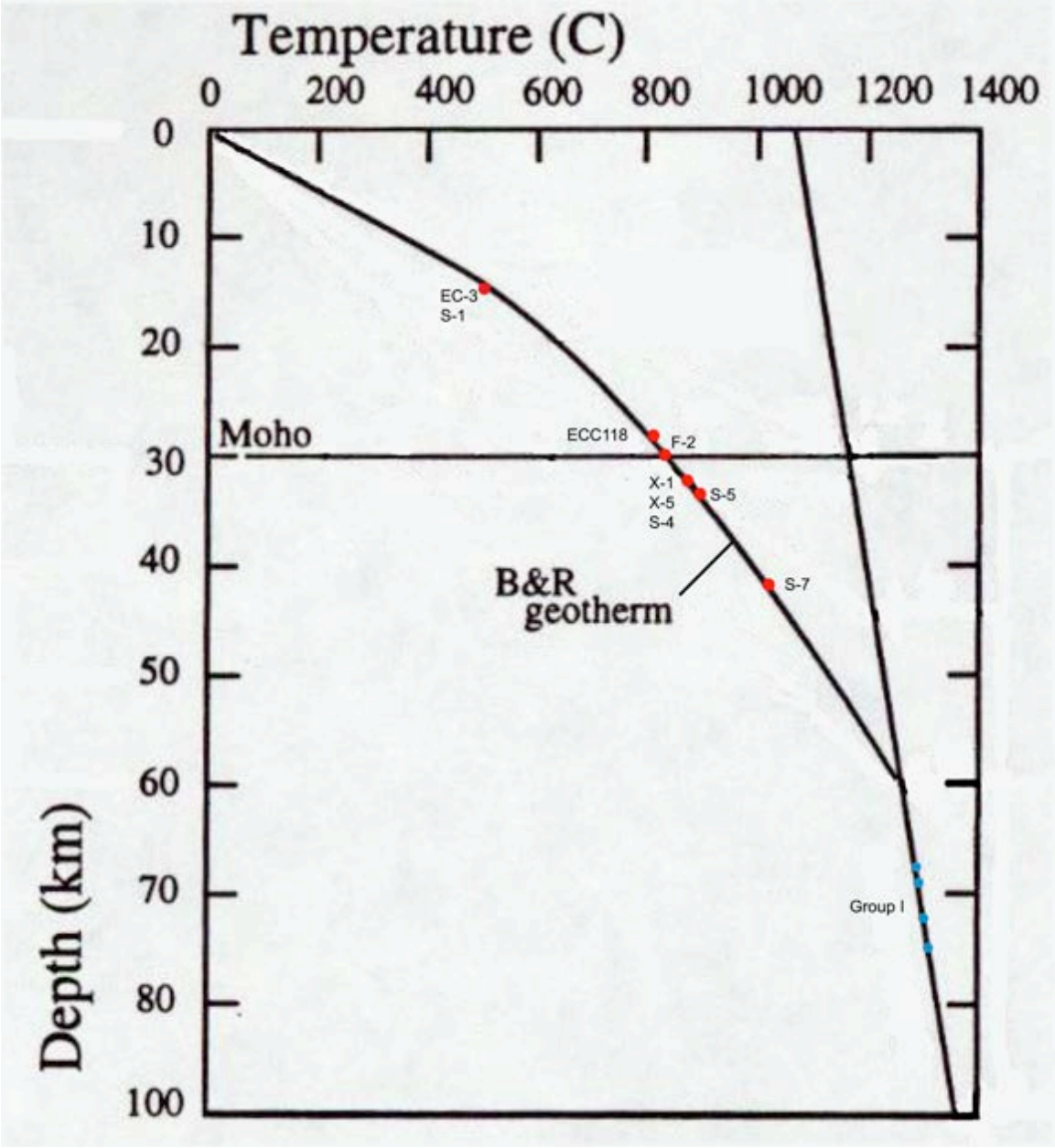


Figure 4.6: Calculated QUILF temperatures of LCVF Group II xenoliths plotted along with representative Group I xenolith LCVF temperatures (Roden & Shimizu, 1983) plotted along basin and range geotherm of Lachenbruch and Sass (1978). Figure adapted from Saltus and Thompson (1995).

### 4.3 Significance of Apatite

Apatite textures can give insight into magmatic conditions. Stubby (roughly equant in dimension) apatite generally forms in a fluid saturated melt, and acicular apatite generally precipitates from a fluid or melt during quenching (Wyllie et al. 1962). Apatites in both samples X-1 and F-2 are comparatively stubby (Figures 3.2 & 3.4), are not acicular, and as such are consistent with crystallization from a fluid-saturated magma and not precipitation from a supercritical fluid.

The apatites in xenoliths X-1 and F-2 are very different from each other in terms of volatile composition. Apatites analyzed in xenolith X-1 are OH-dominated (OH>F+CL) with relatively high Cl/F (Figure 3.9). The apatite in X-1 is unusually Cl-rich for apatite from a Group II xenolith, and is somewhat similar to apatite A (metasomatic) of O'Reilly and Griffin (2000) in its Cl and OH content. Type A apatite is usually associated with Group I xenoliths. In contrast, apatites in xenolith F-2 plot along the F-OH join with highly variable F/OH, but little Cl. The apatite in both X-1 and F-2 have similar Sr concentrations and Sr/FeO ratios to Apatite B (magmatic) of O'Reilly and Griffin (2000; Figure 4.7).

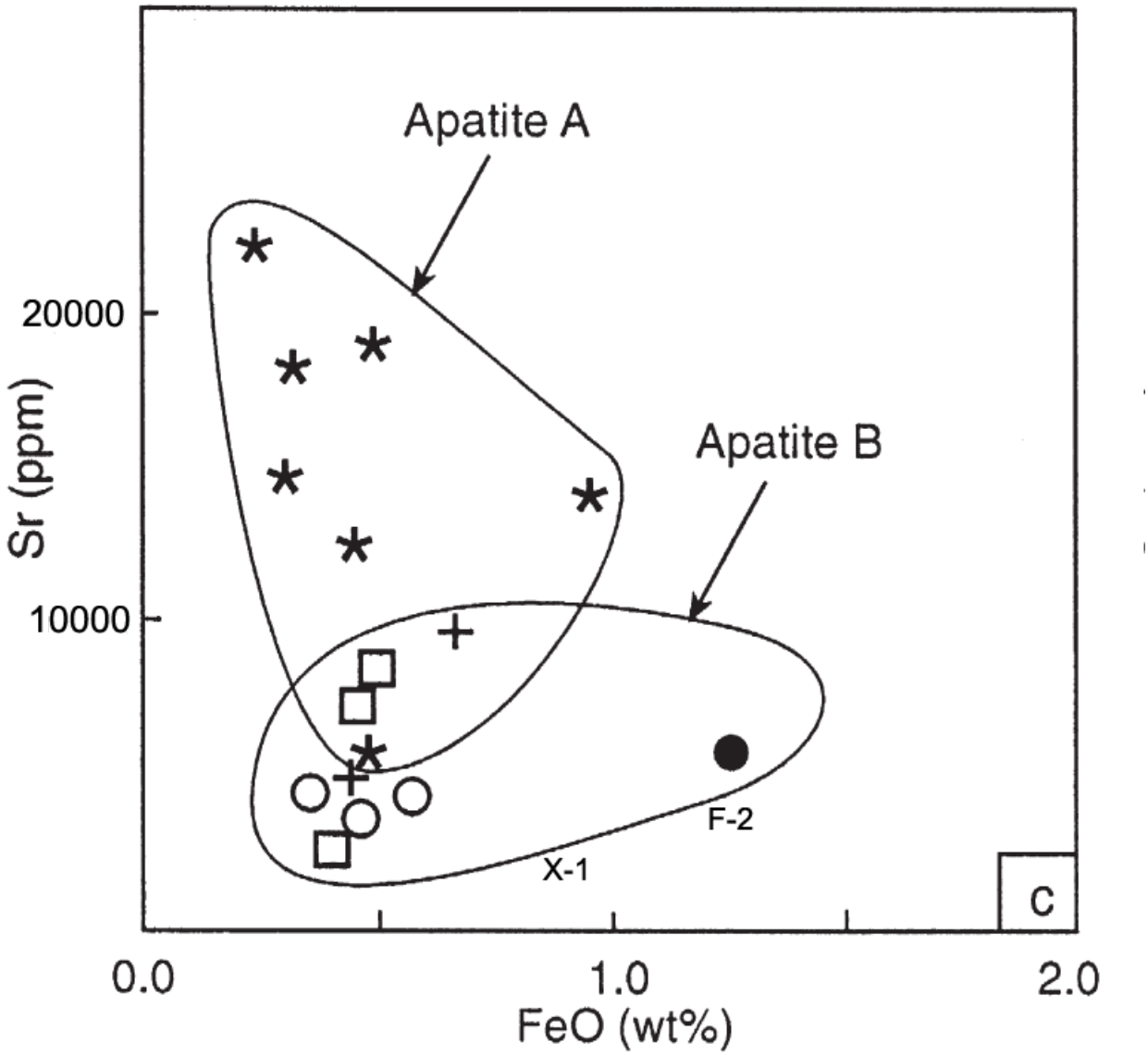


Figure 4.7: Strontium and FeO abundances in apatites from samples X1 and F2. Figure adapted from O'Reilly & Griffin (2000)

Sr values for the host basalt at LCVF range from 510 ppm to 970 ppm, (Kargel, 1987). An interesting observation is that the highest Sr concentration (970 ppm) in Kargel (1987) is in basalt sampled at Easy Chair Crater. The partitioning of Sr between apatite and melt can be used to infer the Sr concentration in the parental melts of the apatites in xenoliths X-1 and F-2. The partition coefficient $D_X$ is the mass concentration of element X in apatite divided by the concentration of X in the melt. Partition coefficients for Sr partitioning between apatite and

melt were experimentally determined by Watson and Green (1981). Their results suggest $D_{Sr}$ apatite/melt values of 1.1 for basanite melts at a temperature of 950°C and 1.4 for basanite melts at a temperature of 1080°C are appropriate. Table 4.1 shows calculated melt Sr concentrations based on these partition coefficients and the measured Sr content of the apatites. The calculated melt values range between 665 ppm and 1923 ppm and are similar to that for the Easy Chair Crater basalt. In a survey of geochemical data for continental basalts Farmer (2004) found a range of Sr concentrations of 300-3000 ppm with an average value of around 900 ppm. Moreover, Sr is typically high in alkaline basalts (≈500-2000 ppm; Clague & Frey, 1982), and thus the calculated Sr content points to an alkalic parent magma similar to that of the host lava.

Table 4.1: Calculated Sr in melts in equilibrium with Easy Chair Crater xenolith apatites

| Sample | X-1 | X-1 | X-1 | F-2 | F-2 | F-2 |
|---|---|---|---|---|---|---|
| Apatite grain | AA | BB | A | A | B | C |
| SrO Wt percent | 0.19 | 0.18 | 0.23 | 0.25 | 0.11 | 0.15 |
| Sr ppm | 1608 | 1523 | 1946 | 2115 | 931 | 1269 |
| Sr in melt D=1.1 | 1461 | 1384 | 1769 | 1923 | 846 | 1154 |
| Sr in melt D=1.4 | 1148 | 1088 | 1390 | 1511 | 665 | 907 |

Apatite A (metasomatic) has been shown to have a higher range of Sr concentrations than Apatite B (magmatic), 4800-22300 ppm vs. 2400-8300 ppm (O'Reilly and Griffin, 2000), and Sr partitions into fluid more readily than melt or minerals (Brenan et al., 1995). Given that the Sr concentrations in the apatites in xenoliths X-1 and F-2 are relatively low compared to metasomatic apatites, it is likely that these apatites formed by crystallization from a silicate melt.

Patiño Douce et al. (2011) noted that F-apatite has the greatest thermal stability, and in fact endmember fluorapatite is the common igneous apatite (Piccoli and Candela, 2002). Both the apatite in X-1 and F-2 are atypical for magmatic apatites because they are OH-rich. The variability that I observed in F/OH contents in apatite from F-2 was first reported in Patiño Douce et al. (2011). This variability in F/OH composition is curious given the relatively small size (≈4 cm) of the xenolith and as discussed in Patiño Douce et al. (2011) could be due to heating of the xenolith during magma ascent, which caused an OH-rich apatite to dehydrate. If so, the original apatite in F-2 may be approximated by the analyzed apatite grain with the highest OH content.

The origin of apatite in X-1 is intriguing because of its high Cl and OH contents. Again, X-1 is a Group II xenolith (high Al, Ti), which most commonly contains Apatite B (Low Cl; O'Reilly and Griffin 2000). Was the original apatite Cl- and OH-rich or was an originally F-rich magmatic apatite enriched in Cl and OH by an OH- and Cl- rich fluid that metasomatized the host rocks? For the latter to be possible a F-rich magmatic apatite would have to encounter a Cl- and water-rich (but relatively Sr-poor) metasomatic fluid. If the apatite in xenolith X-1 was originally Cl- and OH rich, a possible origin for this apatite is crystallization from a hydrous magma enriched in Cl, either generated by melting of a Cl-rich rock or one that incorporated a high-Cl fluid that was liberated from a Cl-rich source.

Apatites in xenolith X-1 are more enriched in Cl than is typical for Group II xenoliths and are more OH-rich in general. The relatively high OH values in these Easy Chair Crater xenolith apatites as well as the predominance of amphibole is indicative of genesis from a relatively hydrous magma. Partition coefficients of hydrogen in apatite obtained from experimental work

by Boyce et al. (2010) and McCubbin et al. (2010) can be used to estimate amount of water in the initial melt. Note that results from experimental partition coefficients for volatiles in apatites should be considered a rough estimate at best and are only applicable for qualitative comparison (Sarafian et al., 2013). A $D_{OH}$ of 0.4 is an average experimental value for apatite/melt obtained by Boyce et al. (2010). Using this partition coefficient with average calculated OH contents in apatites from samples X-1 and F-2, I estimate average water contents of the equilibrium melts to be approximately 1.3-2.8% wt% $H_2O$ (Table 4.2).

Table 4.2: Estimates of melt $H_2O$ from apatite compositions.

| Sample | X-1 | X-1 | X-1 | F-2 | F-2 | F-2 |
|---|---|---|---|---|---|---|
| Grain | AA | BB | A | A | B | C |
| H2O wt. % | 1.27 | 1.32 | 1.52 | 0.5 | 1.06 | 1.04 |
| $D_{OH}$ | 0.4 | 0.4 | 0.4 | 0.4 | 0.4 | 0.4 |
| H2O wt. % (melt) | 3.2 | 3.3 | 3.8 | 1.3 | 2.7 | 2.6 |

The calculations indicate that the melt that crystallized the apatite in xenolith X-1 could have been more hydrous than that responsible for the apatite in xenolith F-2. Hamilton et al. (1964) determined experimentally that the solubility of water in a basaltic melt is 9.4 wt% at 1100°C and 6 kbar and shows increasing solubility as pressure increases. The qualitative estimates of water content in the parental magma(s) for Easy Chair Group II xenoliths are well below that of saturation as determined by Hamilton (1964). This finding does not preclude a role for of a supercritical fluid but does allow for all the water to be dissolved in the melt.

The apatite in xenolith X-1 is relatively devoid of F and enriched in Cl and OH. In systems where a silicate melt and a hydrous fluid exist at equilibrium, F preferentially partitions into the melt and Cl into the fluid (Patiño-Douce et al., 2011; Carroll and Webster, 1994; Mathez and Webster, 2005), thus the parental rock would have to be very Cl-rich to produce apatites with Cl

concentrations similar to those in the apatite of xenolith X-1 (Cl in X-1 apatite is ≈1.0 wt%). Low-pressure (500 bar) experiments by Mathez and Webster (2005) show that to produce apatites of 1.0 wt% Cl composition, a melt of at least 1.0 wt% Cl is needed. It should be noted that this relation is complicated by the fact that melt Cl solubility is strongly dependent on melt composition (Mathez and Webster, 2005), but it can be stated qualitatively that a Cl-enriched magmatic apatite requires a Cl-rich melt which necessitates either a Cl-rich source rock or incorporation of a Cl rich fluid into an existing melt.

Shallow, subhorizontal, subduction of the Farallon plate from the mid-Cretaceous to the late Eocene resulted in compression, crustal shortening, and uplift of large regions in the southwest (e.g., Sangre de Cristos Mountains) during the Laramide orogeny; the subsequent falling away of the slab caused an influx of athenospheric mantle beneath the continental lithosphere and a transition from compression to the extensional tectonics we see now in the Basin and Range Province (Dickinson & Snyder, 1978; Humphreys, 1995). Slab-derived melts or fluids resulting from the subduction of the Farallon plate could be responsible for enrichment of lithospheric mantle in Cl and $H_2O$ resulting in a source rock capable of producing a melt consistent with the OH-enrichment observed in the apatites from xenolith F-2 and the Cl- and OH-enrichment observed in the apatites from X-1.

Altered oceanic crust and sediments have high Cl contents (Rowe & Lassiter, 2009), and it has been shown that many arc and backarc lavas are enriched in Cl relative to other incompatible elements due to devolatilization of subducted oceanic crust into the mantle wedge (Wade et al., 2006). It follows that volatile abundance (Cl, $H_2O$) can be elevated in magmas derived from mantle metasomatized by subducted oceanic crust. Work by Rowe and Lassiter

(2009) quantified this by analyzing melt inclusions in basalts from the Rio Grande Rift (RGR). The RGR is thought to mark the eastern end of subhorizontal Farallon plate subduction (Lawton and McMillan, 1999) and presumably the mantle beneath the RGR could be subject to enrichment by devolatilization of oceanic crust. Because Ba and Sr are more fluid-mobile than Nb and Nd, the ratio of Ba to Nb and Sr to Nd have been used to provide evidence of fluid enrichment of lithospheric mantle (Lee, 2005). In xenolith X-1 the whole-rock Ba/Nb is 14.4 and in xenolith F-2 it is 31.6 (Norris, 1996). These values fall within the range (≈10-35) for RGR melt inclusions analyzed by Rowe & Lassiter (2009). Published values of Ba/Nb for MORB are low (≈7; Rowe & Lassiter, 2009). Published Ba/Nb values for alkali basalts thought to result from decompression melting of convecting mantle with little crustal input range from 7-11 at Potrillo Volcanic Field in New Mexico (Thompson et al., 2005), 7-12 at the Geronimo volcanic field in New Mexico (Kempton et al., 1990) and less than 15 at the Zuni-Bandera volcanic field, also in New Mexico (Rowe & Lassiter, 2009). Wolff et al. (2005) in a study of Jemez volcanic field basalts and related basement rock, reported that exposed Precambrian basement and crustal xenoliths in the western US have elevated Ba/Nb ratios (> 30) thus, high Ba/Nb in RGR basalts and presumably in other Western basalts (i.e. LCVF) could also be indicative of continental crust contamination of a melt. Wolff et al. (2005) also stated however, that the same Precambrian basement has relatively low Sr/Nd ratios (< 10) whereas RGR melt inclusions from a Cl enriched source have higher Sr/Nd ratios averaging from 10-30. LCVF basalts have Sr/Nd ratios of 15-25 (Bergman, 1982, Kargel, 1987), in the same range. Rowe and Lassiter (2009) plotted Ba/Nb, Sr/Nd, and Cl/K all vs. Cl/Nb and were able to differentiate between crustal contamination and subduction-related metasomatism and attributed the Cl enrichment observed in RGR basalts to the

influence of fluids from subducted oceanic lithosphere. Currently no whole rock or melt Cl data exists for LCVF and consequently, a full comparison of trace element ratios is impossible. Thus the possibility of crustal contamination as a source for Ba enrichment of the parental magma to the LCVF xenoliths is not precluded. However, the modal abundance of amphibole and the Cl and OH enrichment of apatite within LCVF xenoliths suggest that hydrous and Cl-rich fluids were present during magma formation possibly derived from the Farallon plate.

## 5.0 CONCLUSION

Group II xenoliths analyzed in this thesis are very hydrous as evidenced by the ubiquity and abundance of amphibole and the nature of the included apatites. This OH enrichment in two xenolith apatites along with the Cl enrichment in one of theses apatites could be the effect of fluids liberated from the subducted Farallon plate. Relatively high Ba/Nb and Sr/Nd of LCVF lavas are also consistent with a role for such a fluid in their petrogenesis.

Relatively high temperatures of equilibration in Group I xenoliths may be the signature of a perturbed geotherm related to subduction related magmatism or even a plume that helped to dehydrate the subducted slab, metasomatizing the lithospheric mantle and providing a source rock for the alkali basalts and associated hydrous xenoliths observed at LCVF. However, geothermometry for the Group II xenoliths indicate a range of temperatures of equilibration. This observed range could be attributed to the fact that the closing temperatures of the geothermometers used are dependent on the mineralogy of the assemblage in a given rock. Those xenoliths that contain exsolved spinel pairs or ilmenite (e.g. S-1, EC-3) are capable of recording the lowest temperatures of equilibrium, in this case ≈500°C. These lower temperature assemblages are pressure independent and could exist at a range of depths but presumably reached equilibrium along the local geotherm.

To truly prove the importance of the inferred fluid enrichment of the source rocks as well as the source of melt generation at LCVF further work is necessitated. For example, more apatite volatile analyses, as well as whole-rock or melt inclusion Cl analyses could help

prove the influence of a Farallon-derived fluid in the petrogenesis of the LCVF. Local heat flow measurements and more precise geobarometry could produce a geotherm that explains the metasomatic and magmatic sequence of events that resulted in LCVF.

**REFERENCES**


Allmendinger, R. W., Hauge, T. A., Hauser, E. C., Potter, C. J., Klemperer, S. L., Nelson, K. D., ... & Oliver, J. (1987). Overview of the COCORP 40 N transect, western United States: The fabric of an orogenic belt. *Geological Society of America Bulletin*, *98*(3), 308-319.

Andersen, D. J., Lindsley, D. H., & Davidson, P. M. (1993). QUILF: A pascal program to assess equilibria among Fe-Mg-Mn-Ti oxides, pyroxenes, olivine, and quartz. *Computers & Geosciences*, *19*(9), 1333-1350.

Aoki, K. I., & Kushiro, I. (1968). Some clinopyroxenes from ultramafic inclusions in Dreiser Weiher, Eifel. *Contributions to Mineralogy and Petrology*, *18*(4), 326-337.

Bergman, S. C. (1982). *Petrogenetic aspects of the alkali basalt lavas and included megacrysts and nodules from the Lunar Crater Volcanic Field, Nevada, USA*.

Boudreau, A. E., & McCallum, I. S. (1989). Investigations of the Stillwater Complex: Part V. Apatites as indicators of evolving fluid composition.*Contributions to Mineralogy and Petrology*, *102*(2), 138-153.

Boyce, J. W., Liu, Y., Rossman, G. R., Guan, Y., Eiler, J. M., Stolper, E. M., & Taylor, L. A. (2010). Lunar apatite with terrestrial volatile abundances. *Nature*,*466*(7305), 466-469.

Brenan, J. M., Shaw, H. F., Ryerson, F. J., & Phinney, D. L. (1995). Mineral-aqueous fluid partitioning of trace elements at 900 C and 2.0 GPa: Constraints on the trace element chemistry of mantle and deep crustal fluids. *Geochimica et Cosmochimica Acta*, *59*(16), 3331-3350.

Brey, G. P., & Köhler, T. (1990). Geothermobarometry in four-phase lherzolites II. New thermobarometers, and practical assessment of existing thermobarometers. *Journal of Petrology*, *31*(6), 1353-1378.

Buddington, A. F., & Lindsley, D. H. (1964). Iron-titanium oxide minerals and synthetic equivalents. *Journal of petrology*, *5*(2), 310-357.

Carroll, M. R., & Webster, J. D. (1994). Solubilities of sulfur, noble gases, nitrogen, chlorine, and fluorine in magmas. *Reviews in Mineralogy and Geochemistry*, *30*(1), 231-279.

Christensen, N. I., & Mooney, W. D. (1995). Seismic velocity structure and composition of the continental crust: A global view. *Journal of Geophysical Research: Solid Earth (1978–2012)*, *100*(B6), 9761-9788.

Clague, D. A., & Frey, F. A. (1982). Petrology and trace element geochemistry of the Honolulu Volcanics, Oahu: implications for the oceanic mantle below Hawaii. *Journal of Petrology*, *23*(3), 447-504.

Dickinson, W. R., & Snyder, W. S. (1978). Plate tectonics of the Laramide orogeny. *Geological Society of America Memoirs*, *151*, 355-366.

Duffield, W. A., & Sass, J. H. (2003). *Geothermal energy: Clean power from the earth's heat* (Vol. 1249). DIANE Publishing.

Farmer, G. L. (2003). Continental basaltic rocks. *Treatise on geochemistry*, *3*, 85-121.

Frey, F. A., & Prinz, M. (1978). Ultramafic inclusions from San Carlos, Arizona: petrologic and geochemical data bearing on their petrogenesis. *Earth and Planetary Science Letters*, *38*(1), 129-176.

Hamilton, D. L., Burnham, C. W., & Osborn, E. F. (1964). The solubility of water and effects of oxygen fugacity and water content on crystallization in mafic magmas. *Journal of Petrology*, *5*(1), 21-39.

Hamilton, W. (1987). Crustal extension in the Basin and Range province, southwestern United States. In *Continental extensional tectonics* (Vol. 28, pp. 155-176). Blackwell Science Incorporated.

Humphreys, E. D. (1995). Post-Laramide removal of the Farallon slab, western United States. *Geology*, *23*(11), 987-990.

Heizler, M.T. (2013) 40Ar/39Ar geochronology results for Lunar Crater Volcanic Field basalts, Nevada. New Mexico Geochronological Research Laboratory Report NMGRL-IR-792. https://vhub.org.resources/2503.

Kargel, J. S. (1987). *The geochemistry of basalts and mantle inclusions from the Lunar Crater Volcanic Field, Nevada: petrogenetic and geodynamic implications* (Doctoral dissertation, The Ohio State University).

Lawton, T. F., & McMillan, N. J. (1999). Arc abandonment as a cause for passive continental rifting: Comparison of the Jurassic Mexican Borderland rift and the Cenozoic Rio Grande rift. *Geology*, *27*(9), 779-782.

Leake, B.E., Woolley, A.R., Arps, C.E.S., Birch, W.D., Gilbert, M.C.,Grice, J.D., Hawthorne, F.C., Kato, A., Kisch, H.J., Krivovichev, V.G.,Linthout, K., Laird, J., Mandarino, J.A., Maresch, W.V., Nickel, E.H.,Rock, N.M.S., Schumacher, J.C., Smith, D.C., Stephenson, N.C.N., Ungaretti,L., Whittaker, E.J.W., and Youzhi, G. (1997) Nomenclature of amphiboles: Report of the Subcommittee on Amphiboles of the International Mineralogical Association, Commission on New Minerals and Mineral Names. The Canadian Mineralogist, 35, 219-246

Lee, C. T. A. (2005). Trace element evidence for hydrous metasomatism at the base of the North American lithosphere and possible association with Laramide low-angle subduction. *The Journal of geology*, *113*(6), 673-685.

Lindsley, D. H., & Spencer, K. J. (1982). Fe-Ti oxide geothermometry: Reducing analyses of coexisting Ti-magnetite (Mt) and ilmenite (Ilm). *EOS Transactions, American Geophysical Union*, *63*(18), 471.

Kempton, P. D., Harmon, R. S., Hawkesworth, C. J., & Moorbath, S. (1990). Petrology and geochemistry of lower crustal granulites from the Geronimo Volcanic Field, southeastern Arizona. *Geochimica et Cosmochimica Acta*,*54*(12), 3401-3426.

Mathez, E. A., & Webster, J. D. (2005). Partitioning behavior of chlorine and fluorine in the system apatite-silicate melt-fluid. *Geochimica et Cosmochimica Acta*, *69*(5), 1275-1286.

McCubbin, F. M., Steele, A., Hauri, E. H., Nekvasil, H., Yamashita, S., & Hemley, R. J. (2010). Nominally hydrous magmatism on the Moon. *Proceedings of the National Academy of Sciences*.

McKenzie, D., & Bickle, M. J. (1988). The volume and composition of melt generated by extension of the lithosphere. *Journal of petrology*, *29*(3), 625-679.

Menzies, M. A., Arculus, R. J., Best, M. G., Bergman, S. C., Ehrenberg, S. N., Irving, A. J., Roden M.F., & Schulze, D. J. (1987). A record of subduction process and within-plate volcanism in lithospheric xenoliths of the southwestern USA.*Mantle xenoliths*, 59-74.

Norris, J. A. (1996). *Geochemistry of mafic and ultramafic xenoliths from the Easy Chair crater basalt flow, Lunar Crater volcanic field, Nevada* (Doctoral dissertation, University of Georgia).

O'Reilly, S. Y., & Griffin, W. L. (2000). Apatite in the mantle: implications for metasomatic processes and high heat production in Phanerozoic mantle.*Lithos*, *53*(3), 217-232.

Patiño Douce, A. E., Roden, M. F., Chaumba, J., Fleisher, C., & Yogodzinski, G. (2011). Compositional variability of terrestrial mantle apatites, thermodynamic modeling of apatite volatile contents, and the halogen and water budgets of planetary mantles. *Chemical Geology*, *288*(1), 14-31.

Piccoli, P. M., & Candela, P. A. (2002). Apatite in igneous systems. *Reviews in Mineralogy and Geochemistry*, *48*(1), 255-292.

Rowe, M. C., & Lassiter, J. C. (2009). Chlorine enrichment in central Rio Grande Rift basaltic melt inclusions: Evidence for subduction modification of the lithospheric mantle. *Geology*, *37*(5), 439-442.

Roden, M. F., & Shimizu, N. (1993). Ion microprobe analyses bearing on the composition of the upper mantle beneath the Basin and Range and Colorado Plateau provinces. *Journal of Geophysical Research: Solid Earth (1978–2012)*,*98*(B8), 14091-14108.

Saltus, R. W., & Thompson, G. A. (1995). Why is it downhill from Tonopah to Las Vegas?: A case for mantle plume support of the high northern Basin and Range. *Tectonics*, *14*(6), 1235-1244.

Sarafian, A. R., Roden, M. F., & Patiño-Douce, A. E. (2013). The volatile content of Vesta: Clues from apatite in eucrites. *Meteoritics & Planetary Science*, *48*(11), 2135-2154.

Sass, J.H. (2005). Summary of supporting data for USGS regional heat-flow studies of the Great Basin, 1970-1990. US Geological Survey, http://pubs.usgs.gov/of/2005/1207/

Scott, D. H., & Trask, N. J. (1971). *Geology of the lunar crater volcanic field, Nye County, Nevada* (pp. 1-22). US Government Printing Office.

Smith, D., & Roden, M. F. (1981). Geothermometry and kinetics in a two-spinel peridotite nodule, Colorado Plateau. *Am. Mineral.;(United States)*, *66*(3-4).

Smith, D. (2000). Insights into the evolution of the uppermost continental mantle from xenolith localities on and near the Colorado Plateau and regional comparisons. *Journal of Geophysical Research: Solid Earth (1978–2012)*,*105*(B7), 16769-16781.

Smith, J. V., Delaney, J. S., Hervig, R. L., & Dawson, J. B. (1981). Storage of F and Cl in the upper mantle: geochemical implications. *Lithos*, *14*(2), 133-147.

Thompson, R. N., Ottley, C. J., Smith, P. M., Pearson, D. G., Dickin, A. P., Morrison, M. A., ... & Gibson, S. A. (2005). Source of the Quaternary alkalic basalts, picrites and basanites of the Potrillo Volcanic Field, New Mexico, USA: lithosphere or convecting mantle?. *Journal of Petrology*, *46*(8), 1603-1643.

Turnock, A. C., & Eugster, H. P. (1962). Fe—Al Oxides: Phase Relationships below 1,000 C. *Journal of Petrology*, *3*(3), 533-565.

Wade, J. A., Plank, T., Melson, W. G., Soto, G. J., & Hauri, E. H. (2006). The volatile content of magmas from Arenal volcano, Costa Rica. *Journal of Volcanology and Geothermal Research*, *157*(1), 94-120.

Wager, L. R., Brown, G. M., & Wadsworth, W. J. (1960). Types of igneous cumulates. *Journal of Petrology*, *1*(1), 73-85.

Watson, E. B., & Green, T. H. (1981). Apatite/liquid partition coefficients for the rare earth elements and strontium. *Earth and Planetary Science Letters*, *56*, 405-421.

Wilshire, H. G., & Shervais, J. W. (1975). Al-augite and Cr-diopside ultramafic xenoliths in basaltic rocks from western United States. *Physics and Chemistry of the Earth*, *9*, 257-272.

Wolff, J. A., Rowe, M. C., Teasdale, R., Gardner, J. N., Ramos, F. C., & Heikoop, C. E. (2005). Petrogenesis of pre-caldera mafic lavas, Jemez Mountains volcanic field (New Mexico, USA). Journal of Petrology, 46(2), 407-439.

Wyllie, P. J., Cox, K. G., & Biggar, G. M. (1962). The habit of apatite in synthetic systems and igneous rocks. *Journal of Petrology*, *3*(2), 238-243.

# Appendix A: Complete Tables of Microprobe Analyses

## Pyroxenes

**Pyroxenes**

| | AF-1 | | AF-1 | | AF-1 | | AF-1 | | | AF-1 | | AF-1 | | AF-2 | | AF-2 | | | AF-2 | | | AF-2 | | AF-2 | | | |
|---|---|---|---|---|---|---|---|---|---|---|---|---|---|---|---|---|---|---|---|---|---|---|---|---|---|---|---|
| grain | a1 | a2 | b1 | b2 | c1 | c2 | d1 | d2 | d3 | e1 | e2 | f1 | f2 | a1 | a2 | b1 | b2 | b3 | c1 | c2 | c3 | d1 | d2 | e1 | e2 | f1 | f2 |
| SiO2 | 45.15 | 44.77 | 45.72 | 45.55 | 45.00 | 45.03 | 46.09 | 46.63 | 46.32 | 44.61 | 44.03 | 44.80 | 45.12 | 44.71 | 44.74 | 45.64 | 44.41 | 46.05 | 47.05 | 45.30 | 45.00 | 45.59 | 46.28 | 44.80 | 45.41 | 45.24 | 45.39 |
| TiO2 | 2.20 | 2.21 | 2.43 | 2.47 | 2.15 | 1.91 | 2.27 | 2.10 | 1.72 | 2.09 | 1.88 | 2.39 | 2.08 | 2.36 | 2.51 | 2.19 | 2.71 | 2.12 | 1.92 | 2.29 | 2.09 | 2.78 | 2.57 | 2.66 | 2.53 | 2.21 | 2.10 |
| Al2O3 | 8.99 | 8.81 | 8.95 | 9.16 | 9.67 | 9.58 | 9.10 | 8.81 | 7.64 | 9.87 | 9.92 | 8.91 | 8.61 | 9.67 | 9.68 | 9.55 | 10.18 | 8.81 | 8.04 | 9.08 | 8.12 | 9.86 | 9.08 | 9.74 | 9.64 | 8.98 | 8.72 |
| FeO | 8.09 | 8.34 | 8.58 | 8.78 | 8.62 | 8.44 | 8.03 | 8.48 | 8.14 | 8.98 | 8.45 | 8.55 | 8.08 | 7.59 | 7.63 | 7.91 | 7.38 | 7.65 | 7.18 | 7.43 | 7.45 | 7.14 | 7.14 | 7.60 | 7.43 | 7.43 | 7.52 |
| Fe2O3 | 0.00 | 0.00 | 0.00 | 0.00 | 0.00 | 0.00 | 0.00 | 0.00 | 0.00 | 0.00 | 0.00 | 0.00 | 0.00 | 0.00 | 0.00 | 0.00 | 0.00 | 0.00 | 0.00 | 0.00 | 0.00 | 0.00 | 0.00 | 0.00 | 0.00 | 0.00 | 0.00 |
| MnO | 0.24 | 0.17 | 0.35 | 0.25 | 0.20 | 0.23 | 0.13 | 0.14 | 0.09 | 0.17 | 0.11 | 0.20 | 0.13 | 0.13 | 0.15 | 0.24 | 0.07 | 0.10 | 0.14 | 0.18 | 0.14 | 0.13 | 0.09 | 0.23 | 0.18 | 0.14 | 0.06 |
| MgO | 11.63 | 11.55 | 11.74 | 11.96 | 11.52 | 11.39 | 11.90 | 11.87 | 12.31 | 11.45 | 11.54 | 11.86 | 11.93 | 11.12 | 11.34 | 11.44 | 10.65 | 11.42 | 12.00 | 11.39 | 11.62 | 11.41 | 11.55 | 11.00 | 10.90 | 11.43 | 11.14 |
| CaO | 21.05 | 21.17 | 20.80 | 20.55 | 21.17 | 21.13 | 20.89 | 21.26 | 21.19 | 20.65 | 19.80 | 21.12 | 20.84 | 22.62 | 21.45 | 20.98 | 22.28 | 22.39 | 22.13 | 22.22 | 22.24 | 21.90 | 22.25 | 22.05 | 21.95 | 22.23 | 22.29 |
| Na2O | 0.80 | 0.82 | 0.75 | 0.86 | 0.85 | 0.79 | 0.90 | 0.77 | 0.82 | 0.96 | 0.95 | 0.72 | 0.80 | 0.69 | 0.90 | 1.16 | 0.69 | 0.76 | 0.72 | 0.78 | 0.77 | 0.80 | 0.72 | 0.82 | 0.81 | 0.79 | 0.76 |
| K2O | 0.00 | 0.00 | 0.00 | 0.00 | 0.00 | 0.00 | 0.00 | 0.00 | 0.00 | 0.00 | 0.00 | 0.00 | 0.00 | 0.00 | 0.00 | 0.00 | 0.00 | 0.00 | 0.00 | 0.00 | 0.00 | 0.00 | 0.00 | 0.00 | 0.00 | 0.00 | 0.00 |
| Cr2O3 | 0.00 | 0.00 | 0.03 | 0.09 | 0.04 | 0.07 | 0.12 | 0.00 | 0.08 | 0.01 | 0.08 | 0.00 | 0.08 | 0.04 | 0.03 | 0.12 | 0.00 | 0.00 | 0.04 | 0.00 | 0.00 | 0.00 | 0.03 | 0.15 | 0.04 | 0.00 | 0.00 |
| **Total** | 98.15 | 97.84 | 99.34 | 99.68 | 99.22 | 98.57 | 99.43 | 100.06 | 98.32 | 98.79 | 96.75 | 98.56 | 97.66 | 98.92 | 98.44 | 99.23 | 98.36 | 99.29 | 99.22 | 98.69 | 97.43 | 99.61 | 99.72 | 99.05 | 98.88 | 98.47 | 97.98 |
| **Mg#** | 59 | 58 | 58 | 58 | 57 | 57 | 60 | 58 | 60 | 56 | 58 | 58 | 60 | 59 | 60 | 59 | 59 | 60 | 63 | 61 | 61 | 61 | 62 | 59 | 59 | 61 | 60 |
| | | | | | | | | | | | | | | | | | | | | | | | | | | | |
| **Cations normalized to 6 oxygens** | | | | | | | | | | | | | | | | | | | | | | | | | | | |
| Si | 1.724 | 1.719 | 1.726 | 1.715 | 1.704 | 1.714 | 1.732 | 1.744 | 1.764 | 1.698 | 1.704 | 1.709 | 1.730 | 1.697 | 1.703 | 1.722 | 1.692 | 1.737 | 1.768 | 1.720 | 1.734 | 1.708 | 1.732 | 1.697 | 1.718 | 1.722 | 1.735 |
| Ti | 0.063 | 0.064 | 0.069 | 0.070 | 0.061 | 0.055 | 0.064 | 0.059 | 0.049 | 0.060 | 0.055 | 0.069 | 0.060 | 0.067 | 0.072 | 0.062 | 0.078 | 0.060 | 0.054 | 0.065 | 0.060 | 0.078 | 0.072 | 0.076 | 0.072 | 0.063 | 0.060 |
| Al | 0.404 | 0.399 | 0.398 | 0.406 | 0.432 | 0.430 | 0.403 | 0.389 | 0.343 | 0.443 | 0.453 | 0.401 | 0.389 | 0.433 | 0.434 | 0.424 | 0.457 | 0.391 | 0.356 | 0.407 | 0.369 | 0.435 | 0.400 | 0.435 | 0.430 | 0.403 | 0.393 |
| Fe 2+ | 0.258 | 0.268 | 0.271 | 0.276 | 0.273 | 0.269 | 0.252 | 0.265 | 0.259 | 0.286 | 0.273 | 0.273 | 0.259 | 0.241 | 0.243 | 0.250 | 0.235 | 0.241 | 0.226 | 0.236 | 0.240 | 0.224 | 0.224 | 0.241 | 0.235 | 0.237 | 0.240 |
| Fe 3+ | 0.000 | 0.000 | 0.000 | 0.000 | 0.000 | 0.000 | 0.000 | 0.000 | 0.000 | 0.000 | 0.000 | 0.000 | 0.000 | 0.000 | 0.000 | 0.000 | 0.000 | 0.000 | 0.000 | 0.000 | 0.000 | 0.000 | 0.000 | 0.000 | 0.000 | 0.000 | 0.000 |
| Mn | 0.008 | 0.005 | 0.011 | 0.008 | 0.007 | 0.007 | 0.004 | 0.004 | 0.003 | 0.006 | 0.004 | 0.006 | 0.004 | 0.004 | 0.005 | 0.008 | 0.002 | 0.003 | 0.004 | 0.006 | 0.005 | 0.004 | 0.003 | 0.007 | 0.006 | 0.005 | 0.002 |
| Mg | 0.662 | 0.661 | 0.661 | 0.671 | 0.650 | 0.646 | 0.667 | 0.661 | 0.699 | 0.650 | 0.666 | 0.674 | 0.682 | 0.629 | 0.643 | 0.643 | 0.604 | 0.642 | 0.672 | 0.645 | 0.667 | 0.637 | 0.645 | 0.621 | 0.615 | 0.648 | 0.635 |
| Ca | 0.861 | 0.871 | 0.841 | 0.829 | 0.859 | 0.862 | 0.841 | 0.852 | 0.864 | 0.842 | 0.821 | 0.863 | 0.856 | 0.920 | 0.875 | 0.848 | 0.909 | 0.905 | 0.891 | 0.904 | 0.918 | 0.879 | 0.892 | 0.895 | 0.890 | 0.907 | 0.913 |
| Na | 0.059 | 0.061 | 0.055 | 0.063 | 0.062 | 0.058 | 0.066 | 0.056 | 0.061 | 0.071 | 0.071 | 0.053 | 0.059 | 0.051 | 0.067 | 0.085 | 0.051 | 0.056 | 0.053 | 0.058 | 0.057 | 0.058 | 0.053 | 0.060 | 0.059 | 0.059 | 0.057 |
| K | 0.000 | 0.000 | 0.000 | 0.000 | 0.000 | 0.000 | 0.000 | 0.000 | 0.000 | 0.000 | 0.000 | 0.000 | 0.000 | 0.000 | 0.000 | 0.000 | 0.000 | 0.000 | 0.000 | 0.000 | 0.000 | 0.000 | 0.000 | 0.000 | 0.000 | 0.000 | 0.000 |
| Cr | 0.000 | 0.000 | 0.001 | 0.003 | 0.001 | 0.002 | 0.004 | 0.000 | 0.002 | 0.000 | 0.002 | 0.000 | 0.002 | 0.001 | 0.001 | 0.004 | 0.000 | 0.000 | 0.001 | 0.000 | 0.000 | 0.000 | 0.001 | 0.004 | 0.001 | 0.000 | 0.000 |
| **Total** | 4.040 | 4.048 | 4.033 | 4.042 | 4.049 | 4.044 | 4.033 | 4.031 | 4.045 | 4.056 | 4.049 | 4.049 | 4.043 | 4.044 | 4.042 | 4.045 | 4.028 | 4.035 | 4.026 | 4.040 | 4.050 | 4.025 | 4.021 | 4.037 | 4.025 | 4.043 | 4.036 |

**Pyroxenes**

| | X-6 | | | X-6 | | | X-6 | | | X-8 | | | X-8 | | | X-8 | | | EC-4 | | | EC-4 | | | EC-4 | | |
|---|---|---|---|---|---|---|---|---|---|---|---|---|---|---|---|---|---|---|---|---|---|---|---|---|---|---|---|
| grain | a1 | a2 | a3 | b1 | b2 | b3 | c1 | c2 | c3 | a1 | a2 | a3 | b1 | b2 | b3 | c1 | c2 | c3 | a1 | a2 | a3 | b1 | b2 | b3 | c1 | c2 | c3 |
| SiO2 | 48.85 | 48.62 | 48.37 | 47.96 | 47.72 | 47.65 | 47.43 | 47.89 | 47.73 | 49.19 | 48.86 | 49.17 | 49.19 | 48.72 | 48.74 | 49.11 | 49.00 | 49.44 | 46.28 | 45.53 | 45.96 | 46.84 | 46.59 | 45.94 | 45.35 | 45.57 | 45.36 |
| TiO2 | 1.26 | 1.11 | 1.18 | 1.18 | 1.21 | 1.19 | 1.37 | 1.18 | 1.36 | 0.94 | 1.04 | 0.95 | 0.72 | 0.68 | 0.94 | 0.92 | 1.06 | 0.96 | 1.35 | 1.49 | 1.59 | 1.41 | 1.26 | 1.12 | 1.93 | 1.91 | 2.10 |
| Al2O3 | 8.64 | 7.70 | 7.85 | 7.75 | 8.05 | 7.93 | 8.15 | 8.16 | 8.27 | 7.21 | 7.43 | 7.14 | 6.24 | 6.31 | 7.14 | 6.17 | 6.46 | 6.13 | 8.74 | 8.78 | 8.73 | 8.73 | 8.57 | 8.47 | 9.14 | 9.04 | 9.12 |
| FeO | 8.12 | 7.67 | 8.00 | 8.55 | 8.62 | 8.46 | 8.85 | 8.81 | 8.76 | 7.29 | 7.48 | 7.47 | 7.58 | 7.74 | 7.43 | 8.79 | 7.06 | 6.94 | 8.85 | 8.90 | 8.87 | 8.32 | 8.91 | 8.90 | 8.79 | 8.75 | 8.62 |
| Fe2O3 | 0.00 | 0.00 | 0.00 | 0.00 | 0.00 | 0.00 | 0.00 | 0.00 | 0.00 | 0.00 | 0.00 | 0.00 | 0.00 | 0.00 | 0.00 | 0.00 | 0.00 | 0.00 | 0.00 | 0.00 | 0.00 | 0.00 | 0.00 | 0.00 | 0.00 | 0.00 | 0.00 |
| MnO | 0.10 | 0.16 | 0.14 | 0.24 | 0.14 | 0.21 | 0.13 | 0.12 | 0.21 | 0.13 | 0.23 | 0.21 | 0.19 | 0.16 | 0.17 | 0.31 | 0.20 | 0.14 | 0.21 | 0.16 | 0.16 | 0.16 | 0.17 | 0.14 | 0.14 | 0.26 | 0.25 |
| MgO | 12.46 | 13.12 | 13.38 | 12.79 | 12.63 | 12.85 | 12.38 | 12.61 | 13.01 | 13.16 | 12.95 | 13.32 | 14.00 | 14.18 | 13.61 | 15.89 | 13.68 | 13.95 | 11.41 | 11.55 | 11.46 | 11.50 | 11.81 | 11.72 | 11.54 | 11.56 | 11.72 |
| CaO | 20.73 | 20.77 | 20.85 | 19.99 | 20.20 | 20.10 | 20.31 | 19.61 | 19.56 | 20.96 | 20.60 | 20.66 | 20.02 | 19.91 | 20.02 | 17.27 | 20.58 | 20.52 | 20.88 | 21.07 | 20.93 | 20.95 | 20.94 | 20.94 | 20.82 | 20.80 | 20.82 |
| Na2O | 0.80 | 0.72 | 0.79 | 0.68 | 0.68 | 0.78 | 0.78 | 0.74 | 0.82 | 0.86 | 0.86 | 0.89 | 0.84 | 0.94 | 0.84 | 0.76 | 0.81 | 0.84 | 0.91 | 0.90 | 0.89 | 0.91 | 0.95 | 0.86 | 0.98 | 1.00 | 0.91 |
| K2O | 0.00 | 0.00 | 0.00 | 0.00 | 0.00 | 0.00 | 0.00 | 0.00 | 0.00 | 0.00 | 0.00 | 0.00 | 0.00 | 0.00 | 0.00 | 0.00 | 0.00 | 0.00 | 0.00 | 0.00 | 0.00 | 0.00 | 0.00 | 0.00 | 0.00 | 0.00 | 0.00 |
| Cr2O3 | 0.02 | 0.00 | 0.00 | 0.01 | 0.00 | 0.00 | 0.00 | 0.01 | 0.00 | 0.07 | 0.18 | 0.00 | 0.14 | 0.11 | 0.33 | 0.41 | 0.28 | 0.40 | 0.03 | 0.00 | 0.00 | 0.00 | 0.00 | 0.00 | 0.00 | 0.00 | 0.00 |
| **Total** | 100.99 | 99.87 | 100.57 | 99.15 | 99.24 | 99.18 | 99.39 | 99.14 | 99.72 | 99.82 | 99.64 | 99.83 | 98.93 | 98.74 | 99.23 | 99.63 | 99.13 | 99.32 | 98.66 | 98.38 | 98.59 | 98.82 | 99.20 | 98.08 | 98.69 | 98.88 | 98.90 |
| **Mg#** | 61 | 63 | 63 | 60 | 59 | 60 | 58 | 59 | 60 | 64 | 63 | 64 | 65 | 65 | 65 | 64 | 66 | 67 | 56 | 56 | 56 | 58 | 57 | 57 | 57 | 57 | 58 |
| | | | | | | | | | | | | | | | | | | | | | | | | | | | |
| **Cations normalized to 6 oxygens** | | | | | | | | | | | | | | | | | | | | | | | | | | | |
| Si | 1.865 | 1.867 | 1.826 | 1.805 | 1.807 | 1.814 | 1.782 | 1.791 | 1.817 | 1.873 | 1.891 | 1.876 | 1.887 | 1.850 | 1.855 | 1.852 | 1.866 | 1.865 | 1.739 | 1.729 | 1.770 | 1.755 | 1.744 | 1.740 | 1.715 | 1.734 | 1.735 |
| Ti | 0.036 | 0.032 | 0.034 | 0.033 | 0.034 | 0.034 | 0.039 | 0.033 | 0.039 | 0.027 | 0.030 | 0.027 | 0.021 | 0.019 | 0.027 | 0.026 | 0.030 | 0.027 | 0.038 | 0.042 | 0.046 | 0.040 | 0.036 | 0.032 | 0.055 | 0.055 | 0.060 |
| Al | 0.389 | 0.349 | 0.349 | 0.344 | 0.359 | 0.356 | 0.361 | 0.360 | 0.371 | 0.323 | 0.339 | 0.321 | 0.282 | 0.282 | 0.320 | 0.274 | 0.290 | 0.273 | 0.387 | 0.393 | 0.396 | 0.386 | 0.378 | 0.378 | 0.408 | 0.405 | 0.411 |
| Fe 2+ | 0.259 | 0.246 | 0.253 | 0.269 | 0.273 | 0.269 | 0.278 | 0.276 | 0.279 | 0.232 | 0.242 | 0.238 | 0.243 | 0.246 | 0.236 | 0.277 | 0.225 | 0.219 | 0.278 | 0.283 | 0.286 | 0.261 | 0.279 | 0.282 | 0.278 | 0.278 | 0.276 |
| Fe 3+ | 0.000 | 0.000 | 0.000 | 0.000 | 0.000 | 0.000 | 0.000 | 0.000 | 0.000 | 0.000 | 0.000 | 0.000 | 0.000 | 0.000 | 0.000 | 0.000 | 0.000 | 0.000 | 0.000 | 0.000 | 0.000 | 0.000 | 0.000 | 0.000 | 0.000 | 0.000 | 0.000 |
| Mn | 0.003 | 0.005 | 0.005 | 0.008 | 0.005 | 0.007 | 0.004 | 0.004 | 0.007 | 0.004 | 0.007 | 0.007 | 0.006 | 0.005 | 0.005 | 0.010 | 0.006 | 0.004 | 0.007 | 0.005 | 0.005 | 0.005 | 0.005 | 0.004 | 0.005 | 0.008 | 0.008 |
| Mg | 0.709 | 0.751 | 0.753 | 0.718 | 0.713 | 0.729 | 0.694 | 0.703 | 0.738 | 0.747 | 0.747 | 0.758 | 0.800 | 0.803 | 0.772 | 0.893 | 0.777 | 0.785 | 0.639 | 0.654 | 0.658 | 0.642 | 0.659 | 0.662 | 0.651 | 0.656 | 0.668 |
| Ca | 0.848 | 0.855 | 0.843 | 0.807 | 0.820 | 0.820 | 0.818 | 0.786 | 0.798 | 0.855 | 0.855 | 0.845 | 0.823 | 0.810 | 0.816 | 0.698 | 0.840 | 0.829 | 0.841 | 0.857 | 0.864 | 0.841 | 0.840 | 0.850 | 0.844 | 0.848 | 0.853 |
| Na | 0.059 | 0.054 | 0.058 | 0.050 | 0.050 | 0.058 | 0.057 | 0.054 | 0.061 | 0.064 | 0.064 | 0.066 | 0.062 | 0.069 | 0.062 | 0.055 | 0.060 | 0.061 | 0.066 | 0.066 | 0.066 | 0.066 | 0.069 | 0.063 | 0.072 | 0.074 | 0.067 |
| K | 0.000 | 0.000 | 0.000 | 0.000 | 0.000 | 0.000 | 0.000 | 0.000 | 0.000 | 0.000 | 0.000 | 0.000 | 0.000 | 0.000 | 0.000 | 0.000 | 0.000 | 0.000 | 0.000 | 0.000 | 0.000 | 0.000 | 0.000 | 0.000 | 0.000 | 0.000 | 0.000 |
| Cr | 0.000 | 0.000 | 0.000 | 0.000 | 0.000 | 0.000 | 0.000 | 0.000 | 0.000 | 0.002 | 0.006 | 0.000 | 0.004 | 0.003 | 0.010 | 0.012 | 0.008 | 0.012 | 0.001 | 0.000 | 0.000 | 0.000 | 0.000 | 0.000 | 0.000 | 0.000 | 0.000 |
| **Total** | 4.170 | 4.158 | 4.120 | 4.034 | 4.060 | 4.088 | 4.033 | 4.007 | 4.110 | 4.127 | 4.182 | 4.138 | 4.129 | 4.087 | 4.105 | 4.099 | 4.103 | 4.075 | 3.996 | 4.029 | 4.092 | 3.996 | 4.009 | 4.012 | 4.027 | 4.059 | 4.078 |

**Pyroxenes**

| | EC-3 | EC-3 | EC-3 | EC-3 | EC-3 | EC-3 | EC-3 | EC-3 | EC-3 | EC-3 | EC-3 | EC-3 | EC-3 | EC-3 | EC-3 | EC-3 | EC-3 | EC-3 |
|---|---|---|---|---|---|---|---|---|---|---|---|---|---|---|---|---|---|---|
| **grain** | 1A1 | 1A2 | 1A3 | 1B1 | 1B2 | 1B3 | 1C1 | 1C2 | 1C3 | 1D1 | 1D2 | 1D3 | 2A1 | 2A2 | 2A3 | 2B1 | 2B2 | 2B3 |
| SiO2 | 45.77 | 45.47 | 44.75 | 43.46 | 41.24 | 43.26 | 27.30 | 26.79 | 26.75 | 27.51 | 27.09 | 27.16 | 44.20 | 44.32 | 45.77 | 45.95 | 44.84 | 44.68 |
| TiO2 | 2.43 | 2.41 | 2.44 | 2.36 | 3.79 | 2.36 | 9.78 | 9.88 | 9.77 | 9.93 | 10.02 | 9.92 | 1.71 | 1.87 | 1.90 | 1.98 | 2.05 | 2.01 |
| Al2O3 | 9.85 | 9.74 | 9.54 | 9.92 | 11.87 | 9.75 | 16.09 | 15.91 | 15.89 | 16.15 | 16.16 | 16.09 | 8.12 | 9.20 | 9.13 | 9.41 | 9.43 | 9.35 |
| FeO | 7.27 | 6.99 | 7.12 | 7.16 | 8.43 | 7.07 | 17.55 | 17.13 | 17.22 | 17.08 | 17.19 | 16.68 | 7.99 | 8.40 | 8.56 | 8.53 | 8.23 | 8.60 |
| Fe2O3 | 0.00 | 0.00 | 0.00 | 0.00 | 0.00 | 0.00 | 0.00 | 0.00 | 0.00 | 0.00 | 0.00 | 0.00 | 0.00 | 0.00 | 0.00 | 0.00 | 0.00 | 0.00 |
| MnO | 0.10 | 0.13 | 0.09 | 0.17 | 0.06 | 0.11 | 0.14 | 0.09 | 0.10 | 0.17 | 0.07 | 0.14 | 0.14 | 0.17 | 0.13 | 0.14 | 0.24 | 0.10 |
| MgO | 12.12 | 11.84 | 11.99 | 11.84 | 11.99 | 12.14 | 16.25 | 15.78 | 15.87 | 15.22 | 15.57 | 15.77 | 11.80 | 12.23 | 12.13 | 12.18 | 12.41 | 12.20 |
| CaO | 22.39 | 22.06 | 21.96 | 22.26 | 18.81 | 22.20 | 11.23 | 11.49 | 11.47 | 11.52 | 11.37 | 11.34 | 20.14 | 20.97 | 21.08 | 20.86 | 20.96 | 21.20 |
| Na2O | 0.92 | 0.89 | 0.81 | 0.83 | 1.43 | 0.85 | 1.59 | 1.54 | 1.60 | 1.61 | 1.74 | 1.62 | 0.95 | 1.00 | 1.05 | 0.88 | 0.87 | 0.93 |
| K2O | 0.00 | 0.00 | 0.00 | 0.00 | 0.00 | 0.00 | 0.00 | 0.00 | 0.00 | 0.00 | 0.00 | 0.00 | 0.00 | 0.00 | 0.00 | 0.00 | 0.00 | 0.00 |
| Cr2O3 | 0.10 | -0.01 | -0.06 | -0.07 | 0.07 | 0.03 | 0.03 | -0.03 | 0.05 | 0.07 | -0.06 | -0.01 | -0.07 | 0.14 | 0.03 | 0.08 | -0.04 | -0.02 |
| **Total** | 100.95 | 99.54 | 98.63 | 97.93 | 97.68 | 97.78 | 99.96 | 98.57 | 98.72 | 99.27 | 99.16 | 98.71 | 94.98 | 98.31 | 99.77 | 100.03 | 98.99 | 99.06 |
| Mg# | 63 | 63 | 63 | 62 | 59 | 63 | 48 | 48 | 48 | 47 | 48 | 49 | 60 | 59 | 59 | 59 | 60 | 59 |
| | | | | | | | | | | | | | | | | | | |
| **Cations normalized to 6 oxygens** | | | | | | | | | | | | | | | | | | |
| Si | 1.748 | 1.746 | 1.689 | 1.636 | 1.562 | 1.647 | 1.026 | 1.002 | 1.018 | 1.047 | 1.049 | 1.036 | 1.695 | 1.683 | 1.742 | 1.733 | 1.708 | 1.685 |
| Ti | 0.070 | 0.070 | 0.069 | 0.067 | 0.108 | 0.068 | 0.276 | 0.278 | 0.280 | 0.285 | 0.292 | 0.285 | 0.049 | 0.053 | 0.054 | 0.056 | 0.059 | 0.057 |
| Al | 0.443 | 0.441 | 0.424 | 0.440 | 0.530 | 0.437 | 0.713 | 0.701 | 0.713 | 0.725 | 0.737 | 0.724 | 0.367 | 0.412 | 0.410 | 0.418 | 0.423 | 0.416 |
| Fe 2+ | 0.232 | 0.225 | 0.225 | 0.225 | 0.267 | 0.225 | 0.552 | 0.536 | 0.548 | 0.544 | 0.557 | 0.532 | 0.256 | 0.267 | 0.272 | 0.269 | 0.262 | 0.271 |
| Fe 3+ | 0.000 | 0.000 | 0.000 | 0.000 | 0.000 | 0.000 | 0.000 | 0.000 | 0.000 | 0.000 | 0.000 | 0.000 | 0.000 | 0.000 | 0.000 | 0.000 | 0.000 | 0.000 |
| Mn | 0.003 | 0.004 | 0.003 | 0.005 | 0.002 | 0.004 | 0.005 | 0.003 | 0.003 | 0.005 | 0.002 | 0.004 | 0.005 | 0.006 | 0.004 | 0.005 | 0.008 | 0.003 |
| Mg | 0.690 | 0.678 | 0.675 | 0.664 | 0.677 | 0.689 | 0.911 | 0.880 | 0.901 | 0.864 | 0.899 | 0.897 | 0.675 | 0.692 | 0.688 | 0.685 | 0.705 | 0.686 |
| Ca | 0.916 | 0.908 | 0.888 | 0.898 | 0.763 | 0.906 | 0.452 | 0.460 | 0.468 | 0.470 | 0.471 | 0.463 | 0.828 | 0.853 | 0.860 | 0.843 | 0.855 | 0.857 |
| Na | 0.068 | 0.067 | 0.059 | 0.061 | 0.105 | 0.063 | 0.116 | 0.111 | 0.118 | 0.119 | 0.131 | 0.120 | 0.071 | 0.073 | 0.077 | 0.065 | 0.064 | 0.068 |
| K | 0.000 | 0.000 | 0.000 | 0.000 | 0.000 | 0.000 | 0.000 | 0.000 | 0.000 | 0.000 | 0.000 | 0.000 | 0.000 | 0.000 | 0.000 | 0.000 | 0.000 | 0.000 |
| Cr | 0.003 | 0.000 | -0.002 | -0.002 | 0.002 | 0.001 | 0.001 | -0.001 | 0.001 | 0.002 | -0.002 | 0.000 | -0.002 | 0.004 | 0.001 | 0.002 | -0.001 | -0.001 |
| **Total** | 4.173 | 4.137 | 4.031 | 3.995 | 4.016 | 4.039 | 4.051 | 3.970 | 4.051 | 4.061 | 4.136 | 4.061 | 3.943 | 4.043 | 4.108 | 4.077 | 4.083 | 4.043 |

# Amphiboles

**Amphiboles**

| | AF-1 | | | AF-1 | | | AF-1 | | | AF-2 | | | AF-2 | | | AF-2 | | |
|---|---|---|---|---|---|---|---|---|---|---|---|---|---|---|---|---|---|---|
| Grain | a1 | a2 | a3 | b1 | b2 | b3 | c1 | c2 | c3 | a1 | a2 | a3 | b1 | b2 | b3 | c1 | c2 | c3 |
| SiO2 | 39.92 | 38.97 | 39.42 | 40.56 | 40.03 | 38.18 | 39.49 | 39.53 | 39.18 | 39.08 | 38.87 | 39.98 | 38.95 | 38.13 | 38.41 | 39.99 | 39.59 | 39.26 |
| TiO2 | 4.53 | 4.85 | 4.77 | 4.49 | 4.68 | 4.50 | 5.49 | 5.19 | 5.44 | 4.91 | 4.79 | 4.82 | 5.73 | 5.72 | 5.69 | 5.16 | 5.20 | 5.23 |
| Al2O3 | 14.23 | 14.42 | 14.40 | 14.14 | 13.87 | 14.48 | 14.27 | 14.23 | 14.15 | 14.63 | 14.40 | 14.50 | 14.60 | 14.37 | 14.38 | 14.23 | 14.12 | 14.19 |
| FeO | 11.71 | 11.80 | 11.63 | 11.39 | 11.15 | 11.48 | 11.33 | 11.19 | 10.95 | 11.78 | 10.90 | 11.63 | 11.06 | 10.85 | 10.89 | 10.70 | 10.74 | 11.22 |
| MnO | 0.00 | 0.20 | 0.00 | 0.00 | 0.15 | 0.17 | 0.00 | 0.00 | 0.00 | 0.20 | 0.00 | 0.00 | 0.00 | 0.00 | 0.00 | 0.00 | 0.00 | 0.00 |
| MgO | 12.13 | 12.25 | 12.05 | 12.14 | 12.03 | 12.37 | 11.95 | 11.98 | 11.90 | 12.56 | 12.43 | 12.46 | 12.37 | 12.16 | 11.80 | 12.19 | 11.82 | 12.09 |
| CaO | 11.52 | 11.56 | 11.54 | 11.86 | 11.72 | 11.71 | 11.78 | 11.63 | 11.67 | 11.53 | 11.37 | 11.76 | 11.57 | 11.71 | 11.75 | 11.94 | 11.61 | 11.59 |
| Na2O | 2.32 | 2.29 | 2.34 | 2.40 | 2.31 | 2.37 | 2.45 | 2.35 | 2.39 | 2.62 | 2.50 | 2.70 | 2.50 | 2.55 | 2.59 | 2.41 | 2.45 | 2.62 |
| K2O | 1.14 | 1.03 | 1.14 | 0.90 | 1.07 | 0.89 | 0.98 | 0.99 | 1.16 | 0.99 | 1.05 | 1.14 | 0.90 | 0.94 | 0.86 | 0.97 | 1.09 | 0.97 |
| Cl | 0.00 | 0.00 | 0.00 | 0.00 | 0.00 | 0.00 | 0.00 | 0.00 | 0.00 | 0.00 | 0.00 | 0.00 | 0.00 | 0.00 | 0.00 | 0.00 | 0.00 | 0.00 |
| F | 0.00 | 0.00 | 0.00 | 0.00 | 0.00 | 0.00 | 0.00 | 0.00 | 0.00 | 0.00 | 0.00 | 0.00 | 0.00 | 0.00 | 0.00 | 0.00 | 0.00 | 0.00 |
| **Total** | 97.51 | 97.37 | 97.29 | 97.89 | 97.02 | 96.14 | 97.72 | 97.10 | 96.85 | 98.31 | 96.32 | 98.99 | 97.68 | 96.42 | 96.37 | 97.58 | 96.62 | 97.18 |
| Mg# | 51 | 51 | 51 | 52 | 52 | 52 | 51 | 52 | 52 | 52 | 53 | 52 | 53 | 53 | 52 | 53 | 52 | 52 |
| **Cations normalized to 23 O+OH** | | | | | | | | | | | | | | | | | | |
| Si | 5.923 | 5.809 | 5.868 | 5.976 | 5.960 | 5.765 | 5.846 | 5.880 | 5.851 | 5.773 | 5.830 | 5.854 | 5.764 | 5.728 | 5.768 | 5.905 | 5.910 | 5.846 |
| Ti | 0.506 | 0.543 | 0.534 | 0.498 | 0.524 | 0.511 | 0.611 | 0.581 | 0.611 | 0.546 | 0.541 | 0.531 | 0.638 | 0.646 | 0.643 | 0.573 | 0.584 | 0.585 |
| Al | 2.489 | 2.534 | 2.526 | 2.456 | 2.434 | 2.578 | 2.490 | 2.494 | 2.490 | 2.548 | 2.546 | 2.502 | 2.546 | 2.545 | 2.546 | 2.476 | 2.484 | 2.490 |
| Fe | 1.453 | 1.471 | 1.447 | 1.403 | 1.388 | 1.449 | 1.402 | 1.392 | 1.368 | 1.455 | 1.368 | 1.424 | 1.369 | 1.363 | 1.367 | 1.321 | 1.340 | 1.398 |
| Mn | 0.000 | 0.025 | 0.000 | 0.000 | 0.018 | 0.021 | 0.000 | 0.000 | 0.000 | 0.024 | 0.000 | 0.000 | 0.000 | 0.000 | 0.000 | 0.000 | 0.000 | 0.000 |
| Mg | 2.683 | 2.723 | 2.674 | 2.667 | 2.670 | 2.784 | 2.636 | 2.657 | 2.649 | 2.766 | 2.779 | 2.719 | 2.730 | 2.724 | 2.642 | 2.684 | 2.629 | 2.684 |
| Ca | 1.831 | 1.846 | 1.840 | 1.872 | 1.870 | 1.894 | 1.868 | 1.853 | 1.868 | 1.824 | 1.828 | 1.845 | 1.835 | 1.885 | 1.891 | 1.889 | 1.856 | 1.850 |
| Na | 0.668 | 0.663 | 0.675 | 0.686 | 0.668 | 0.693 | 0.703 | 0.679 | 0.691 | 0.752 | 0.727 | 0.767 | 0.718 | 0.743 | 0.754 | 0.691 | 0.710 | 0.758 |
| K | 0.217 | 0.196 | 0.217 | 0.170 | 0.204 | 0.171 | 0.185 | 0.188 | 0.221 | 0.187 | 0.201 | 0.213 | 0.170 | 0.179 | 0.164 | 0.184 | 0.207 | 0.184 |
| **TOTAL** | 15.769 | 15.811 | 15.781 | 15.726 | 15.736 | 15.867 | 15.742 | 15.725 | 15.749 | 15.876 | 15.820 | 15.854 | 15.769 | 15.814 | 15.775 | 15.721 | 15.722 | 15.794 |

# Olivine

**Olivines**

| Sample | EC-3 | EC-3 | EC-3 | EC-3 | EC-3 | EC-3 | EC-3 | EC-3 | EC-3 | EC-3 | EC-3 | EC-3 | EC-3 | EC-3 | EC-3 | EC-3 | EC-3 | EC-3 | EC-3 | X-1 | X-1 | X-1 | X-1 | X-1 | X-1 | X-1 | X-1 | X-1 |
|---|---|---|---|---|---|---|---|---|---|---|---|---|---|---|---|---|---|---|---|---|---|---|---|---|---|---|---|---|
| grain | A1a | A1b | A1c | A2a | A2b | A2c | A3a | A3b | A3c | B1a | B1b | B1c | B2a | B2b | B2c | B3a | B3b | B3c | | A1a | A1b | A1c | A2a | A2b | A2c | A3a | A3b | A3c |
| SiO2 | 34.86 | 35.12 | 34.75 | 36.18 | 36.13 | 35.69 | 37.19 | 37.16 | 37.57 | 27.69 | 34.25 | 34.01 | 35.12 | 35.12 | 35.48 | 35.10 | 34.93 | 35.08 | | 35.48 | 35.47 | 34.84 | 36.79 | 36.72 | 36.23 | 36.85 | 36.74 | 35.72 |
| TiO2 | 0.00 | 0.00 | 0.00 | 0.00 | 0.00 | 0.00 | 0.00 | 0.00 | 0.00 | 0.00 | 0.00 | 0.00 | 0.00 | 0.00 | 0.00 | 0.00 | 0.00 | 0.00 | | 0.00 | 0.00 | 0.00 | 0.00 | 0.00 | 0.00 | 0.00 | 0.00 | 0.00 |
| Al2O3 | 0.00 | 0.00 | 0.00 | 0.00 | 0.00 | 0.00 | 0.00 | 0.00 | 0.00 | 0.00 | 0.00 | 0.00 | 0.00 | 0.00 | 0.00 | 0.00 | 0.00 | 0.00 | | 0.00 | 0.00 | 0.00 | 0.00 | 0.00 | 0.00 | 0.00 | 0.00 | 0.00 |
| FeO | 27.78 | 27.56 | 28.12 | 27.97 | 27.75 | 28.29 | 27.71 | 27.78 | 28.03 | 28.05 | 27.74 | 28.08 | 27.59 | 27.18 | 27.16 | 27.59 | 27.59 | 28.07 | | 25.69 | 26.20 | 26.05 | 25.68 | 26.00 | 25.53 | 26.10 | 25.23 | 25.96 |
| Fe2O3 | 0.00 | 0.00 | 0.00 | 0.00 | 0.00 | 0.00 | 0.00 | 0.00 | 0.00 | 0.00 | 0.00 | 0.00 | 0.00 | 0.00 | 0.00 | 0.00 | 0.00 | 0.00 | | 0.00 | 0.00 | 0.00 | 0.00 | 0.00 | 0.00 | 0.00 | 0.00 | 0.00 |
| MnO | 0.37 | 0.25 | 0.38 | 0.45 | 0.50 | 0.21 | 0.27 | 0.25 | 0.40 | 0.45 | 0.25 | 0.30 | 0.36 | 0.33 | 0.26 | 0.20 | 0.34 | 0.46 | | 0.20 | 0.41 | 0.29 | 0.19 | 0.36 | 0.21 | 0.30 | 0.34 | 0.36 |
| MgO | 35.34 | 34.60 | 35.00 | 34.71 | 34.23 | 34.67 | 34.16 | 34.84 | 34.13 | 37.16 | 35.43 | 35.59 | 34.94 | 35.40 | 35.75 | 34.98 | 35.53 | 36.56 | | 37.26 | 37.62 | 37.65 | 36.63 | 37.63 | 36.69 | 37.95 | 37.17 | 36.45 |
| CaO | 0.00 | 0.11 | 0.08 | 0.00 | 0.09 | 0.09 | 0.10 | 0.13 | 0.00 | 0.08 | 0.00 | 0.10 | 0.12 | 0.12 | 0.07 | 0.07 | 0.12 | 0.00 | | 0.12 | 0.08 | 0.08 | 0.08 | 0.09 | 0.07 | 0.00 | 0.08 | 0.09 |
| Na2O | 0.00 | 0.00 | 0.00 | 0.00 | 0.00 | 0.00 | 0.00 | 0.00 | 0.00 | 0.00 | 0.00 | 0.00 | 0.00 | 0.00 | 0.00 | 0.00 | 0.00 | 0.00 | | 0.00 | 0.00 | 0.00 | 0.00 | 0.00 | 0.00 | 0.00 | 0.00 | 0.00 |
| K2O | 0.00 | 0.00 | 0.00 | 0.00 | 0.00 | 0.00 | 0.00 | 0.00 | 0.00 | 0.00 | 0.00 | 0.00 | 0.00 | 0.00 | 0.00 | 0.00 | 0.00 | 0.00 | | 0.00 | 0.00 | 0.00 | 0.00 | 0.00 | 0.00 | 0.00 | 0.00 | 0.00 |
| Cr2O3 | 0.00 | 0.00 | 0.00 | 0.00 | 0.00 | 0.00 | 0.00 | 0.00 | 0.00 | 0.00 | 0.00 | 0.00 | 0.00 | 0.00 | 0.00 | 0.00 | 0.00 | 0.00 | | 0.00 | 0.00 | 0.00 | 0.00 | 0.00 | 0.00 | 0.00 | 0.00 | 0.00 |
| NiO | 0.03 | 0.03 | 0.01 | -0.01 | -0.02 | 0.10 | -0.06 | 0.09 | 0.05 | 0.04 | 0.00 | 0.09 | -0.02 | 0.02 | 0.11 | 0.00 | 0.00 | 0.00 | | 0.07 | -0.02 | 0.07 | 0.01 | 0.05 | 0.10 | 0.15 | 0.09 | 0.10 |
| **Total** | 98.38 | 97.67 | 98.35 | 99.31 | 98.69 | 99.07 | 99.38 | 100.25 | 100.19 | 93.47 | 97.67 | 98.17 | 98.10 | 98.16 | 98.82 | 97.93 | 98.51 | 100.17 | | 98.82 | 99.77 | 98.98 | 99.38 | 100.85 | 98.83 | 101.35 | 99.65 | 98.70 |
| Mg# | 56 | 56 | 55 | 55 | 55 | 55 | 55 | 56 | 55 | 57 | 56 | 56 | 56 | 57 | 57 | 56 | 56 | 57 | | 59 | 59 | 59 | 59 | 59 | 59 | 59 | 60 | 58 |
| | | | | | | | | | | | | | | | | | | | | | | | | | | | | |
| **Cations normalized to 4 oxygens** | | | | | | | | | | | | | | | | | | | | | | | | | | | | |
| Si | 0.955 | 0.967 | 0.955 | 0.979 | 0.983 | 0.971 | 1.000 | 0.991 | 1.003 | 0.822 | 0.947 | 0.938 | 0.964 | 0.961 | 0.963 | 0.964 | 0.955 | 0.945 | | 0.957 | 0.950 | 0.942 | 0.982 | 0.968 | 0.974 | 0.967 | 0.977 | 0.965 |
| Ti | 0.000 | 0.000 | 0.000 | 0.000 | 0.000 | 0.000 | 0.000 | 0.000 | 0.000 | 0.000 | 0.000 | 0.000 | 0.000 | 0.000 | 0.000 | 0.000 | 0.000 | 0.000 | | 0.000 | 0.000 | 0.000 | 0.000 | 0.000 | 0.000 | 0.000 | 0.000 | 0.000 |
| Al | 0.000 | 0.000 | 0.000 | 0.000 | 0.000 | 0.000 | 0.000 | 0.000 | 0.000 | 0.000 | 0.000 | 0.000 | 0.000 | 0.000 | 0.000 | 0.000 | 0.000 | 0.000 | | 0.000 | 0.000 | 0.000 | 0.000 | 0.000 | 0.000 | 0.000 | 0.000 | 0.000 |
| Fe 2+ | 0.637 | 0.635 | 0.646 | 0.633 | 0.632 | 0.643 | 0.623 | 0.620 | 0.626 | 0.697 | 0.641 | 0.648 | 0.633 | 0.622 | 0.617 | 0.634 | 0.631 | 0.632 | | 0.579 | 0.587 | 0.589 | 0.573 | 0.573 | 0.574 | 0.573 | 0.561 | 0.587 |
| Fe 3+ | 0.000 | 0.000 | 0.000 | 0.000 | 0.000 | 0.000 | 0.000 | 0.000 | 0.000 | 0.000 | 0.000 | 0.000 | 0.000 | 0.000 | 0.000 | 0.000 | 0.000 | 0.000 | | 0.000 | 0.000 | 0.000 | 0.000 | 0.000 | 0.000 | 0.000 | 0.000 | 0.000 |
| Mn | 0.008 | 0.006 | 0.009 | 0.010 | 0.012 | 0.005 | 0.006 | 0.006 | 0.009 | 0.011 | 0.006 | 0.007 | 0.008 | 0.008 | 0.006 | 0.005 | 0.008 | 0.011 | | 0.005 | 0.009 | 0.007 | 0.004 | 0.008 | 0.005 | 0.007 | 0.008 | 0.008 |
| Mg | 1.444 | 1.421 | 1.433 | 1.400 | 1.388 | 1.406 | 1.369 | 1.386 | 1.358 | 1.645 | 1.460 | 1.464 | 1.429 | 1.444 | 1.447 | 1.432 | 1.448 | 1.468 | | 1.498 | 1.502 | 1.517 | 1.457 | 1.479 | 1.470 | 1.484 | 1.473 | 1.469 |
| Ca | 0.000 | 0.003 | 0.002 | 0.000 | 0.003 | 0.003 | 0.003 | 0.004 | 0.000 | 0.002 | 0.000 | 0.003 | 0.003 | 0.004 | 0.002 | 0.002 | 0.003 | 0.000 | | 0.003 | 0.002 | 0.002 | 0.002 | 0.002 | 0.002 | 0.000 | 0.002 | 0.003 |
| Na | 0.000 | 0.000 | 0.000 | 0.000 | 0.000 | 0.000 | 0.000 | 0.000 | 0.000 | 0.000 | 0.000 | 0.000 | 0.000 | 0.000 | 0.000 | 0.000 | 0.000 | 0.000 | | 0.000 | 0.000 | 0.000 | 0.000 | 0.000 | 0.000 | 0.000 | 0.000 | 0.000 |
| K | 0.000 | 0.000 | 0.000 | 0.000 | 0.000 | 0.000 | 0.000 | 0.000 | 0.000 | 0.000 | 0.000 | 0.000 | 0.000 | 0.000 | 0.000 | 0.000 | 0.000 | 0.000 | | 0.000 | 0.000 | 0.000 | 0.000 | 0.000 | 0.000 | 0.000 | 0.000 | 0.000 |
| Cr | 0.000 | 0.000 | 0.000 | 0.000 | 0.000 | 0.000 | 0.000 | 0.000 | 0.000 | 0.000 | 0.000 | 0.000 | 0.000 | 0.000 | 0.000 | 0.000 | 0.000 | 0.000 | | 0.000 | 0.000 | 0.000 | 0.000 | 0.000 | 0.000 | 0.000 | 0.000 | 0.000 |
| Ni | 0.001 | 0.001 | 0.000 | 0.000 | 0.000 | 0.002 | -0.001 | 0.002 | 0.001 | 0.001 | 0.000 | 0.002 | 0.000 | 0.000 | 0.002 | 0.000 | 0.000 | 0.000 | | 0.002 | 0.000 | 0.002 | 0.000 | 0.001 | 0.002 | 0.003 | 0.002 | 0.002 |
| **Total** | 3.045 | 3.033 | 3.045 | 3.021 | 3.017 | 3.029 | 3.000 | 3.009 | 2.997 | 3.178 | 3.053 | 3.062 | 3.036 | 3.039 | 3.037 | 3.036 | 3.045 | 3.055 | | 3.043 | 3.050 | 3.058 | 3.018 | 3.032 | 3.026 | 3.033 | 3.023 | 3.035 |

**Olivines**

| Sample | X-1 | X-1 | X-1 | X-1 | X-1 | X-1 | X-1 | X-1 | X-1 | S-1 | S-1 | S-1 | S-1 | S-1 | S-1 |
|---|---|---|---|---|---|---|---|---|---|---|---|---|---|---|---|
| grain | B1a | B1b | B1c | B2a | B2b | B2c | B3a | B3b | B3c | A1a | A1b | A1c | B1a | B1b | B1c |
| SiO2 | 36.76 | 36.26 | 36.59 | 35.86 | 35.82 | 35.56 | 34.65 | 34.81 | 34.84 | 34.87 | 34.91 | 36.62 | 35.64 | 34.91 | 34.96 |
| TiO2 | 0.00 | 0.00 | 0.00 | 0.00 | 0.00 | 0.00 | 0.00 | 0.00 | 0.00 | 0.00 | 0.00 | 0.00 | 0.00 | 0.00 | 0.00 |
| Al2O3 | 0.00 | 0.00 | 0.00 | 0.00 | 0.00 | 0.00 | 0.00 | 0.00 | 0.00 | 0.00 | 0.00 | 0.00 | 0.00 | 0.00 | 0.00 |
| FeO | 25.35 | 26.11 | 25.52 | 25.91 | 25.45 | 25.35 | 25.64 | 26.01 | 25.47 | 25.58 | 24.92 | 25.04 | 28.53 | 28.84 | 28.49 |
| Fe2O3 | 0.00 | 0.00 | 0.00 | 0.00 | 0.00 | 0.00 | 0.00 | 0.00 | 0.00 | 0.00 | 0.00 | 0.00 | 0.00 | 0.00 | 0.00 |
| MnO | 0.32 | 0.36 | 0.36 | 0.44 | 0.32 | 0.34 | 0.32 | 0.27 | 0.26 | 0.31 | 0.20 | 0.32 | 0.32 | 0.33 | 0.33 |
| MgO | 37.03 | 36.60 | 36.78 | 37.18 | 36.99 | 36.53 | 37.02 | 37.14 | 36.62 | 38.02 | 38.37 | 37.87 | 35.70 | 35.55 | 35.07 |
| CaO | 0.10 | 0.11 | 0.11 | 0.09 | 0.00 | 0.09 | 0.12 | 0.00 | 0.08 | 0.10 | 0.08 | 0.07 | 0.00 | 0.09 | 0.10 |
| Na2O | 0.00 | 0.00 | 0.00 | 0.00 | 0.00 | 0.00 | 0.00 | 0.00 | 0.00 | 0.00 | 0.00 | 0.00 | 0.00 | 0.00 | 0.00 |
| K2O | 0.00 | 0.00 | 0.00 | 0.00 | 0.00 | 0.00 | 0.00 | 0.00 | 0.00 | 0.00 | 0.00 | 0.00 | 0.00 | 0.00 | 0.00 |
| Cr2O3 | 0.00 | 0.00 | 0.00 | 0.00 | 0.00 | 0.00 | 0.00 | 0.00 | 0.00 | 0.00 | 0.00 | 0.00 | 0.00 | 0.00 | 0.00 |
| NiO | 0.14 | -0.03 | 0.16 | 0.07 | 0.10 | 0.15 | 0.05 | 0.10 | 0.18 | 0.03 | 0.00 | -0.09 | 0.00 | -0.02 | 0.06 |
| **Total** | 99.70 | 99.44 | 99.36 | 99.49 | 98.59 | 97.87 | 97.75 | 98.24 | 97.27 | 98.87 | 98.48 | 99.92 | 100.18 | 99.72 | 98.94 |
| Mg# | 59 | 58 | 59 | 59 | 59 | 59 | 59 | 59 | 59 | 60 | 61 | 60 | 56 | 55 | 55 |
| | | | | | | | | | | | | | | | |
| **Cations normalized to 4 oxygens** | | | | | | | | | | | | | | | |
| Si | 0.978 | 0.971 | 0.976 | 0.960 | 0.965 | 0.966 | 0.947 | 0.947 | 0.954 | 0.941 | 0.943 | 0.971 | 0.959 | 0.948 | 0.955 |
| Ti | 0.000 | 0.000 | 0.000 | 0.000 | 0.000 | 0.000 | 0.000 | 0.000 | 0.000 | 0.000 | 0.000 | 0.000 | 0.000 | 0.000 | 0.000 |
| Al | 0.000 | 0.000 | 0.000 | 0.000 | 0.000 | 0.000 | 0.000 | 0.000 | 0.000 | 0.000 | 0.000 | 0.000 | 0.000 | 0.000 | 0.000 |
| Fe 2+ | 0.564 | 0.585 | 0.570 | 0.580 | 0.574 | 0.576 | 0.586 | 0.592 | 0.583 | 0.577 | 0.563 | 0.555 | 0.642 | 0.655 | 0.651 |
| Fe 3+ | 0.000 | 0.000 | 0.000 | 0.000 | 0.000 | 0.000 | 0.000 | 0.000 | 0.000 | 0.000 | 0.000 | 0.000 | 0.000 | 0.000 | 0.000 |
| Mn | 0.007 | 0.008 | 0.008 | 0.010 | 0.007 | 0.008 | 0.007 | 0.006 | 0.006 | 0.007 | 0.005 | 0.007 | 0.007 | 0.008 | 0.008 |
| Mg | 1.468 | 1.462 | 1.463 | 1.485 | 1.486 | 1.479 | 1.508 | 1.506 | 1.496 | 1.530 | 1.545 | 1.496 | 1.432 | 1.439 | 1.428 |
| Ca | 0.003 | 0.003 | 0.003 | 0.003 | 0.000 | 0.003 | 0.003 | 0.000 | 0.002 | 0.003 | 0.002 | 0.002 | 0.000 | 0.003 | 0.003 |
| Na | 0.000 | 0.000 | 0.000 | 0.000 | 0.000 | 0.000 | 0.000 | 0.000 | 0.000 | 0.000 | 0.000 | 0.000 | 0.000 | 0.000 | 0.000 |
| K | 0.000 | 0.000 | 0.000 | 0.000 | 0.000 | 0.000 | 0.000 | 0.000 | 0.000 | 0.000 | 0.000 | 0.000 | 0.000 | 0.000 | 0.000 |
| Cr | 0.000 | 0.000 | 0.000 | 0.000 | 0.000 | 0.000 | 0.000 | 0.000 | 0.000 | 0.000 | 0.000 | 0.000 | 0.000 | 0.000 | 0.000 |
| Ni | 0.003 | -0.001 | 0.003 | 0.002 | 0.002 | 0.003 | 0.001 | 0.002 | 0.004 | 0.001 | 0.000 | -0.002 | 0.000 | 0.000 | 0.001 |
| **Total** | 3.019 | 3.029 | 3.020 | 3.038 | 3.032 | 3.031 | 3.052 | 3.051 | 3.042 | 3.058 | 3.057 | 3.031 | 3.041 | 3.052 | 3.044 |

# Oxides

Oxides

| | EC-3 | | | EC-3 | | | EC-3 | | | EC-3 | | | AF-1 | | AF-1 | | S-1 | | | |
|---|---|---|---|---|---|---|---|---|---|---|---|---|---|---|---|---|---|---|---|---|
| MINERAL | Spinel | Spinel | Spinel | Ilmenite | Ilmenite | Ilmenite | Spinel | Spinel | Spinel | Ilmenite | Ilmenite | Ilmenite | ? | Spinel | Spinel | ? Bad result | Spinel | Magnetite | Magnetite | Magnetite |
| grain | A1a | A1b | A1c | A2a | A2b | A2c | B1a | B1b | B1c | B2a | B2b | B2c | A1b | A2c | B1a | B2b | A1a | A2a | A3a | A4b |
| SiO2 | 0.00 | 0.00 | 0.00 | 0.00 | 0.00 | 0.00 | 0.00 | 0.00 | 0.00 | 0.00 | 0.00 | 0.00 | 0.12 | 0.00 | 0.00 | 0.00 | 0.05 | 0.12 | 0.26 | 0.12 |
| TiO2 | 0.37 | 0.40 | 0.40 | 53.33 | 52.97 | 52.93 | 0.45 | 0.54 | 0.50 | 53.37 | 52.50 | 53.09 | 5.55 | 0.81 | 0.95 | 39.80 | 0.44 | 0.06 | 0.01 | 0.09 |
| Al2O3 | 59.94 | 60.42 | 60.94 | 0.41 | 0.42 | 0.35 | 56.15 | 58.14 | 56.26 | 0.10 | 0.10 | 0.10 | 8.33 | 52.89 | 52.91 | 0.78 | 60.95 | 1.08 | 0.20 | 0.24 |
| MnO | 0.11 | 0.25 | 0.20 | 0.41 | 0.44 | 0.34 | 0.14 | 0.10 | 0.21 | 0.40 | 0.44 | 0.38 | 0.40 | 0.22 | 0.14 | 0.23 | 0.08 | 0.06 | 0.09 | 0.00 |
| MgO | 16.05 | 16.29 | 16.58 | 8.42 | 8.38 | 8.18 | 14.19 | 13.93 | 14.25 | 8.43 | 8.31 | 8.15 | 4.68 | 13.23 | 12.85 | 4.18 | 13.53 | 0.14 | 0.26 | 0.02 |
| CaO | 0.00 | 0.00 | 0.00 | 0.00 | 0.00 | 0.00 | 0.00 | 0.00 | 0.00 | 0.00 | 0.00 | 0.00 | 0.00 | 0.00 | 0.02 | 0.00 | 0.03 | 0.00 | 0.00 | 0.04 |
| Cr2O3 | 0.30 | 0.40 | 0.21 | 0.00 | 0.00 | 0.00 | 0.42 | 0.26 | 0.14 | 0.00 | 0.00 | 0.00 | 0.14 | 0.19 | 0.10 | 0.07 | 0.34 | 0.00 | 0.00 | 0.00 |
| FeO | 22.91 | 22.57 | 22.66 | 36.84 | 37.02 | 36.20 | 26.84 | 27.03 | 27.22 | 36.97 | 36.70 | 36.55 | 74.97 | 30.08 | 31.31 | 49.61 | 22.52 | 29.28 | 87.77 | 90.12 |
| Fe2O3 | 0.00 | 0.00 | 0.00 | 0.00 | 0.00 | 0.00 | 0.00 | 0.00 | 0.00 | 0.00 | 0.00 | 0.00 | 0.00 | 0.00 | 0.00 | 0.00 | 0.00 | 57.65 | 0.00 | 0.00 |
| **Total** | 99.67 | 100.32 | 100.99 | 99.40 | 99.22 | 98.01 | 98.19 | 100.00 | 98.57 | 99.27 | 98.04 | 98.27 | 94.19 | 97.42 | 98.28 | 94.67 | 97.94 | 88.39 | 88.59 | 90.63 |
| Mg# | 41.21 | 41.92 | 42.25 | 18.60 | 18.46 | 18.44 | 34.58 | 34.01 | 34.37 | 18.57 | 18.46 | 18.24 | 5.88 | 30.55 | 29.10 | 7.77 | 37.53 | 0.16 | 0.30 | 0.02 |
| Fe total | 22.91 | 22.57 | 22.66 | 36.84 | 37.02 | 36.20 | 26.84 | 27.03 | 27.22 | 36.97 | 36.70 | 36.55 | 74.97 | 30.08 | 31.31 | 49.61 | 22.52 | 86.93 | 87.77 | 90.12 |
| Fe2+/Fe3+ | 1.00 | 1.00 | 1.00 | 1.00 | 1.00 | 1.00 | 1.00 | 1.00 | 1.00 | 1.00 | 1.00 | 1.00 | 1.00 | 1.00 | 1.00 | 1.00 | 1.00 | 0.33 | 1.00 | 1.00 |
| **Oxygen #** | 4 | 4 | 4 | 3 | 3 | 3 | 4 | 4 | 4 | 3 | 3 | 3 | 4 | 4 | 4 | 4 | 4 | 4 | 4 | 4 |
| Si | 0.000 | 0.000 | 0.000 | 0.000 | 0.000 | 0.000 | 0.000 | 0.000 | 0.000 | 0.000 | 0.000 | 0.000 | 0.005 | 0.000 | 0.000 | 0.000 | 0.001 | 0.005 | 0.014 | 0.006 |
| Ti | 0.007 | 0.008 | 0.008 | 0.965 | 0.962 | 0.971 | 0.009 | 0.011 | 0.010 | 0.969 | 0.966 | 0.973 | 0.179 | 0.017 | 0.020 | 1.096 | 0.009 | 0.002 | 0.000 | 0.004 |
| Al | 1.883 | 1.883 | 1.885 | 0.012 | 0.012 | 0.010 | 1.836 | 1.860 | 1.835 | 0.003 | 0.003 | 0.003 | 0.420 | 1.781 | 1.775 | 0.034 | 1.941 | 0.055 | 0.013 | 0.015 |
| Fe 2+ | 0.511 | 0.499 | 0.497 | 0.741 | 0.747 | 0.738 | 0.623 | 0.614 | 0.630 | 0.746 | 0.751 | 0.745 | 2.682 | 0.719 | 0.745 | 1.519 | 0.509 | 1.064 | 3.928 | 3.954 |
| Fe 3+ | 0.000 | 0.000 | 0.000 | 0.000 | 0.000 | 0.000 | 0.000 | 0.000 | 0.000 | 0.000 | 0.000 | 0.000 | 0.000 | 0.000 | 0.000 | 0.000 | 0.000 | 1.885 | 0.000 | 0.000 |
| Mn | 0.002 | 0.006 | 0.004 | 0.008 | 0.009 | 0.007 | 0.003 | 0.002 | 0.005 | 0.008 | 0.009 | 0.008 | 0.014 | 0.005 | 0.003 | 0.007 | 0.002 | 0.002 | 0.004 | 0.000 |
| Mg | 0.638 | 0.642 | 0.648 | 0.302 | 0.302 | 0.297 | 0.587 | 0.564 | 0.588 | 0.303 | 0.303 | 0.296 | 0.298 | 0.563 | 0.545 | 0.228 | 0.545 | 0.009 | 0.021 | 0.002 |
| Ca | 0.000 | 0.000 | 0.000 | 0.000 | 0.000 | 0.000 | 0.000 | 0.000 | 0.000 | 0.000 | 0.000 | 0.000 | 0.000 | 0.000 | 0.001 | 0.000 | 0.001 | 0.000 | 0.000 | 0.002 |
| Cr | 0.006 | 0.008 | 0.004 | 0.000 | 0.000 | 0.000 | 0.009 | 0.006 | 0.003 | 0.000 | 0.000 | 0.000 | 0.005 | 0.004 | 0.002 | 0.002 | 0.007 | 0.000 | 0.000 | 0.000 |
| **Total** | **3.048** | **3.046** | **3.047** | **2.029** | **2.032** | **2.024** | **3.068** | **3.056** | **3.071** | **2.030** | **2.032** | **2.025** | **3.604** | **3.090** | **3.091** | **2.886** | **3.015** | **3.023** | **3.979** | **3.983** |

## Apatite

| Sample | X-1 | X-1 | X-1 | X-1 | X-1 | F-2 | F-2 | F-2 | F-2 | F-2 | F-2 |
|---|---|---|---|---|---|---|---|---|---|---|---|
| Grain | AA1 | BB1 | BB2 | BB3 | A1 | A2 | A3 | B1 | B2 | C1 | C1 |
| FeO | 0.930 | 0.515 | 0.731 | 0.404 | 0.604 | 1.281 | 3.599 | 0.315 | 0.496 | 0.571 | 1.022 |
| MgO | 0.576 | 0.537 | 0.547 | 0.500 | 0.375 | 0.607 | 0.776 | 0.315 | 0.325 | 0.399 | 0.562 |
| CaO | 55.007 | 54.124 | 54.323 | 54.248 | 54.446 | 53.604 | 51.575 | 53.901 | 53.917 | 55.154 | 55.234 |
| Na2O | 0.192 | 0.210 | 0.228 | 0.226 | 0.125 | 0.124 | nd | nd | 0.117 | 0.312 | 0.221 |
| P2O5 | 41.897 | 41.349 | 41.136 | 41.812 | 42.213 | 40.535 | 41.081 | 42.001 | 42.655 | 42.407 | 42.278 |
| SO3 | nd | nd | nd | 0.045 | 0.102 | 0.088 | 0.139 | nd | nd | nd | nd |
| SrO | 0.191 | 0.184 | 0.143 | 0.210 | 0.229 | 0.237 | 0.267 | nd | 0.115 | 0.149 | 0.151 |
| Ce2O3 | nd | nd | nd | nd | nd | nd | nd | nd | nd | nd | nd |
| Y2O3 | nd | nd | nd | nd | nd | 0.245 | nd | 0.211 | nd | nd | nd |
| F | 0.614 | 0.354 | 0.355 | 0.611 | nd | 2.677 | 2.137 | 1.245 | 1.279 | 1.256 | 1.427 |
| Cl | 0.907 | 0.953 | 0.952 | 0.970 | 0.997 | 0.550 | 0.319 | 0.495 | 0.468 | 0.449 | 0.552 |
| Total | 100.375568 | 98.6994 | 98.678741 | 99.178269 | 99.653953 | 99.948809 | 100.138496 | 99.096844 | 99.384488 | 100.906614 | 101.517871 |
| O=F, Cl | -0.463258099 | -0.363958901 | -0.364132162 | -0.476067165 | -0.240819224 | -1.251331946 | -0.971776266 | -0.635772774 | -0.643993634 | -0.630151846 | -0.725427083 |
| total | 99.9123099 | 98.3354411 | 98.31460884 | 98.70220184 | 99.41313378 | 98.69747705 | 99.16671973 | 98.46107123 | 98.74049437 | 100.2764622 | 100.7924439 |
| cations norm to 25 oxygen equivalents | | | | | | | | | | | |
| Fe | 0.13 | 0.07 | 0.10 | 0.06 | 0.08 | 0.18 | 0.51 | 0.04 | 0.07 | 0.08 | 0.14 |
| Mg | 0.14 | 0.14 | 0.14 | 0.13 | 0.09 | 0.16 | 0.20 | 0.08 | 0.08 | 0.10 | 0.14 |
| Ca | 9.85 | 9.84 | 9.88 | 9.80 | 9.75 | 9.84 | 9.39 | 9.76 | 9.68 | 9.82 | 9.82 |
| Na | 0.06 | 0.07 | 0.08 | 0.07 | 0.04 | 0.04 | 0.02 | 0.02 | 0.04 | 0.10 | 0.07 |
| P | 5.93 | 5.94 | 5.91 | 5.97 | 5.98 | 5.88 | 5.91 | 6.01 | 6.05 | 5.97 | 5.94 |
| S | 0.00 | 0.00 | 0.00 | 0.01 | 0.01 | 0.01 | 0.02 | 0.00 | 0.00 | 0.00 | 0.00 |
| Sr | 0.02 | 0.02 | 0.01 | 0.02 | 0.02 | 0.02 | 0.03 | 0.00 | 0.01 | 0.01 | 0.01 |
| Ce | 0.00 | 0.03 | 0.01 | 0.00 | 0.03 | 0.00 | 0.00 | 0.03 | 0.00 | 0.01 | 0.00 |
| Y | 0.01 | 0.00 | 0.01 | 0.01 | 0.00 | 0.02 | 0.02 | 0.02 | 0.00 | 0.00 | 0.01 |
| F | 0.32 | 0.19 | 0.19 | 0.33 | 0.02 | 1.45 | 1.15 | 0.67 | 0.68 | 0.66 | 0.75 |
| Cl | 0.26 | 0.27 | 0.27 | 0.28 | 0.28 | 0.16 | 0.09 | 0.14 | 0.13 | 0.13 | 0.16 |
| OH | 1.42 | 1.54 | 1.54 | 1.40 | 1.70 | 0.39 | 0.76 | 1.19 | 1.19 | 1.21 | 1.10 |
| Sum cations | 18.14 | 18.11 | 18.15 | 18.07 | 18.02 | 18.16 | 18.10 | 17.97 | 17.94 | 18.09 | 18.13 |